

THESIS ON MECHANICAL ENGINEERING E102

Experimental and Analytical Modelling of Pelvic Motion

SERGEI ŽIGAILOV

TUT
PRESS

TALLINN UNIVERSITY OF TECHNOLOGY
Faculty of Mechanical Engineering
Department of Mechatronics

This dissertation was accepted for the defense of the degree of Doctor of Philosophy in Engineering on 15th June 2016.

Supervisors: Assoc. Prof. Gennadi Arjassov,
Department of Mechatronics, Tallinn University of Technology,
Prof. Victor Musalimov,
Department of Mechatronics, Saint Petersburg National Research University of
Information Technologies, Mechanics and Optics

Opponents: Prof. Mati Pääsuke, Institute of Sport Sciences and Physiotherapy,
University of Tartu,
Assoc. Prof. Julius Griškevičius, Department of Biomechanics, Vilnius
Gediminas Technical University

Defense of the thesis: 30th August 2016

Declaration:

Hereby I declare that this doctoral thesis, my original investigation and achievement, submitted for the doctoral degree at Tallinn University of Technology has not been submitted for any academic degree.

/Sergei Žigailov/

Copyright: Sergei Žigailov, 2016
ISSN 1406-4758
ISBN 978-9949-23-997-9 (publication)
ISBN 978-9949-23-998-6 (PDF)

MEHHA NOTEHNIKA E102

**Vaagna liikumise eksperimentaalne ja
analüütiline modelleerimine**

SERGEI ŽIGAILOV

CONTENTS

LIST OF PUBLICATIONS	7
ABBREVIATIONS	8
SYMBOLS	8
INTRODUCTION	11
Background	11
1. OVERVIEW OF THE MATHEMATICAL MODELS OF HUMAN LOWER LIMBS	13
1.1. The simplest mechanisms: inverted pendulum	14
1.2. Multilink mechanisms imitating human lower-limb motion	17
1.3. Mathematical models of human motion obtained from experiments.....	20
1.4. Identification of motion transfer from the human heel to the pelvis.....	21
1.5. Experimental and analytical approach	23
Chapter 1. Results and discussion.....	24
2. DESIGN OF EXPERIMENTAL PROTOTYPE CONSTRUCTION AND MEASUREMENT SYSTEM	27
2.1. The mechanical construction of the experimental prototype	27
2.2. System of link motions generation	30
2.3. Measurement system of experimental prototype	33
2.4. Completed tasks creating an experimental prototype: evaluation of obtained results	34
Chapter 2. Results and discussion.....	34
3. EXPERIMENTS, SIGNAL PROCESSING, AND OUTPUT SIGNAL DETERMINATION	35
3.1. Selection of experimental parameters.....	35
3.2. Experimental data processing	36
3.3. Interpolation with 3 order splines	44
3.4. Laws of plate motion in measured points	46
Chapter 3. Results and discussion.....	47
4. IDENTIFICATION OF MECHANICAL HEEL-PELVIS SYSTEM	49
4.1. Description of identification method	49
4.2. State-space representation. Vector-matrix form	51
4.3. Solution of discrete state-space equations using Laplace transform: calculation of the transfer function	54
4.4. Dynamic parameters of automatic systems.....	58
4.4.1. Bode diagram.....	58
4.4.2. Damping.....	59
4.5. Inverse Laplace transform: determination of the law of plate plane pelvic motion	61
Chapter 4. Results and discussion.....	63
CONCLUSION.....	64
Scientific Results	64
Novelties	64
Future work.....	64

REFERENCES	66
OTHER PUBLICATIONS	74
ACKNOWLEDGEMENTS	75
ABSTRACT	76
KOKKUVÕTE	78
APPENDICES	80
Appendix 1. Experimental prototype work description	80
Appendix 2. Statistical evaluation of signals (<i>F</i> -test).....	82
Appendix 3. Filtered accelerations averaging.....	87
Appendix 4. Determination of outliers presence (<i>Q</i> -test).....	89
ELULOOKIRJELDUS	93
CURRICULUM VITAE.....	94

LIST OF PUBLICATIONS

1. Zhigailov, S., Musalimov, V., Aryassov, G., Design of experimental stand for human gait imitation. *Proceedings of the 9th International Conference of DAAAM Baltic*, Tallinn, 2014, 300–304.
2. Zhigailov, S., Kuznetcov, A., Musalimov, V., Aryassov, G., Measurement and Analysis of Human Lower Limbs Movement Parameters during Walking. *Solid State Phenomena*, 2015, 220–221, 538–543.
3. Zhigailov, S., Verchenko, A., Musalimov, V., Aryassov, G., Calculation of plate plane motion parameters using inertial measurement system. *Proceedings of the 10th International Conference of DAAAM Baltic*, Tallinn, 2015, 192–198.
4. Zhigailov, S., Musalimov, V., Aryassov, G., Penkov, I., Modelling and simulation of human lower-limb motion. *International Review on Modelling and Simulations (I.RE.MO.S.)*, 2016, 9(2), 114-123.

The contribution of the dissertant to the completing the doctoral thesis

The contribution of the author to the papers as follows:

Publication 1,2 and 4 – I was the main author responsible for literature overview, analysis, design of the first version of the construction of experimental prototype. I had a major role in writing this paper.

Publication 3 – I was responsible for composition of the paper.

ABBREVIATIONS

CAD – Computer-aided Design;
DOF – Degrees of Freedom;
IIR – Infinite Impulse Response;
IMU – Inertial Measurement Unit;
MEMS – Micro-electro Mechanical System;
MSS – Musculoskeletal System;
TF – Transfer Function.

SYMBOLS

A – Functional matrix of size $nu \times nu$ (matrix system state (object));
 $Acc(i + 1, i, i - 1)$ – Acceleration;
 Amp – Amplitude;
 B – Functional matrix sized $nu \times r$ (control matrix (input));
 C – Functional matrix with size $m \times nu$ (matrix of output state);
 Ch_i – Cubic function;
 Ch'_i, Ch''_i – Boundary conditions for cubic function;
 D – Functional matrix with size $m \times r$ (matrix of output control);
 $Diff_{y,z}$ – Deviation of accelerometers filtered data from average acceleration by y and z axes;
 $Diff_{ymid,zmid}$ – Average difference between each measurement of filtered accelerometers data and average acceleration data by y and z axes;
 $Dis(i + 2)$ – Displacement;
 $D_{y,z}(s), D_{y,z}(z)$ – Arrays of displacements by y and z axes;
 Dy_{max}, Z_{max} – Maximal values of samples by y and z axes;
 Dy_{min}, Z_{min} – Minimal values of samples by y and z axes;
 $F(s)$ – Laplace image of the function $f(t)$;
 F_{emp} – Empirical value of F -test;
 F_{table} – Table value of F -test;
 G_r – Gyroscope data for small period of time;
 $H(z)$ – Transfer characteristics of Butterworth filter;
 H_0, H_1 – Hypotheses;
 I – Identity matrix;
 K – Matrix impulse transition function of system;
 L – Logarithmic ratio;
 $Lap(t), Lap(s)$ – Laplace transform of Euler function;
 M_y – Median by axis y ;
 M_z – Median by axis z ;
 $N_i(i = 1, \dots, nu)$ – Equation of the system state;
 $O_k(k = 1, \dots, m)$ – Equation defining the output variables with dependence from state variables and inputs;
 $P(s)$ – Matrix whose elements are polynomials of s ;

R – Radius;
 Res – Residue;
 S_i – Spline function;
 T_s – Sample time (time of discretisation);
 T_{exp} – Pure time of experiments;
 T_{total} – Total time of measurements for corresponding experimental mode;
 $V(i + 1, i, i - 1)$ – Linear velocity;
 W – Weight coefficient;
 $W_{y,z}(s, z)$ – Transfer functions;
 a, b, c, d – Coefficients in spline function;
 e – Euler constant;
 $er(t)$ – Random disturbance;
 f – Natural frequency;
 f_{cut} – Cutoff frequency;
 $f(t)$ – Function of Newton`s differential equation;
 $f_y(t), f_z(t)$ – Fourier functions;
 $g_{y,z}$ – Angular velocity;
 i – Number of element in vectors and equations;
 j – Imaginary unit;
 m – Number of outputs;
 n – Arrays of time intervals with some number of points;
 n_d – Damping Coefficients;
 nl – Pole of multiplicity;
 n_u – Number of state variables of system;
 num – Number of periods;
 pr – Processed signal;
 r – Number of inputs;
 s – Variables of continuous-time function;
 s_i – Singular point;
 $t(i + 1, i, i - 1)$ – Time;
 $t_m(1,2,3)$ – Step duration in time;
 $u(t), u(s), u(z)$ – Input signal;
 un – Unprocessed signal;
 u_q – Input variables;
 u^T, y^T, x^T – Transposed vectors;
 \ddot{u}, \dot{u} – Derivatives of input signal;
 $w(1,2,3)$ – Weight;
 x – Intermediate variable;
 $x_0(t)$ – Initial condition;
 x_i – Total number of variable states;
 \dot{x} – Differential operator;
 y, z – Directions, axes;
 $y(t), y(s), y(z)$ – Output signals;
 \bar{y}, \bar{z} – Arithmetic means by axes y and z ;

$\tilde{y}(t)$ – Theoretical yield of the object;
 z – Variables of discrete-time function.

Ψ – Operator of identification function;
 Φ – Integrand;
 α – Angle of rotation around supporting bearing;
 $\beta(1,2,3)$ – Angle of rotation around axis x ;
 γ – Values of displacements in ascending order;
 δ – Real number;
 λ_i – Characteristic number of matrix A ;
 $\mu_{y,z}$ – Expected values by y and z axes;
 $\sigma_{y,z}$ – Standard deviations by y and z axes;
 $\sigma_{y(un)}^2, \sigma_{y(pr)}^2$ – Dispersion of unprocessed and processed signals by axis y ;
 $\sigma_{z(un)}^2, \sigma_{z(pr)}^2$ – Dispersion of unprocessed and processed signals by axis z .

\mathcal{L} – Operation of Laplace transform.

INTRODUCTION

Background

Among the diseases that most people face sooner or later are illnesses connected with dysfunctions of the musculoskeletal system (MSS) and spine. Because the MSS is our frame, support, and foundation, it provokes imbalance causing disease in other systems and individual organs as well as decreased mobility and deterioration of general condition of the body. Diseases of the spine, bones, and joints are equally typical for young and elderly people. Apart from mechanical traumas and excessive loads on separate parts of MSS, there are some other diseases that are not directly connected with illnesses of the MSS components (for example – stroke), but cause the loss of locomotion activity. Statistics of morbidity of different types of diseases, according to the information of European Occupational Disease Statistics is shown in Fig. 1.1 [1]:

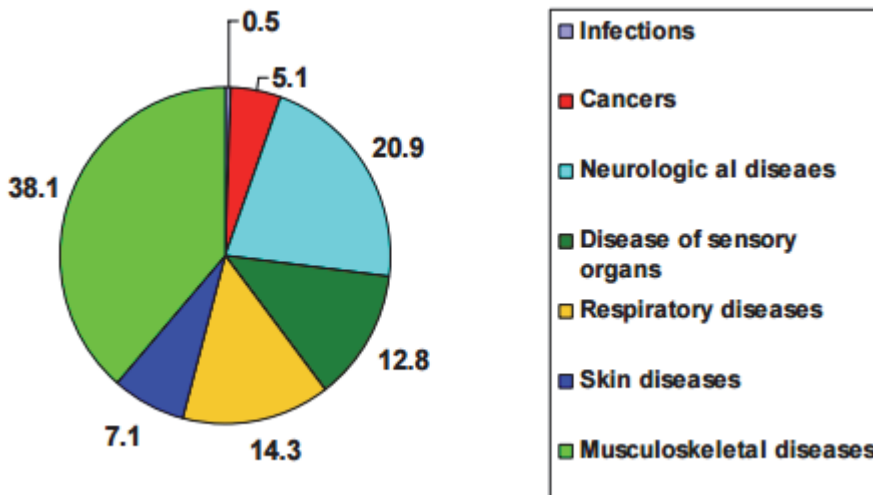


Figure 1.1. Proportional distribution of occupational diseases in EU (2005) [1].

Many modifications of medical rehabilitation facilities and trainers have been designed in recent years for successful treatment of diseases of the MSS. Some of them have proved to have high efficiency in practice. The most successful models of such systems make it possible to provide feedback to the patient as well as to take into account individual physiological and anthropometric characteristics of a particular patient in the preparation of the course of restoration programs. However, the possibility of using these trainers at each facility is inappropriate primarily because of their high cost.

One of the main ways to reduce the high cost of medical rehabilitation systems is using lower-cost inertial measurement units (IMUs) for the study of human

motion. Nowadays, there is no single mathematical model or complete description of human MSS using IMUs. Therefore, this area of biomechanics requires further study.

The human pelvis, connecting the upper and lower parts of the body and transporting an individual's own weight, has always been one of the highest priorities in the research of the human MSS. The description of the kinematics and dynamics of the pelvis during walking is especially difficult. Therefore, a large portion of mathematical models begin with study of the plane pelvic motion.

Subsequently, the results of this work will be used during the development of a new rehabilitation trainer for people suffering from MSS diseases and will be used in restoration of the quality of pelvic motion abilities restoration (for sitting-in-saddle patients). From the famous trainers, only Zander's models were equipped with a saddle, but they had only one degree of freedom (DOF) and became out of date.

The main objective of this work is to model and construct a mechanical system for human heel-pelvis motion simulation in the frontal plane, and to find parameters of its mathematical model for subsequent use in human lower-limb recovery in the near future.

1. OVERVIEW OF THE MATHEMATICAL MODELS OF HUMAN LOWER LIMBS

Up to this day, the most successful moving legged mechanisms are musculoskeletal system of living things, past centuries of adaptation. Depending on the lifestyle, living beings daily are successful in performing the functions of movement in different climates (temperature, humidity, etc.) and landscape (elevation, the presence of obstacles on the path of research, the nature of the soil, etc.) conditions. By this way, the basic principle of designing two-leg mechanisms (lower limbs) is to copy the movements of the musculoskeletal system existing in the nature of living beings. However, copying of bipedal biological systems is complicated because of some technical reasons such as the power consumption, the stability and the biological and mechanical complexity of legs [2].

According to physical interpretation, the mechanism simulating human motion can be introduced with different parts of the legs (conditional one-leg mechanism with partial motion and bipedal mechanism with full motion), wheels, rails etc.

Because of the object of study, the present overview is basically aimed to describe of different types of human lower-limb motion mathematical interpretations for bipedal construction.

The representation of the human locomotor apparatus depends on the tasks of the study and assuming complexity and precision of the model [3].

Therefore, according to the difficulty of measuring and simulating constructions, the human motion mathematical description can be divided into several groups of mathematical models [4]:

- Models based on the inverted pendulum principles, having up to 2 springs or dampers in it, describing simplified human motion models.
- Models of multilink mechanisms are usually more complicated and precise than the inverted pendulum mechanisms and able to describe the motion of the separate parts of the lower limbs (heels, ankles, knees, thighs, hips, pelvis, etc.).
- Models obtained with human motion measurements made during real experiments with human walking which are the most precise and provide close results to real human motion.

All examples of mechanisms and corresponding mathematical models presented in sections 1.1 – 1.4 describe the plane motion.

1.1. The simplest mechanisms: inverted pendulum

The first group of biomechanical lower-limb and pelvic constructions consists of models based on inverted pendulum models [5–7]. The best way to use inverted pendulum models is by providing energy transfer during construction motion.

The model with one spring is described in [8] and is illustrated in Fig. 1.1.

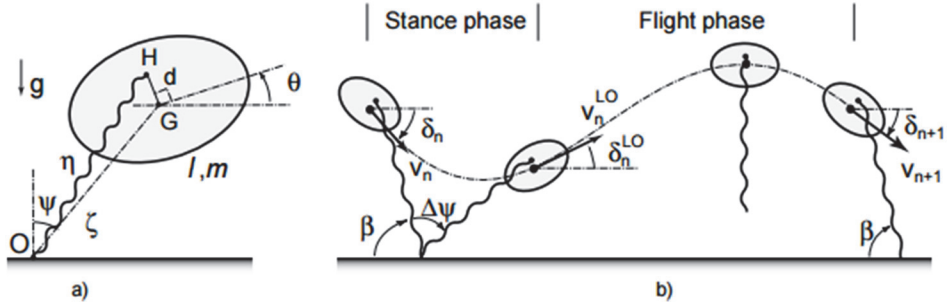


Figure 1.1. a) The hopping rigid body, b) stance and flight phases comprising a full stride [8].

The distance between point O and the point of spring-leg fixation on the hip can be calculated from Eq. (1.1):

$$\eta = \sqrt{d^2 + \zeta^2 + 2d\zeta\cos(\psi + \theta)}, \quad (1.1)$$

where d is the distance from the centre of mass (COM), point G to point H , where a massless spring leg is attached to the hip joint; θ is the pitch angle; ψ is the angle formed between the line joining foothold O to the COM and the vertical (gravity) axis, and ζ is the distance from foothold to the COM.

The kinetic energy of the body is:

$$T = \frac{1}{2}m(\dot{\zeta}^2 + \zeta^2\dot{\psi}^2) + \frac{1}{2}I\dot{\theta}^2, \quad (1.2)$$

where m is the body mass, I – moment of inertia.

The potential energy of the body is:

$$V_{tot} = mg\zeta\cos\psi + V(\eta(\zeta, \psi, \theta)), \quad (1.3)$$

where g is the gravitational acceleration, and $V = V_{spr}$ denotes the spring potential. Forming the Lagrangian $L = T - V$ and writing $\frac{\partial V}{\partial \eta} = V_\eta$, we obtain differential equations of construction motion in the phase of stance (equations 1.4 – 1.6):

$$\ddot{\zeta} = \zeta\dot{\psi}^2 - g\cos\psi - \frac{v_\eta(\eta)}{m\eta}(\zeta + d\cos(\psi + \theta)), \quad (1.4)$$

$$\zeta\dot{\psi} = -2\dot{\zeta}\dot{\psi} + g\sin(\psi) + \frac{v_\eta(\eta)}{m\eta}(\sin(\psi + \theta)), \quad (1.5)$$

$$\ddot{\theta} = d\dot{\zeta}\frac{v_\eta(\eta)}{m\eta}\sin(\psi + \theta). \quad (1.6)$$

The change of coordinates x_G, y_G , LO indicates the state of system at the moment of liftoff and angle θ in time is (equations 1.7 – 1.9):

$$x_G(t) = x^{LO} + \dot{x}^{LO}t, \quad (1.7)$$

$$y_G(t) = y^{LO} + \dot{y}^{LO}t - \frac{1}{2}gt^2, \quad (1.8)$$

$$\theta(t) = \theta^{LO} + \dot{\theta}^{LO}t. \quad (1.9)$$

More complicated models of inverted pendulums can have up to 2 damping elements. The simple models include concentrated in one point body mass (the COM) and a maximum of 2 variables (the COM) [4].

We observe a model simulating feet lifting during the running process [9] and having 2 springs. By the type of construction, this model can be related to spring-loaded inverted models (SLIP) (Fig. 1.2).

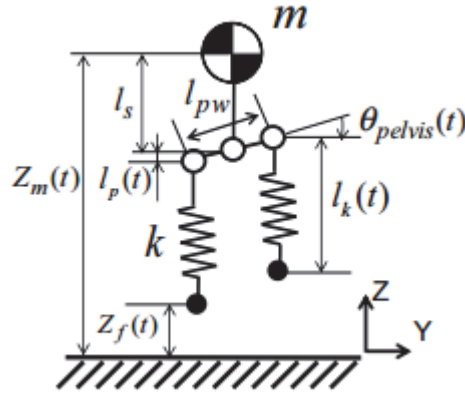


Figure 1.2. Mass-spring model [9].

The pelvic oscillation control method allows storage and release of energy in different phases of gait through the use of springs in the construction (Fig. 1.2). The axis of pelvic movements aligns with the axes of movements of the hips. The process of controlling natural frequencies of oscillation of the pelvis occurs, taking into account pre-known values of stiffness of the supporting leg and mass. Furthermore, pelvic tilt angles are selected such that the vibrations of the springs would be sufficient for the correct work of the mechanism. A

mathematical model of pelvic vertical motion, in the form of differential equations, can be written as:

$$m\ddot{z}_m(t) + k \left(z_m(t) - l_s - l_p(t) - l_k(0) \right) - mg = 0, \quad (1.10)$$

where m is the body mass; $z_m(t)$ indicates the vertical displacement of the mass; l_s is the distance between the pelvis and the body mass; $l_p(t)$ denotes the vertical displacement of the pelvis caused by its rotation; $l_k(t)$ is the leg springs length; k denotes leg stiffness; g is gravitational acceleration; t indicates time of stance phase.

The angle of pelvic tilt (θ_{pelvis}) can be found for 2 positions of the leg: touching the floor, and in the air (without touching the floor).

For the leg, touching the floor, the law of pelvic tilt angle change can be found as follows:

$$\theta_{pelvis}(t_{stance}) = A \sin(\omega t_{stance} + \varphi), \quad (1.11)$$

where A is the amplitude of pelvic rotation; ω is the natural frequency; t_{stance} is duration of the stance phase, and φ denotes the phase difference between pelvic movement and mass vertical movement.

For a lifted leg, pelvic tilt angle can be expressed as:

$$\theta_{pelvis}(t_{flight}) = \begin{cases} \frac{(\theta_{pelvis_{ini}} - \theta_{pelvis_{off}})}{T_{landing}} t_{flight}, \\ \theta_{pelvis_{ini}} \end{cases}, \quad (1.12)$$

where $\theta_{pelvis_{ini}}$ is the initial angle of the pelvis at landing; $\theta_{pelvis_{off}}$ indicates the angle of the pelvis at take-off; and t_{flight} is the time of the flight phase.

The higher equation in the figure bracket describes the pelvic tilt angles when the initial angles are not reached, while the lower equation applies when the tilt angle has reached the initial angle (Eq. (1.13)).

Since the movement of the mass has a trajectory of a parabola in the flight phase, the next landing time $T_{landing}$ is given by:

$$T_{landing} = \frac{2v_z}{g}, \quad (1.13)$$

where $T_{landing}$ denotes the time of landing, and v_z indicates the velocity of the mass in the vertical direction at take-off.

In spite of the visual simplicity of inverted pendulum and SLIP models, the observed models cannot realistically represent human lower-limb motion.

1.2. Multilink mechanisms imitating human lower-limb motion

The next group of mathematical models consists of multilink constructions simulating human lower-limb motion. Different types of biped mechanisms can be related to this group. In dependence on certain mechanisms, models of this type can be partial (only lower limbs) or full body [2].

The mechanism limited to only human lower-limb simulation is described in [10] and shown in Fig. 1.3.

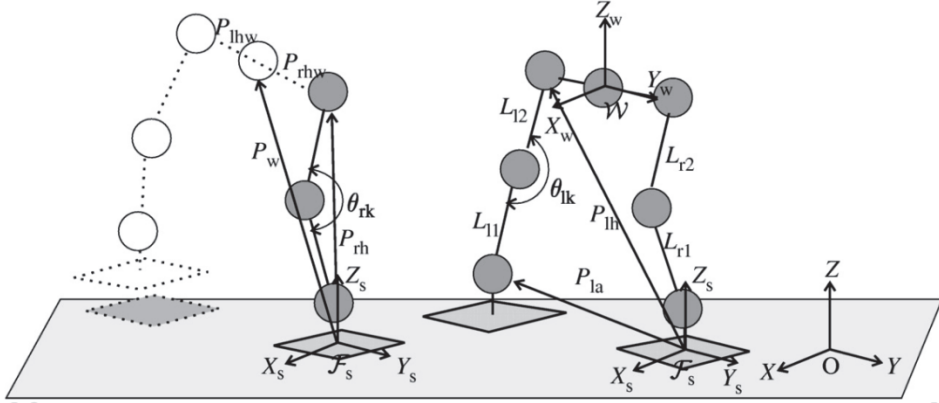


Figure 1.3. Coordinates and parameters [10].

The mechanical construction [10] shown in Fig. 1.3 has 16 DOF and consists of two identical legs (each has 7 DOF) and a waist (2 DOF).

Leg motion of the illustrated walking simulator can be divided into 2 parts: supporting and swinging phases. Working angles of rotation of the elements of construction are selected to be the same as real angles of bending of human lower limbs while walking. Supporting leg flexion angle of the knee is defined in advance. Conditional waist position adjustment depends on the chosen working mode (pattern) of the mechanical structure and is not determined before the start of simulator work.

To describe the position and orientation of elements of the mechanical construction in space, three different coordinate systems are used. The world coordinates system $O(X, Y, Z)$ has a zero reference point fixed to the ground, the coordinate system $W(X_w, Y_w, Z_w)$ takes account of the geometric centre of the conditional waist, and the zero point of the coordinate system $F_s(X_s, Y_s, Z_s)$ is located in the centre of the supporting legs.

The position of the hip of the leg staying on the ground, in the swinging phase, P_s , can be calculated as follows:

$$P_s = P_w + E_w P_{hw}, \quad (1.14)$$

where P_w is the vector of position of the waist in coordinate system W of the supporting leg (F_s); E_w is the identity matrix of the waist; and P_{hw} the vector of position of the hip in relation to the moving frame.

The distance between the supporting leg's hip and the foot, L_{ah} , is calculated as follows:

$$L_{ah} = \sqrt{L_{r1}^2 + L_{r2}^2 - 2L_{r1}L_{r2}\cos\theta_{rk}}, \quad (1.15)$$

where L_{r1} and L_{r2} are the lengths of the supporting leg's calf and thigh; θ_{rk} is the knee angle of the same leg.

The position of the supporting leg's hip by the vertical coordinate in relation to the leg coordinate system (F_s), P_{rhz} , is written as follows from Eq. (1.16):

$$P_{rhz} = \sqrt{L_{ah}^2 - (P_{rhx}^2 + P_{rhy}^2)}, \quad (1.16)$$

where P_{rhx} is x and P_{rhy} is the y position of the hip of the supporting leg's hip.

Then, the position of the swinging leg's hip relativ to F_s , P_{lh} , can be calculated mutually using the following equations (equations 1.17–1.19):

$$|P_{lh} - P_{la}| = \sqrt{L_{l1}^2 + L_{l2}^2 - 2L_{l1}L_{l2}\cos\theta_{lk}}, \quad (1.17)$$

$$|P_{lh} - P_{rh}| = P_{lhw} + P_{rhw}, \quad (1.18)$$

$$(P_{lh} - P_{rh}) \cdot O_{wx} = 0, \quad (1.19)$$

where P_{la} is the position of the swinging leg's ankle in coordinate system of supporting leg F_s ; P_{rh} denotes the position of the hip of the supporting leg; L_{lhw} indicates the pitch position of the left hip, L_{rhw} denotes the pitch position for the right hip relative to the coordinate system W , and O_{wx} is a vector of unity for the waist.

In [11], it is possible to see a multilinked mechanism representing the human body (Fig. 1.4).

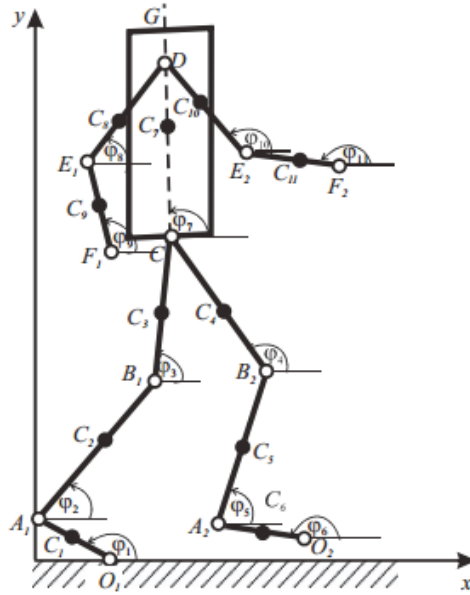


Figure 1.4. Construction of multilinked biped mechanism [11].

The mechanism consists of 11 rod-like links. To find the equations of link motion, the Lagrange equations of the second kind are used. The Lagrange equation of the second kind in common view can be found from Eq. (1.20):

$$\frac{d}{dt} \left(\frac{\partial L}{\partial \dot{q}_i} \right) - \frac{\partial L}{\partial q_i} = Q_i, (i = 1 \dots 11), \quad (1.20)$$

where q_i indicates the generalised coordinates; Q_i are the generalised non-conservative forces; $L = T - V$, where L indicates Lagrangian; T is the kinetic energy, while V is the potential energy.

After the equations of generalised coordinates change for each link were composed; kinetic and potential energies have been found using well-known formulas from theoretical mechanics. Then, substituting the equation of generalised force for the first link of the mechanism can be written as:

$$Q_1 = gl_1(m + m_2 + m_3 + m_1 n_1) \cos \varphi_1 + M_1 - M_2, \quad (1.21)$$

where g is the gravitational acceleration; m, \dots, m_3 are the masses of the links; n_1 indicates an additional coefficient; l_1 denotes the first link length; φ_1 is the angle between the ground and the first link, while M_1, M_2 are moments of friction forces.

Solving analytically with the use of Mathematica 6.0 software a system of 22 differential equations [11], the final laws of angles φ_2 and φ_3 changing in time are obtained and shown graphically (Fig. 1.5).

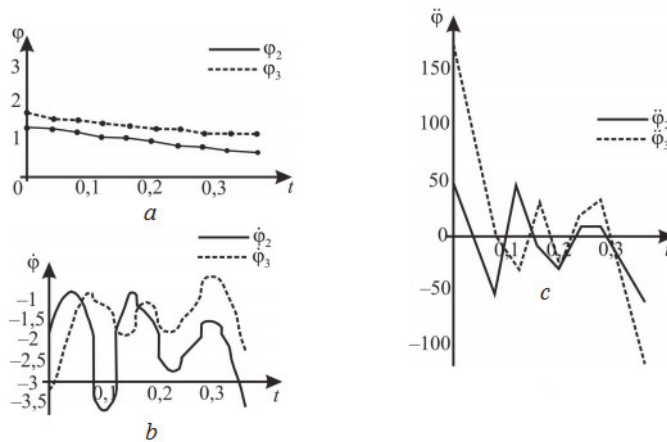


Figure 1.5. Dependence on time during the full period of a step (full cycle): a) rotation angle, b) angular velocity, c) angular acceleration [11],

where number 2 is related to the supporting leg shank; number 3 is related to the hip; the horizontal axis is measured in seconds, and the vertical axis in angles (degrees).

1.3. Mathematical models of human motion obtained from experiments

The last group of lower-limb mathematical models consists of models created on the basis of captured data from sensors during real experiments of human walking. Such models can simulate human walking much better than previous groups of models and can be used for many research purposes, but the main reason such technologies are not so widely revealed is the high cost of equipment and absence of the necessary number of patients (researches).

This class of mathematical models can be related to the captured data with subsequent mathematical models obtained with different measuring systems, such as optical systems [12–14], sensors installed on certain parts of human lower limbs [15,16], special force plates equipped by force sensors [17–19], trainers for lower-limb motion function rehabilitation [20,21], and so on.

A multilink mechanical model of the lower part of the human body is represented in [22]. The upper part of the body is shown schematically and simplified in the form of a rod, located geometrically centrally between the left and right hip joints (Fig. 1.6). Thus, the upper body position is determined only by the angle θ_L . More accurate mechanical models (anatomically) should display the distance between the hip joint centres and spinal joint outer surface, which ultimately leads to a dependence between the position of the pelvic joint and the upper body angle θ_P , which is a function of the angle of inclination of the upper body with respect to the pelvis in the frontal plane of angles θ_S and θ_L .

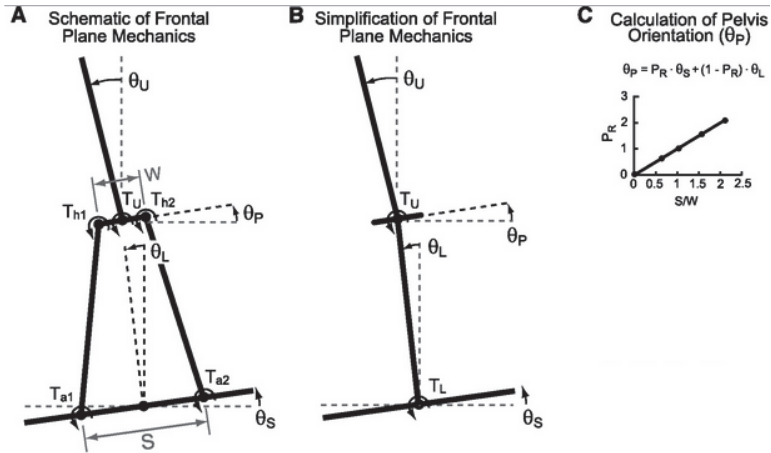


Figure 1.6. Construction of body mechanics: a) full model of introduced mechanism, b) simplified model; c) calculation of pelvis orientation [22],

where θ_U is the upper body orientation; θ_L is the lower body orientation; θ_P is the pelvis orientation; θ_S is the support surface tilt angle; P_R is the pelvic ratio that was used to define θ_P as a function of θ_S and θ_L and depends on the relationship S/W (S is the distance between heels, and W is the width of the pelvis).

The linear approximation of the dependance shown in the right part of Fig. 1.6 was determined by calculating an defined set of θ_P , θ_L , and θ_S angles at a given S/W and then fitting the Eq. (1.22) to this data set:

$$\theta_P = P_R \cdot \theta_S + (1 - P_R) \theta_L. \quad (1.22)$$

1.4. Identification of motion transfer from the human heel to the pelvis

Identification methods are based on work with input and output data. The principles of identification methods are described in section 4.1. This part of the overview is dedicated to the scientific research of human lower-limb motion based on identification methods and described in different types of literature.

The identification algorithm of locomotion introduced in [23] can be described as follows:

The entire process of model identification may be divided into two parts: a preliminary subsystem (PS) and subsystem (S_i) identification. The input signal for the PS model is the pelvis position in Cartesian coordinates, and output signals are pelvic rotations described in Euler angles. After identifying the PS model and estimating its output (rotations of pelvis by the trajectory of its movements), the modelling of 3 corrected pelvic rotations is possible. Then the obtained rotations after representation in exp-map play the role of the output

signals for S_i . The output signals for S_i are identified by Euler angles of corresponding to the chain (Fig. 1.7) presented in the form of an exp-map.

There are 5 submodels. The inputs for chains 1 to 3 are pelvic rotations in exp-map representations. The inputs for chains 4 and 5 are the lower neck rotations in exp-map representations. The different output for chains 1 and 2 are the bottom part of the legs. The output for chain 3 is lower neck rotations, and for chains 4 and 5 are the output signals at the end of the hands.

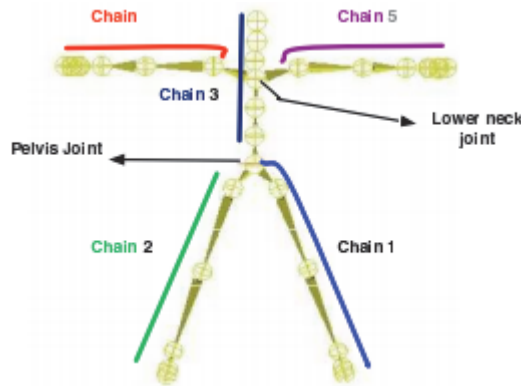


Figure 1.7. Description of the 5 open kinematic chains of human 3D articulated structure [23].

In [24] identification is used to find parameters of the knee tilt angle in the sagittal plane for an Intelligent Bionic Leg (IBL), constructed in Northeastern University (China). As input data, the values of torques of motors set at the hip are used. The output (ethalon) data is the angle of knee bending used. After the comparison of the few different models of identification was conducted, the best results were shown by an autoregressive model with external input (ARX model).

Work [25] describes modelling, identification and simulation of the inverted pendulum PS600 (model of laboratory equipment developed by Amira GmbH).

In [26,27] different aspects for the identification of motion transfer from the points touching the floor to the COMs are described for the sagittal plane. Based on the construction of a few simple SLIP elements [27,28], identification is described with the help of a transfer function.

In [29], common aspects for identifying experiments connected with motion capturing using markers are represented.

Another work [30] introduces possibilities for identifying artificial lower limbs (2 dynamic neural networks). After optimising and identifying using nonlinear identification and using the Quasi-Newton unconstrained optimisation

algorithm, the plots of the angles of knee rotations in the sagittal plane are close to real.

In [31], the method to obtain linear transfer functions between muscle activation and joint angles of cats is shown.

In addition, [32] is about exoskeleton (BLEEX) with a description of identification for motors torques installed in simulated exoskeleton ankles, knees, and hips. Results are similar enough for a series of experiments and can be estimated as sufficient.

Of particular interest is [33], in which the transmission work is exchanged with transfer functions for 3 different combinations. As a result, the key parameters of motor work were found, such as angular acceleration, torques, and so on, for bipedal robot construction offered by the authors.

The main conclusion that can be made is that identification methods for creation of a mathematical model of the mechanical heel-pelvis system in the frontal plane, as described in Chapter 2 has not yet been described in scientific literature.

1.5. Experimental and analytical approach

The experimental and analytical approach to transfer motion from the heel to the pelvis of a human in the modelling of the process of bipedal walking is used in this work.

The experimental approach can be expressed as follows: we work with the input and output signals obtained from real experiments. To obtain the input signal, the results of 2 different experiments of human walking have been chosen. Finally, the curves of heel displacements from both experiments were combined and averaged. As output signals curve, we used the displacements obtained from the processed accelerations and angular velocities received from the IMUs mounted on the plate of the prototype, simulating human pelvic motion within 27 independent experiments (Chapter 3).

The principle of the black box as a mechanical system with unknown parameters between input and output signals is used to describe the work of the mechanical construction (section 2.1) of the experimental prototype. The resulting differential equation of motion of the second kind, hidden in the black box, means the motion of the system transferring movements from the input (motion of the heel) signal to the output (motion of the pelvis) signal. Thus, the analytical component used in this PhD thesis approach is based on the use of the black box and working with differential equations.

As a working tool, the application System Identification Toolbox (one of the MATLAB toolboxes) was used. The toolbox functionality allows using the identification method to determine the desired differential equation.

The proposed mixed experimental and analytical approach has not yet been described in scientific literature for identifying mechanical heel-pelvis system parameters or for finding its mathematical model (differential equation hidden in the black box).

Chapter 1. Results and discussion

Based on the survey of mathematical models of lower-limb mechanisms discussed in the first part of Chapter 1 (sections 1.1 – 1.3), the mathematical models have been divided into 3 parts:

- 1) Models based on the inverted pendulum mechanisms, having up to 2 springs or dampers in it, describing simplified human motion models.
- 2) Models of multilink mechanisms are usually more complicated and precise than the inverted pendulum mechanisms and able to describe the motion of the separate parts of the lower limbs (heels, ankles, knees, thighs, hips, pelvis, etc.).
- 3) Models obtained with human motion measurements made during real experiments with human walking which are the most precise and provide close results to real human motion.

The main goals of this work are as follows:

1. Modelling and simulation of mechanical heel-pelvis system motion in the frontal plane.
2. Creation of a mathematical model of the motion of the mechanical heel-pelvis system, based on identification methods.

According to the goals of this work, the scientific objectives are as follows:

- Creation of experimental prototype construction, simulating pelvis motion during walking within experiments, taking into account later studied movement use in the therapeutic simulator.
- Creation of an algorithm for IMU data processing considering the possibilities of measuring systems, construction of an experimental prototype, and the action of damping elements. Statistical evaluation of results ((Fisher test (F -test) and Dixon's test (Q -test)).
- Identification of damping and frequency coefficients of a mechanical system heel-pelvis in the frontal plane for both axes.
- Development of a mathematical model of the motion of the mechanical heel-pelvis system, based on identification methods. Determination of transfer functions and differential equations of motion, describing the mathematical patterns between input and output signals.

The main steps of conducting this PhD thesis are shown in Fig. 1.8.

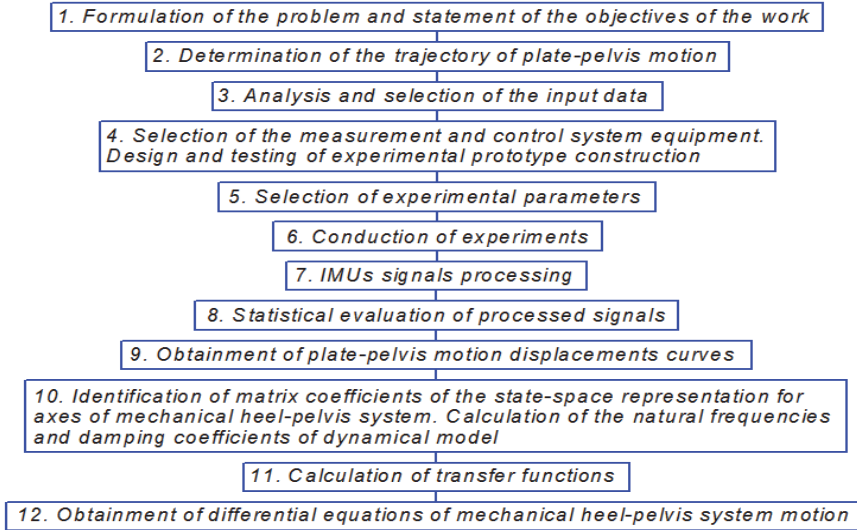


Figure 1.8. The main steps of PhD work.

Step 1 is described in the introduction section. The determination of the trajectory of the plate-pelvis motion (Step 2) will be chosen as the possible motion for future construction of a complex medical prototype for human lower-limb motion restoration to make it more effective. The next step is selection of input data (Step 3). The input data (vertical heel displacements) will be obtained from experiments capturing human walking parameters using IMUs [53,54]. Selection of the measurement and control system equipment (Step 4) should be made according to the necessity of the experimental prototype (Chapter 2). After that, the experimental parameters (Step 5) will be chosen, which include three combinations of angle α (Fig. 2.3) and additional loads where weights are defined as maximal with no influence on the motion of the plate pelvis, and 3 durations of stepper motor steps were selected in advance, while programming the stepper motors (Section 3.1). Then, the experiments with the prototype will be conducted (every experiment began with calibration of IMUs using software) (Step 6) to attain the practical motion of the plate pelvis. After that, the signals of IMUs will be processed by the algorithm described in Section 3.2 (Step 7). For statistical evaluation and the numerical parameters of signals, some mathematical operations (Appendix 3) and statistical tests (F -test in Appendix 2 and Q -test in Appendix 4) will be completed (Step 8). Next, after averaging the curves of the full one-step cycles of the experimental prototype, the shapes of displacement curves will be improved using MATLAB standard commands and a spline with different numbers of points (section 3.3) (Step 9). Afterwards, the curves of displacements will be obtained, and the identification of dynamical systems for both axes will be made. For the input and output data, the heel displacements

from the real experiments are used as input signals, and the plate-pelvis displacements will be used as the output signals. The dynamical system for each axis of plane motion will be designed consisting of one input, the black box, and output. The logical end of Step 10 will be calculating the coefficients in matrices of state-space representation and the damping and natural frequency numerical values found with the computational enumerative technique and integration from Newton's equation ($f(t) = \ddot{u} + 2n_d\dot{u} + f^2u$) (where u is input signal, \ddot{u}, \dot{u} are derivatives of the input signal, f is the natural frequency and n_d is the damping coefficients). Using Eq. (4.31), the transfer functions for dynamical systems of both axes will be found (Step 11). Finally, using the Laplace inverse transform, the final differential equations of mechanical heel-pelvis motion for both axes will be found (Step 12).

Apart from the statistics described in the Introduction section, the statistics of separate human pelvic disturbances are of particular interest. The question to be discussed can be formulated as 'What are the descriptive statistics for human pelvic disturbances and how useful is the scientific research related to this work?' Since the question is very vast and deserves a separate study, it is possible to restrict with only small part of it on example of few diseases. To find the answer to discussive question, we have to understand what types of illnesses can be successfully treated using physical therapy (mechanotherapy). According to the existing methods of treatment, rehabilitative gymnastics with assistance from a therapist are used in late rehabilitation of motion functions in cases of some pelvic bone fractures and some dysfunctions or traumas of the pelvic muscles [34,35]. According to the official statistics, one of the most often traumas in sports is the groin strain. This trauma is approximately 10% to 11% of all injuries in soccer and ice-hockey [36]. The frequency of pelvic bone fractures is 3% to 8% of all the traumas of the human MSS [37] and the incidence of pelvic fracture is 14.97/100000 persons per year [38]. The age group of adults most predisposed to such types of traumas [39,40] comprises people older than 80 years (0.00052% from the total population). The group of people aged 65 to 80 years (0.00021%) is in second place, while the third place comprises the group of people aged 18 to 64 years (0.00017%). Looking at genders, women suffer from pelvic fractures more often than men (53.6% against 46.4%) [39]. In spite of the mentioned directly pelvic diseases and traumas, there are illnesses leading to full (or partial) impossibility of human lower-limb motion abilities, some of which could be successfully treated with the help of medical facility and pelvic motion (stroke, full or partial paralyses, and so on). There are many factors influencing the quality of recovering motion abilities, such as the quality and functionality of medical trainer, experience of the therapist (orthopaedist, physiotherapists), specific particularities of the disease (or complex of diseases) and its severity, the state of muscles, bones, and joints, etc. That is why it is hard to estimate the benefits of use of the represented pelvic motion. The high efficiency of the use of rehabilitation trainers was approved on example of Lokomat in cases of subacute stroke [41] and multiple sclerosis [42,43].

2. DESIGN OF EXPERIMENTAL PROTOTYPE CONSTRUCTION AND MEASUREMENT SYSTEM

The main task of this chapter is describing the experimental prototype design aimed to obtain output signals.

An additional condition is the use of accelerometers and gyroscope as IMUs. The installation of IMUs at the human pelvic, in reality, is quite problematic because a large part of the hipbone is covered with muscle and/or fatty tissues (fat and muscle tissues contract and fluctuate during walking, causing substantial errors in the measurements). The decision of this problem is modelling an experimental prototype – a mechanical system for simulating the plane movements of a sitting at the saddle human pelvis and calculating its main parameters (acceleration, velocity, displacement) has been accepted.

All systems of the designed prototype can be functionally divided into 3 separate parts:

- 1) The mechanical construction transmits drive signal movements from the heel to the pelvis (imitation of motion transmission from heel to pelvis).
- 2) The system of the prototype simulates movements of the heel while walking.
- 3) The measuring system captures accelerations and angular velocities of the plate.

The mechanical construction (section 2.1) was assembled, and experiments were held by the author personally. The parts touching the stepper motor control (section 2.2) and the IMUs signal processing (section 3.2) were made together with MSc student Anton Verchenko and have already been described in [44]. The measurement system used in this work and in [44] was created by MSc student Aleksander Lazarev during his practice work.

2.1. The mechanical construction of the experimental prototype

The simplest method for human lower-limb simulation is connected with replacing the human lower-limb functional parts with mechanical elements. Representation of bones as rigid body elements, joints as hinges, and springs as muscles is a standard solution in such constructions [45,46].

The mechanical construction of the prototype schematically shown in Fig. 2.1 consists of metal elements (profiles, plates, frames, fasteners, bearings, gear elements, and springs), wooden elements (the stick to lift the prototype to the required height and fix it), sensors, and other types of elements. To determine the size of the prototype, real intertrochanteric distance of adult men (32 cm) [47] and the horizontal angle of the pelvis during human gait are used (difference in elevation between the thighs; 3° – 5° is shown in Fig. 2.4) [48].

Damping elements were chosen with sufficient damping and stiffness characteristics.

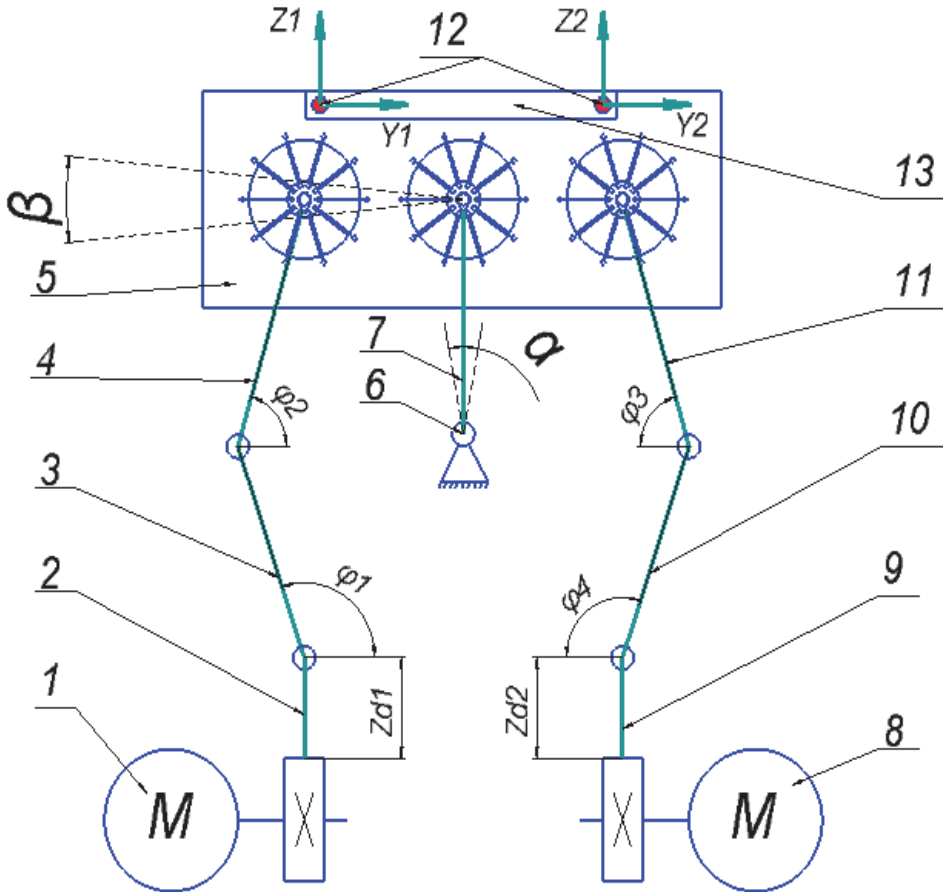


Figure 2.1. Elements of experimental prototype, where (1), (8) are stepper motors; (2), (9) are rack gears (link-ankles); (3), (10) are compensating plates (link-knees); (4), (11) are connecting plates (link-thighs); (5) is the upper plate (link-pelvis); (6) is a supporting bearing; (7) is a connecting plate; (12) are the IMUs; (13) is the additional loads; y and z are directions, and α and β are angles of plate motion; z_{d1}, z_{d2} are directions of vertical linear motion; ϕ_1, \dots, ϕ_4 are angles of links rotations, y_1 and z_1 are axes of IMU number 1 and y_2 and z_2 are the axes of IMU number 2, which were calibrated using special software being on the plate-pelvis situated horizontally.

Although calibration was made in the horizontal position of the plate-pelvis, the starting point of each experiment was chosen as a maximally lifted right leg.

A short description of the experimental prototype follows: when motors 1 and 20 launch (accepted numeration is the same as in Appendix 1, where experimental prototype work is described in detail), rack (2) starts to go up, plate (3) begins to rotate counterclockwise, and plate (4) does not change its position in

height. At the same time, rack (9) goes down and plates (10) and (11) stand in a row. The position of plate (11) gets higher, and plate-pelvis (5) turns left. After the angle of plate-pelvis rotation exceeds a critical angle, plate (5) goes to the left side and rotates around hinge (6), until supporting plate (7) will not reach its final value. Described motion simulates left leg lifting (Fig. 2.2(c)). After that, the right leg begins to lift and the left leg goes down in the same way (Figure 2.2(a)). At the midpoint of the left or right leg lifting, plate-pelvis (5) is in the horizontal position (Fig. 2.2(b)). The second half step occurs in a similar manner, but the left foot goes down, and the right leg goes up.

Three combinations of angles are needed for different models of the experiment. In addition, load (13) is also used in various models of experiments (Chapters 3 and 4 of this thesis).

In Fig. 2.2, an experimental prototype is shown in different work positions.

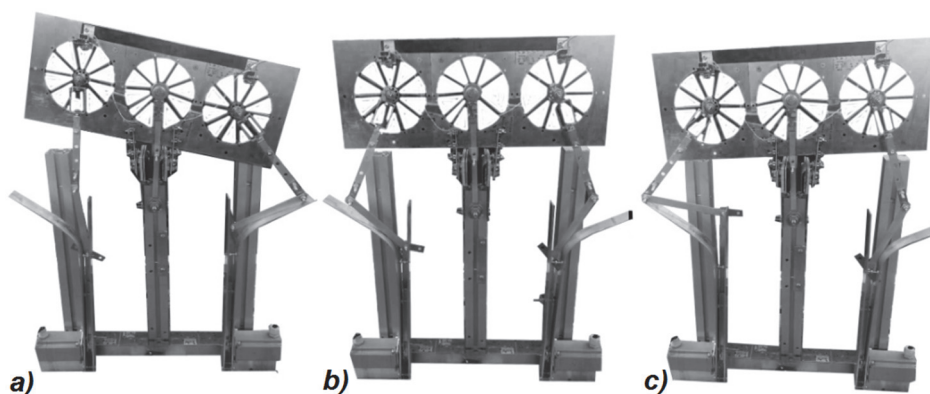


Figure 2.2. Work positions of experimental prototype; a) lifting of the right leg, b) two-leg supporting phase; c) lifting of the left leg.

The realised logic of the experimental prototype (the heel is lower, the corresponding thigh is higher) coincides with the real movement of the pelvis while walking and is shown in Fig. 2.4 [48]. Additional description of pelvis motion during walking can be found in [49].

The explanation of experimental work in detail can be found in Appendix 1.

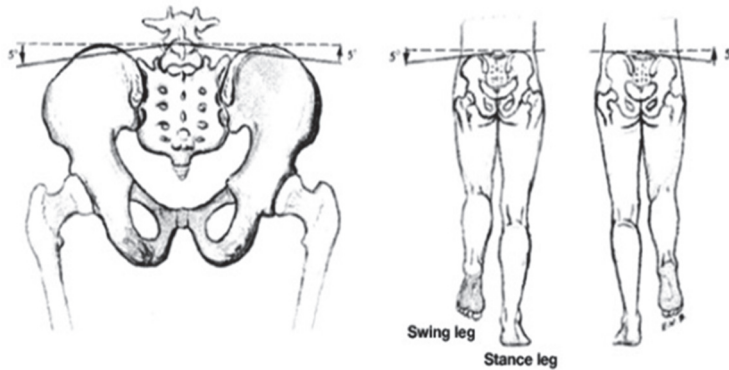


Figure 2.4. Pelvic rotations in frontal plane during walking [49].

Construction with very similar principles of work and design has been described in [50].

2.2. System of link motions generation

For reducing the size of the engines, driving the links of the mechanical construction of the prototype, and smoother work of motors, it was decided to use stepper motors, giving relatively high torques at low frequencies. Because there were available stepper motors from the company Optimum, stepper motor control systems from the company National Instruments (drive, controller, and connecting cables), and software from Labview, it was chosen to use the standard solution offered by National Instruments for stepper motor control (Fig. 2.5).

As a result we have got that system for control of links movements consisting of a drive stepper motors National Instruments MID-7602, stepper motor controller NXI 7332 and 2 identical stepper motors Optimum, connecting cables, software Labview.

To find data of the heel vertical displacements, a short overview of the scientific literature has been made, according to results of which 4 curves of displacements of the heel were chosen.

While [51] has some curves of heel displacements, it is based on a more biomechanical approach to walking than a mechanical approach.

Another curve of foot vertical displacements in time was captured with wearable sensors and discussed in [52], but the sensors were not installed on the heel, but on the side of the foot. Therefore, the averaged input data for the experimental curves of the heel vertical displacements captured with accelerometers [53,54] was chosen.

One step duration in time is 1,2 s. Two identical heel step durations for the right and left legs were defined as shifted from each other in time of 0,6 s (Fig. 2.5).

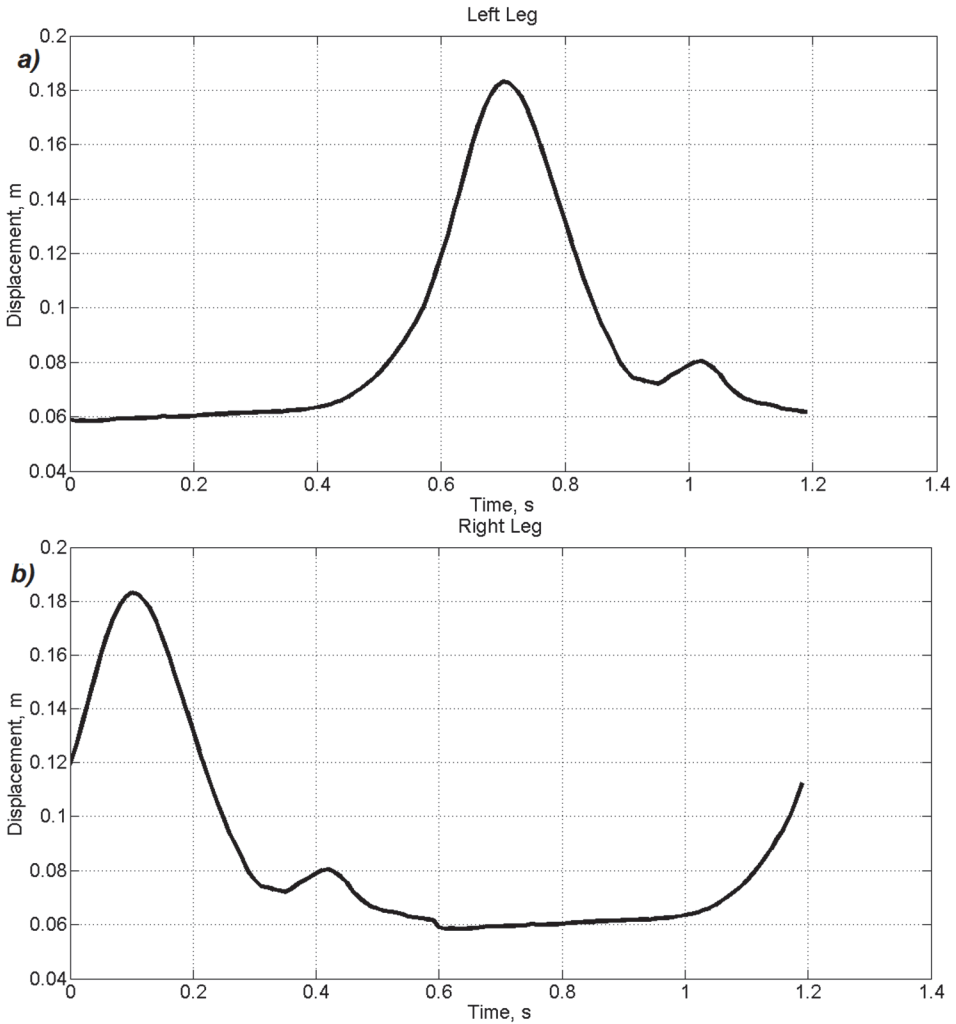


Figure 2.5. Human left and right heels displacements during walking captured with and accelerometers [53,54] as input signals; a) displacements of the left heel; b) displacements of the right heel.

After that, values of vertical displacements that describe the trajectory of heels using stepper motors were selected. Such values coincide with human real heel movements. Then, it was decided to program 24 step segments of 10 steps in each to describe the trajectory of the heel. One complete revolution of the output shaft of the motor is equal to 5000 steps or 0,05 m of the rack linear displacement (Numbers (2) and (9) in Fig. 2.1). Selected values of steps for each of the separate 240 steps were determined to repeat the profile of heel motion.

Selection of parameters for stepper motors was made using the software application Motion Assistant from National Instruments. It allowed the simultaneous running of 2 stepper motors and the ability to select profile programming speed movement parameters as well as the direction of the conventional point (straight line, arc, S-shaped movement) and character reference motion (absolute or relative). Experimental choice of the minimum time duration for each step was connected with such durations of the stepper motors for which a discrete profile is fully described and the motor returns to the starting point without shifting. Finally, 3 different models of time step durations for future experiments: 0,021 s, 0,025 s, and 0,035 s were selected. The total time for each cycle of the experimental prototype (simulation of full human step) is as follows: 48,825 s for the regime with the duration time of one step 0,021 s; 52,545 s for duration of step time 0,025 s; 61,845 s for duration of step time 0,035 s.

Then, the movement of a certain point in a straight line and a programmable motion profile as trapeze were chosen. After this we continued with the selection of parameters for acceleration, deceleration and constant movement of stepper motors.

Picking up speed motor parameters for each step, using the software Labview, the block-diagram of the program was compiled to control stepper motors (Fig. 2.6).

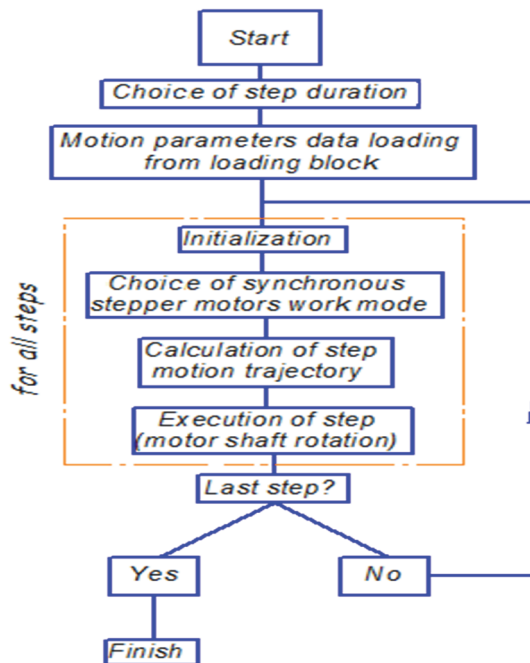


Figure 2.6. Block-diagram of stepper motors control,

where 1) block for loading parameters of steps from files, 2) initialisation of motors, 3) element of simultaneous control of 2 stepper motors, 4) calculation of motor revolutions and the element that unites and strengthens by 1000 times the speed parameters, 5) direct execution of movements, 6) block for saving speed parameters and step parameters in files.

2.3. Measurement system of experimental prototype

This work is a continuation of scientific work aimed to create a mathematic model of motion for the human lower limbs with IMUs. In [54,55], human steps during walking were measured. Thus, IMUs were chosen as measurement units [56,57]. Finally, the measuring system consists of controller Arduino Nano v.3 and 2 IMUs of model MPU 6050. IMU MPU 6050 contains a 3 DOF Micro-electro Mechanical System (MEMS) accelerometer and a 3 DOF MEMS gyro in a single chip. The Arduino NanoV3 (Fig. 2.7) is a board based on the Atmega328 chip.

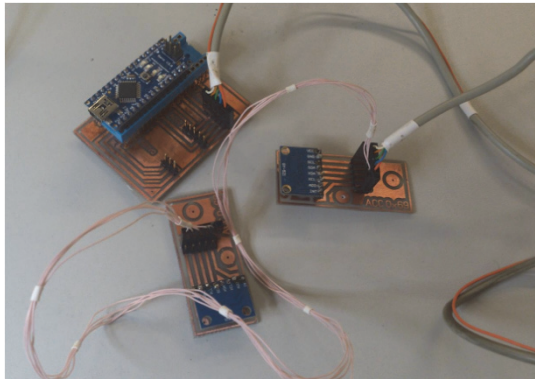


Figure 2.7. Measurement system in assembly.

After the measurement system was assembled, it was necessary to write a program for the fixation of measurement data. As a result, a program in MATLAB was written. It collects measurement data into the com-port with frequency 17,7 Hz and draws plots in real time.

For description of plane motion, we use accelerations by y -axis and z -axis and rotation velocity around the x -axis (Fig. 2.1).

In order to establish the effect of the delay controller Arduino NanoV3, a program was written, sending the symbol from the controller to the MATLAB environment and recording the symbol return time from MATLAB back to controller. As a result, the average time of symbol exchange is 0,011 s. From this, it follows that the controller includes a delay period between the previous and subsequent measurements of the IMU without affecting acceleration values obtained with inertial sensors.

2.4. Completed tasks creating an experimental prototype: evaluation of obtained results

During the design of the experimental prototype, the following tasks have been resolved:

- Designing the mechanical construction of the experimental prototype in 3D CAD (computer-aided design) using the software package SolidWorks.
- Selection parameters of steps to repeat the trajectory of the original heel profile discrete movements were determined.
- Creating a block-diagram for simultaneous control of stepper motors using the software package Labview.
- Assembling and testing the experimental prototype.
- Assembling and programming the measurement system.
- Writing the program for obtainment of visible results of accelerations and angular speeds in the real-time model in the software package MATLAB.

Chapter 2. Results and discussion

The main result of Chapter 2 is the creation of an experimental mechanical construction, transmitting motion from the heel to the pelvis of an individual person, and creation of the measuring system, which allows fixing the acceleration and angular velocity of the captured motion of the pelvic plate at two points (output signal for subsequent identification), considering the subsequent use of such construction for therapeutic purposes.

The logical question appearing after Chapter 2 is about the difference between the designed pelvic motion working as part of a medical complex for human motion ability rehabilitation and the real work of the pelvis during walking.

As a result of designing and assembling an experimental prototype, it can be concluded that its work differs from the real plane movements of the pelvis with the following parameters:

- Lack of vertical displacements of the centre of masses of the plate in simulation, while in reality, during walking it is up to 5 cm [58].
- Two angles describing the motion of the plate (Section 2.2) are experiencing a much greater influence on inertia elements than the hip joint. In other words, changes occur at the designated angles, making walking smoother than it does in the case of the experimental prototype.
- The legs of a real person are not attached to the pelvis at right angles [59].
- Friction forces in the joints of the experimental prototype exceed the friction in the human MSS.

3. EXPERIMENTS, SIGNAL PROCESSING, AND OUTPUT SIGNAL DETERMINATION

3.1. Selection of experimental parameters

After design, assembly, and testing of a prototype, there were experimental measurements made of the plane motion of the plate, simulating the pelvis to acquire the output curves of the displacements. There are 3 different changing parameters during experiments: angle of plate-pelvis rotation on the supporting bearing, duration of steps of the stepper motors in time, and additional loads, which were defined. Additional load and angle of rotation on the supporting bearing can be seen in Fig. 2.1. The principles of the choice of step durations of stepper motors are described in section 2.2. The total number of combinations of experiments is 27 (3 angles x 3 additional loads x 3 durations of steps). Numerical data of selected parameters is shown in Table 3.1 [44,56,57].

Table 3.1. Selected parameters of experiment.

Number of IMU	Marking of parameter	Value (°)	Marking of parameter	Value (N)	Marking of parameter	Value (s)
1	$\alpha 1$ (angle)	4,8	w1 (weight)	16,54	$t_m 1$ (duration of step)	0,021
1	$\alpha 2$ (angle)	6,4	w2 (weight)	13,44	$t_m 2$ (duration of step)	0,025
1	$\alpha 3$ (angle)	8,0	w3 (weight)	9,08	$t_m 3$ (duration of step)	0,035
2	$\alpha 1$ (angle)	4,8	w1 (weight)	16,54	$t_m 1$ (duration of step)	0,021
2	$\alpha 2$ (angle)	6,4	w2 (weight)	13,44	$t_m 2$ (duration of step)	0,025
2	$\alpha 3$ (angle)	8,0	w3 (weight)	9,08	$t_m 3$ (duration of step)	0,035

After the experiments were conducted, the accelerations for axes y , z , and angular velocity for the rotation axis x were obtained with 2 IMUs.

It was decided to sign the experimental parameters as $y(z, g_x)(1 \dots 2)$, $\alpha(1 \dots 3)$, $w(1 \dots 3)$, $t_m(1 \dots 3)$, where $y(z, g_x)$ are names of axes y , and z we measure accelerations, g_x is the rotation over axis x we measure angular velocity, numbers (1 ... 2) indicate the number of sensor we used, $\alpha(1..3)$ is the current angle of rotation of the supporting bearing, $w(1 \dots 3)$ denotes current load value, $t_m(1 \dots 3)$ is the current duration of the step according to Table 3.1. For example, experimental mode $\alpha 2 w 2 t_m 2$ observing later is the next combinations of parameters: $\alpha 2$ is the angle $6,4^\circ$, $w 2$ denotes weight 13,44 N, and $t_m 2$ indicates duration of step in time: 0,025 s.

3.2. Experimental data processing

Straight integration of experimental accelerations does not give adequate results because of the effect of springs and damping elements on plate-pelvis motion and the substantial noise of the signals. That is why a special algorithm was needed to process the signals of IMUs.

Considering the angles of rotation and distances between the centre point of the plate-pelvis and the measuring points in which IMUs are installed, it is possible to assume the approximate values of the final displacements for every experimental mode.

Finally, the only algorithm levelling the effect of the springs has been found and represented in this section. The algorithm can be divided into a few steps to ensure every experimental mode attains the final experimental curves (output signals):

- 1) Preparation of IMU signals.
- 2) The choice of low-pass Butterworth filter for accelerometer signal filtering.
- 3) Averaging signals of IMU accelerometers to simplify data processing and evaluate the accelerometer similarity results (Appendix 3).
- 4) Use of complimentary filter to exclude the effect of angle floating.
- 5) Assignment of gravity forces acting on IMUs during experiments.
- 6) Obtaining filtered accelerations without gravity forces.
- 7) Choosing a method of integration to obtain velocities and displacements from filtered accelerations without gravity force.
- 8) Evaluation of results of the unprocessed and filtered signal comparison (F -test, Appendix 2) and determination of the outliers from the obtained maximal values of displacements (Q -test, Appendix 4).

In order to make the acceleration corresponding to the planned work of the prototype, it was decided to align the acceleration along the horizontal axis. To do this, all the elements of acceleration arrays were summed and the overall rate of accelerations that were shifted from the horizontal axis was obtained. Then, the overall rate was divided by the number of measurements (elements of acceleration array), and the resulting quotient of the division was subtracted from all elements of the array. Some measurements from the initial data were eliminated (filtering curve in Fig. 3.1 is situated higher or lower than the average values) to gain more logical signals because it is hard to understand how the experimental plate moves (up or down). Preparing signals for every experimental mode, we reduced the influence of the effect of the springs on the unprocessed experimental data. It can be considered improvement of the IMUs data processing introduced in [44,56,57]. As a result, after using the Butterworth low-pass filter, we obtained the data shown in Fig. 3.1.

Calibration of the initial measurements is connected to the work with unprocessed signals. It can be reached with the use of the Butterworth filter, which eliminates the peaks of initial accelerations and removes the time trends.

Another aspect of calibration is connected with the calibration of IMU6050 with specialised programs for calibration.

The need for some additional filters for signal processing is approved with results of the F -test (Appendix 2).

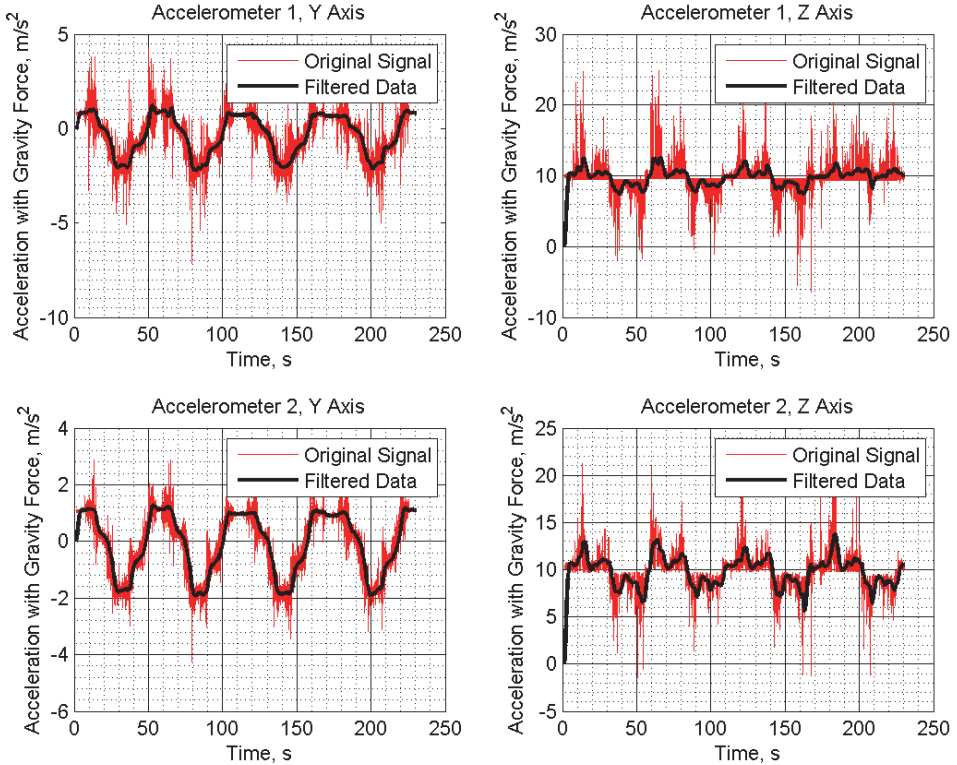


Figure 3.1. Acceleration with Gravity Force for experiment $a2w2t_m2$.

The low-pass Butterworth filter was chosen after compilation and testing of various kinds of filters created in the DSP System Toolbox [60–63].

The parameters of the designed filter are infinite impulse response (IIR), low-pass second order discrete Butterworth filter, stable, and without linear phase. In addition, the normalised frequency value at 3 dB point is 0,02, and the gain is equal to 0,0009. The output gain is 1, and the transfer characteristic of the Butterworth filter is the following:

$$H(z) = \frac{1+2z^{-1}+z^{-2}}{1-1,9112z^{-1}+0,9150z^{-2}} \quad (3.1)$$

Figure 3.2 represents the magnitude and phase response plot of the designed filter.

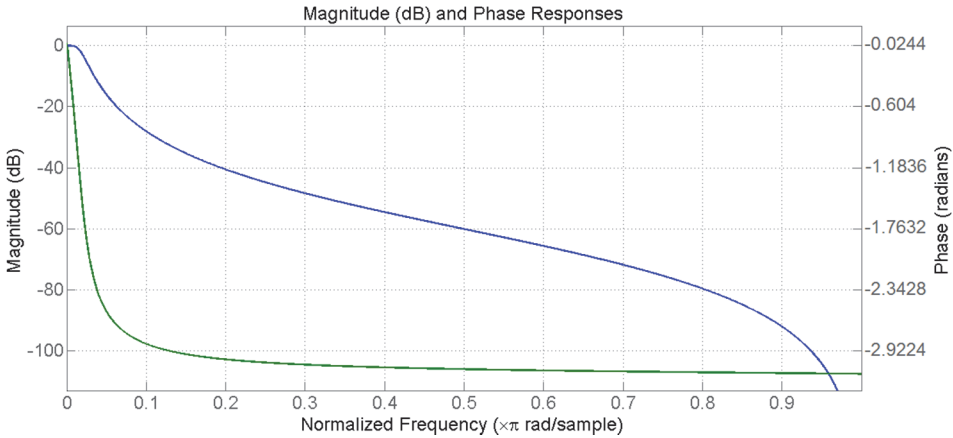


Figure 3.2 Magnitude and phase response of designed filter.

After accelerations were aligned on an axis, it was necessary to calculate how good the mechanical prototype has been assembled and tested.

Since the obtained discrete accelerations were very noisy, it was difficult to evaluate the accelerometer data. Therefore, it made sense to evaluate the curves of the filtered data. Furthermore, as a comparative standard, an additional middle curve, whose coordinates were received from adding the filtered first and second IMU and dividing by 2, were obtained (Fig. 3.3).

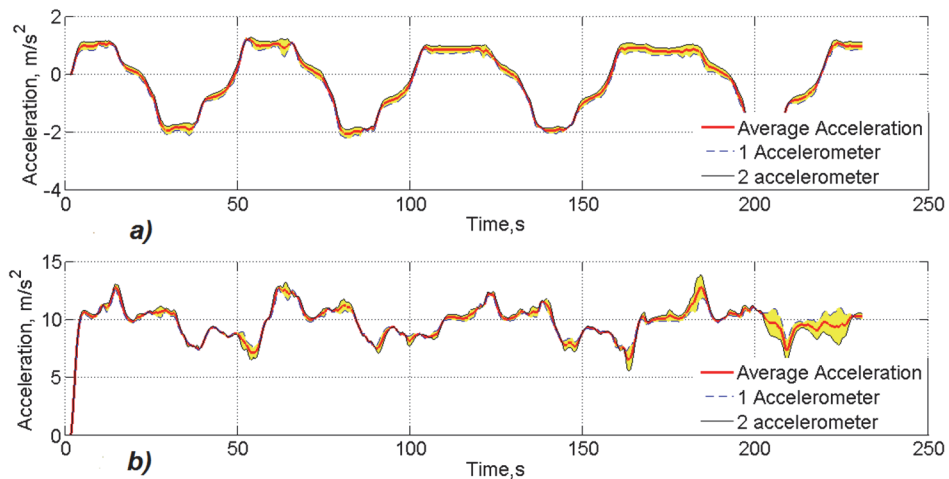


Figure 3.3. Comparison of filtered data of both IMUs accelerometers with averaged acceleration for experimental mode $a2w2t2$ for: a) y-axis, b) z-axis.

Blue dotted line marks filtered acceleration curve for the first IMU accelerometer, and the black solid line represents the filtered acceleration curve of the second IMU accelerometer, while the red solid line is the average curve of the filtered accelerations, and yellow area refers to the difference between the measurements of the first and second IMUs accelerometers.

Parameters of the calculated area (marked in yellow, the numerical difference between the accelerations obtained with 2 IMUs) for axes y and z for every experimental mode is represented in Appendix 3.

Since data of accelerations for both sensors should be identical, Table A3.1 (Appendix 3) numerically describes defects in the design and assembly of the prototype. Some of these defects are:

- Possible errors in the installation IMUs on the plate,
- Incomplete relevant elements of the mechanical system of the prototype,
- Gaps in the joints,
- Incomplete fixation of the plate in the frontal plane. Full fixation of the plate in the frontal plane with bearings was not possible due to the occurrence of friction forces between the plate and bearings.

In the analysis, the biggest difference between the filtered acceleration sensors and the curve of averaged filtered acceleration is in those places where the angle between the filtered data and the horizontal axis (absolute zero) is the least. In fact, these places represent a break between running separate experiments and should not be taken into calculations of deviations. Thus, data of deviations shown in Table A3.1 (Appendix 3) mean the maximum possible deviation from experiments that were not really achieved.

For greater consistency and to reduce the amount of data to be processed, we continue to process signals only for the curve of average values of the filtered accelerations.

Then, it was necessary to determine the gravity force for every measured axis and experimental mode to subtract it from the averaged curves shown in Fig. 3.3. After that, we obtained curves of accelerations that we can integrate to obtain the curves of linear velocities and displacements.

It is worth noting that the coefficients of gravity forces would be impossible to find with only accelerometers. It is necessary to combine the accelerometers and gyroscopes for matching measured angles with accelerations to determine the tilt of the plate and to see how the gravity coefficient is distributed along the y (horizontal axis) and z (vertical axis) axes.

To compensate for drifts in angles, the complementary filter is used. It plays the role of a compromise between the data collected from the accelerometer and gyroscope. The accelerometer is under the influence of external forces that do

not affect the gyroscope. Conversely, the gyro drift has no influence on the accelerometer [64,65]. The complementary filter eliminates the drift angle of up to 10 degrees. The equation of the complimentary filter calculation is:

$$\beta(i) = W \cdot (\beta(i - 1) + G_r \cdot dt) + (1 - W)(Acc \cdot dt), \quad (3.2)$$

where W is the weight coefficient (this mode is 0,98); β is the angle; G_r denotes the gyroscope data for a small period of time, and Acc is the acceleration value [44,56,57].

Results of the complimentary filter in the case of the chosen experimental mode are shown in Fig. 3.4.

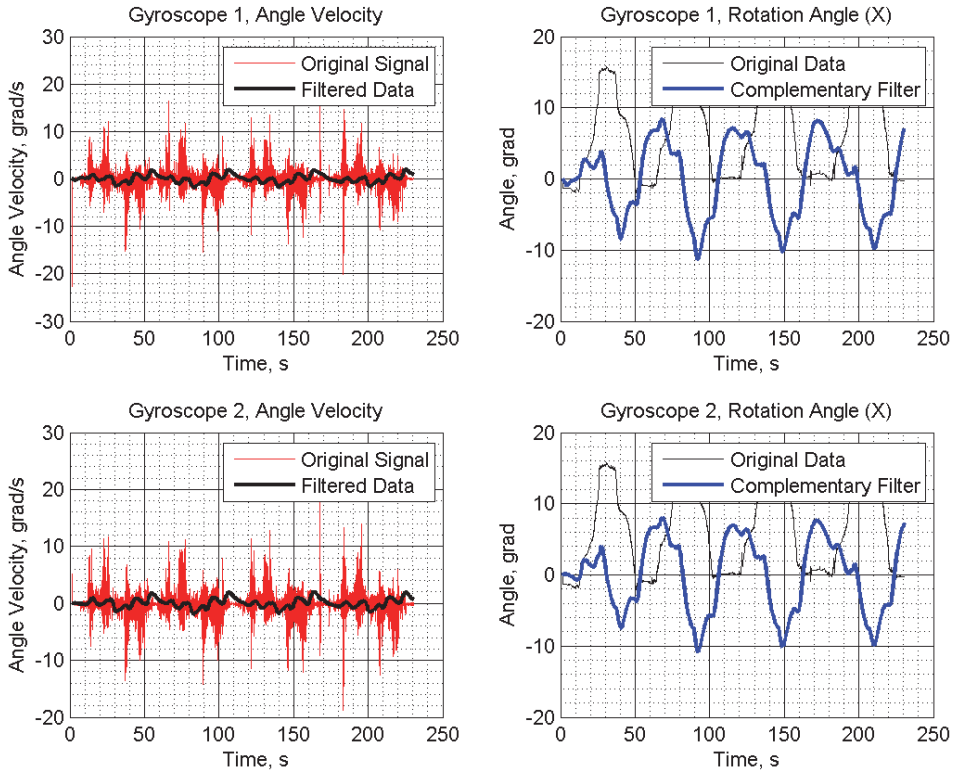


Figure 3.4. Angular velocity and angles obtained from gyroscopes for experiment $a_2w_2t_m^2$.

At a straight plate position, when the rails are at the same height, the gravitational component affects only the z-axis. Fig. 3.5 shows the distribution of gravity forces depending on the time and position of the plate by axes y and z .

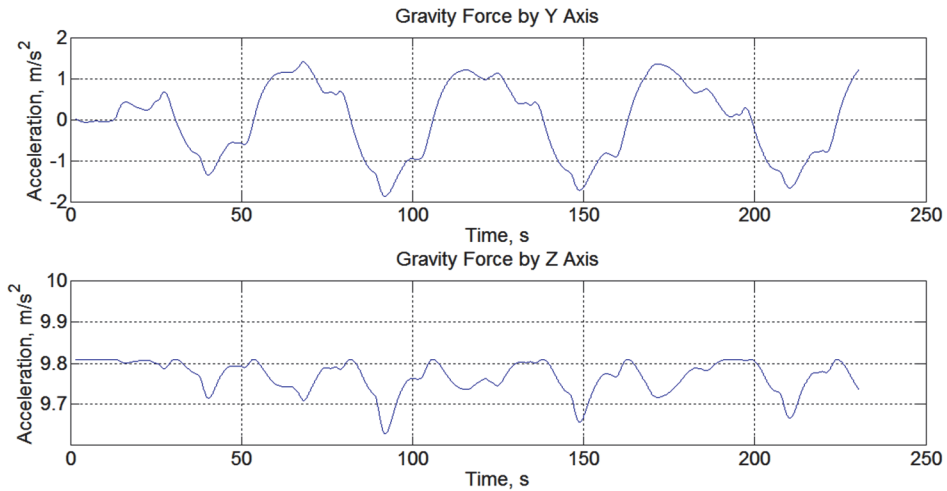


Figure 3.5. Gravity force by y and z axes for experiment $a2w2t_m2$.

After the average curve of the filtered accelerations was found, the values of changing gravitational constant g (gravity forces) were subtracted from it (Fig. 3.6). Red on the graph represents the original signal; black indicates the signal after passing through the filter.

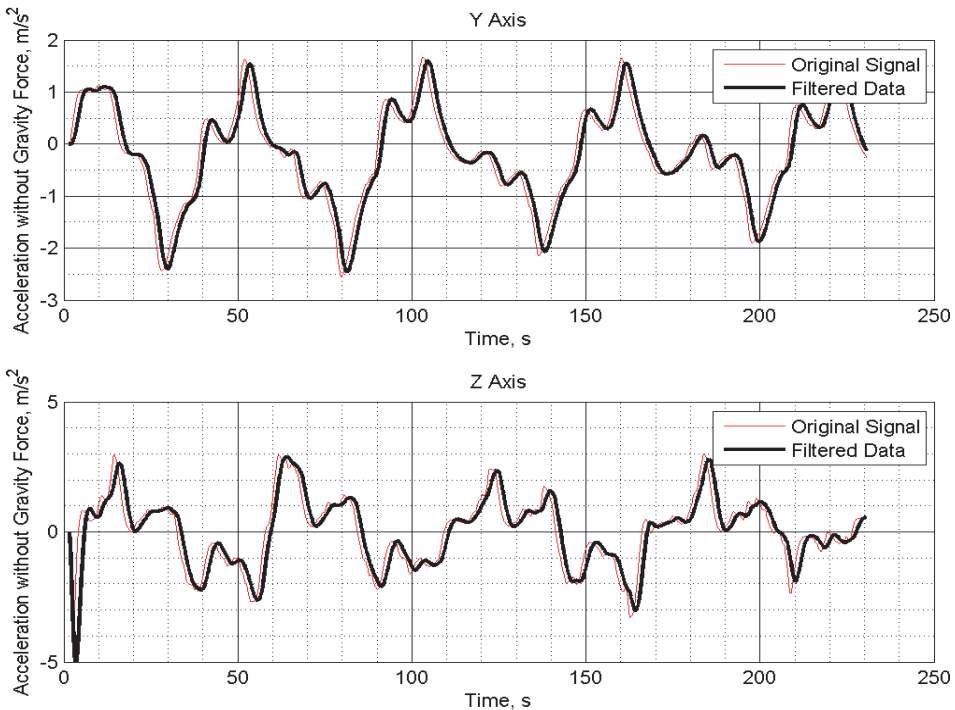


Figure 3.6. Accelerations without gravity forces for experiment $a2w2t_m2$ by axes y and z.

Next, it is possible to find the linear velocities by axes y and z (Fig. 3.7).

The integration of the vector of accelerations to find linear velocity values is made according to the next expression [66]:

$$V(i + 1) = Acc(i) \cdot (t(i + 1) - t(i)), \quad (3.3)$$

where V is the value of linear velocity, Acc is the value of acceleration, t is time, and i is the number of elements in the vectors of acceleration, velocity, and displacement in time.

Since integration is based on work with numerical values, it is easy to follow the results of this mathematical operation.

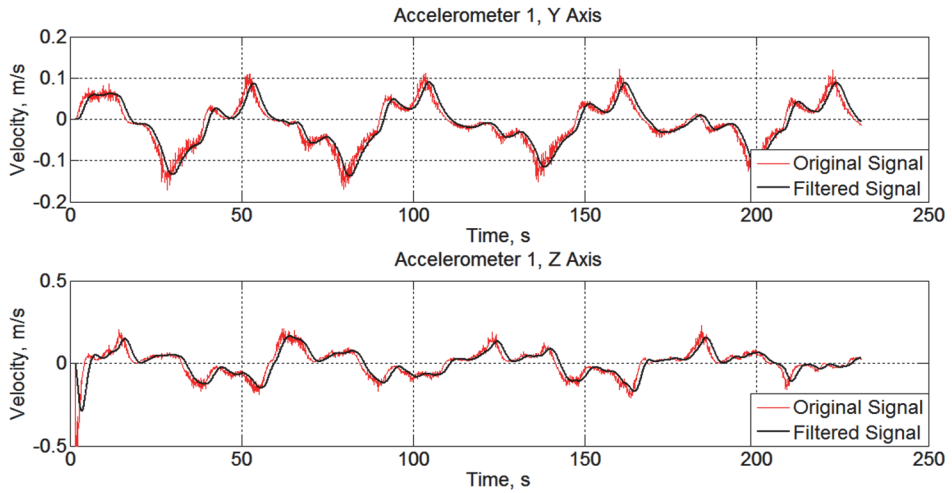


Figure 3.7. Obtained linear velocity from filtered average acceleration curve for experiment $a2w2t_m2$.

After we have found values of linear velocity, we integrate velocities to obtain the real displacements by axes y and z (Fig. 3.8).

The formula for linear velocity integration can be written as:

$$Dis(i + 2) = V(i + 1) \cdot (t(i + 1) - t(i)) + \frac{Acc(i) \cdot (t(i + 1) - t(i))^2}{2}, \quad (3.4)$$

where Dis is the value of displacement, V is the value of linear velocity, Acc is the value of acceleration, t is the time, and i is the number of elements in the vectors of acceleration, velocity, and displacement in time.

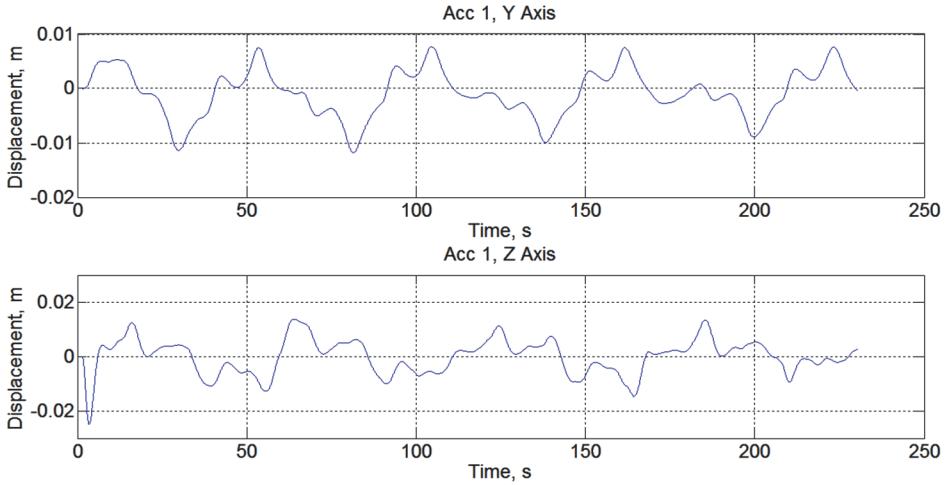


Figure 3.8. Measured displacements by axes y and z for experiment $\alpha 2 w 2 t_m 2$.

Finally, the values of maximal displacements for each experimental mode for axes y and z were found taking into account visually and analytically successful full steps (displacements related to separate steps) (Table 3.2).

Table 3.2. Values of maximal displacements for experimental displacements on axes y and z .

Number of IMU	Experimental mode	Maximal displacements by y -axis (m)	Maximal displacements by z -axis (m)
1	$\alpha 1 w 1 t_m 1$	0,0170	0,0252
2	$\alpha 1 w 1 t_m 2$	0,0166	0,0246
3	$\alpha 1 w 1 t_m 3$	0,0156	0,0223
4	$\alpha 1 w 2 t_m 1$	0,0161	0,0264
5	$\alpha 1 w 2 t_m 2$	0,0169	0,0246
6	$\alpha 1 w 2 t_m 3$	0,0169	0,0232
7	$\alpha 1 w 3 t_m 1$	0,0181	0,0291
8	$\alpha 1 w 3 t_m 2$	0,0163	0,0262
9	$\alpha 1 w 3 t_m 3$	0,0151	0,0263
10	$\alpha 2 w 1 t_m 1$	0,0195	0,0260
11	$\alpha 2 w 1 t_m 2$	0,0178	0,0226
12	$\alpha 2 w 1 t_m 3$	0,0171	0,0253
13	$\alpha 2 w 2 t_m 1$	0,0167	0,0232
14	$\alpha 2 w 2 t_m 2$	0,0178	0,0265
15	$\alpha 2 w 2 t_m 3$	0,0203	0,0259
16	$\alpha 2 w 3 t_m 1$	0,0207	0,0305
17	$\alpha 2 w 3 t_m 2$	0,0197	0,0258
18	$\alpha 2 w 3 t_m 3$	0,0210	0,0257
19	$\alpha 3 w 1 t_m 1$	0,0202	0,0263
20	$\alpha 3 w 1 t_m 2$	0,0190	0,0270
21	$\alpha 3 w 1 t_m 3$	0,0196	0,0274

22	$\alpha_3 w_2 t_m 1$	0,0215	0,0282
23	$\alpha_3 w_2 t_m 2$	0,0232	0,0276
24	$\alpha_3 w_2 t_m 3$	0,0215	0,0288
25	$\alpha_3 w_3 t_m 1$	0,0202	0,0297
26	$\alpha_3 w_3 t_m 2$	0,0210	0,0280
27	$\alpha_3 w_3 t_m 3$	0,0213	0,0283

The results of the Q -test for found displacements are introduced in Appendix 3.

3.3. Interpolation with 3 order splines

The main idea of the 3 order (cubic) spline is representation of the function of theoretical displacement profiles by some 3 order function on each interval of time, limited by the step of interpolation. That is, if there are n arrays of time intervals with some number of points, the spline $S(t)$ is the function [67]:

$$S(t) = \begin{cases} Ch_1(t), & t_0 \leq t \leq t_1 \\ Ch_i(t), & t_{i-1} \leq t \leq t_i, \\ Ch_n(t), & t_{n-1} \leq t \leq t_n \end{cases} \quad (3.5)$$

where each Ch_i is a function of order 3. Commonly, the cubic function has the form

$$Ch_i(t) = a_i + b_i t + c_i t^2 + d_i t^3. \quad (3.6)$$

To calculate the spline, we have to find the coefficients, a_i , b_i , c_i , and d_i for each i . Having n intervals, the total number of coefficients needed for every interval is $4n$. First, the spline must be equal to real values at the beginning and end of the intervals:

$$\begin{aligned} Ch_i(t_{i-1}) &= y_{i-1}; \\ Ch_i(t_i) &= y_i, \end{aligned} \quad (3.7)$$

at every time interval border. Therefore, it becomes

$$\begin{aligned} a_i + b_i t_{i-1} + c_i t_{i-1}^2 + d_i t_{i-1}^3 &= y_{i-1}; \\ a_i + b_i t_i + c_i t_i^2 + d_i t_i^3 &= y_i \end{aligned} \quad (3.8)$$

It is worth noticing that totally we have $2n$ conditions. Then, to find the smoothest function $S(t)$, we need to express:

$$\begin{aligned} Ch'_i(t_i) &= Ch'_{i+1}(t_i); \\ Ch''_i(t_i) &= Ch''_{i+1}(t_i) \end{aligned} \quad (3.9)$$

at all the internal points in the same time interval (i.e. $t_1, t_2, t_3 \dots t_n$). In the main form, it is possible to write named conditions as:

$$b_i + 2c_i t_i + 3d_i t_i^2 = b_{i+1} + 2c_{i+1} t_i + 3d_{i+1} t_i^2;$$

$$2c_i + 6d_i t_i = 2c_{i+1} + 6d_{i+1} t_i \quad (3.10)$$

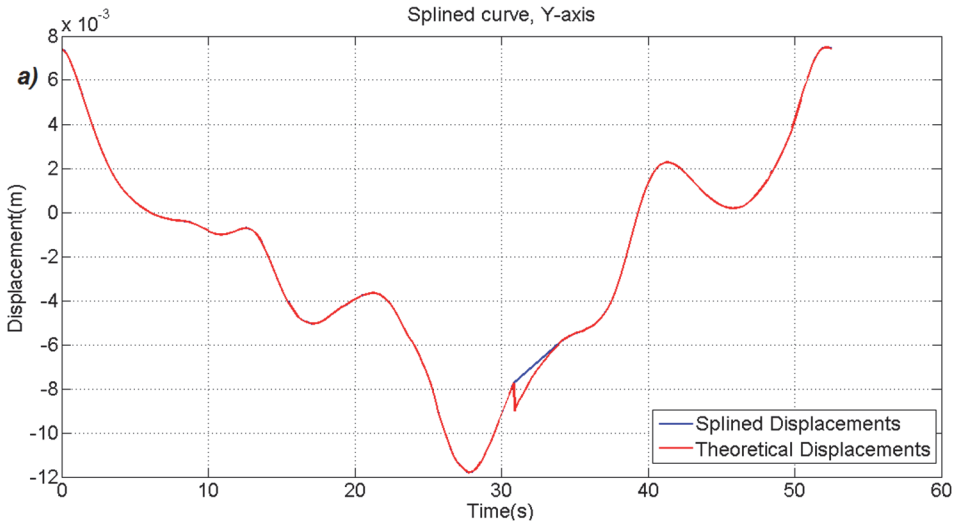
The total number of such conditions is $2(n - 1)$. Taking into account that Ch_i has 3 order, we have $4n$ coefficients determining $S(t)$. As a result, we obtain $4n - 2$ equations, what is 2 equations less of determination all the needed coefficients. For this moment of time, we have to choose of boundary. The standard operation is finding

$$Ch''_1(t_0) = Ch''_n(t_n) = 0 \quad (3.11)$$

The last expression denotes the natural boundary conditions. Eq. (3.12) has the name of clamped boundary conditions:

$$Ch'_1(t_0) = Ch'_n(t_n) = 0 \quad (3.12)$$

The main aim of spline usage and the last steps of spline operations can be seen from Fig. 3.9. In our case, splines are used to make some areas of displacement curves smooth, reducing sharp spots of filtered displacements. Moreover, cubic splines reduce the dispersions of processed signals.



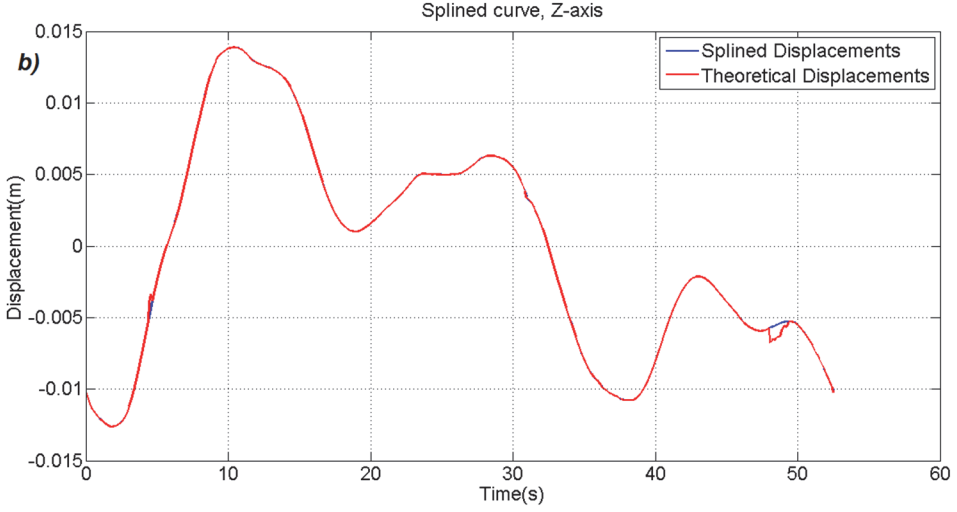


Figure 3.9. The last steps of spline usage for: a) y-axis displacements; b) z-axis displacements.

3.4. Laws of plate motion in measured points

After all the experimental signals from IMUs were processed using the proposed algorithm considering the influence of springs and damping elements, it was necessary to find the laws of plate-pelvis motion.

For experimental mode $\alpha 2w 2t_m 2$, the mathematical laws of plate motion in measured points have been found using the Curve Fitting Toolbox (MATLAB).

Function of plate motion in time for axis y (in Fourier series form):

$$\begin{aligned}
 f_y(t) = & -0,00176 + 0,00622\cos(0,116t) - 0,00063\sin(0,116t) - \\
 & 0,00028\cos(0,232t) - 0,00107\sin(0,232t) + 0,00141\cos(0,348t) + \\
 & 0,00057\sin(0,348t) + 0,00071\cos(0,464t) - 0,00080\sin(0,464t) + \\
 & 0,00143\cos(0,58t) - 0,00048\sin(0,58t) - 0,00065\cos(0,696t) - \\
 & 0,00031\sin(0,696t) + 0,00023\cos(0,812t) + 0,00022\cos(0,928t) - \\
 & 0,00013\sin(0,928t)
 \end{aligned} \quad (3.13)$$

For the y axis, an R-square value of splined curve fitting is equal to 0,9976.

Function of plate motion in time for axis z (in Fourier series form):

$$\begin{aligned}
 f_z(t) = & -0,00017 - 0,00427\cos(0,119t) + 0,00699\sin(0,119t) - \\
 & 0,00211\cos(0,238t) + 0,00049\sin(0,238t) - 0,00501\cos(0,357t) - \\
 & 0,00368\sin(0,357t) - 0,00045\sin(0,476t) + 0,00114\cos(0,595t) - \\
 & 0,00057\sin(0,595t) - 0,00019\cos(0,714t) - 0,00110\sin(0,714t) + \\
 & 0,00022\cos(0,833t) - 0,00049\sin(0,833t) - 0,00039\cos(0,952t)
 \end{aligned} \quad (3.14)$$

For the z axis, an R -square value of splined curve fitting is equal to 0,9979.

The number of decimal points is chosen as the minimum required for the description of curve matching with a splined curve of displacements. For both curves, the R -square values do not change with increasing numbers of decimal points (cases of 5–7 points were observed).

Chapter 3. Results and discussion

In Chapter 3 of this PhD thesis, an algorithm of IMU signal processing is shown and tested with an example using one experimental mode. To process the initial experimental data, a low-pass Butterworth filter of the second order was designed. Using the complimentary filter allowed avoidance of angle floating. The curve of output data (signal) was measured at 2 points of the plate-simulating pelvis motion, and was obtained for 2 axes. The cubic spline usage improved the shape of the output signals curves. Then, the mathematical functions (laws) of the change in time in plate position by 2 measured axes in time were found. The algorithm of IMU initial data processing gives an opportunity to avoid complicated mathematical calculations connected with damping elements motion as a part of the experimental prototype.

Of particular interest is a discussion about the comparison of obtained values of displacements of the plate-pelvis in axes y and z , and experimental plane motion of the human pelvis captured with sensors. In Fig. 3.10, the plate-pelvis motion in the frontal plane simulated with the experimental prototype is represented.

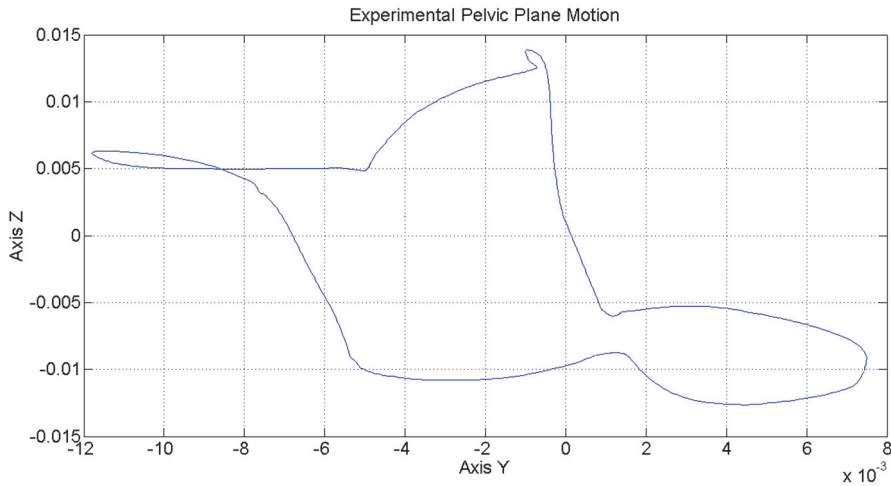


Figure 3.10. Experimental plate-pelvis motion in the frontal plane.

A simple way to estimate the plotted results with Vicon displacements (taken from experimental data described in [68]) is finding the deviation vector con-

sisting of differences between elements with the same numbers. In Fig. 3.11 histograms for deviation vectors for axes y and z are shown.

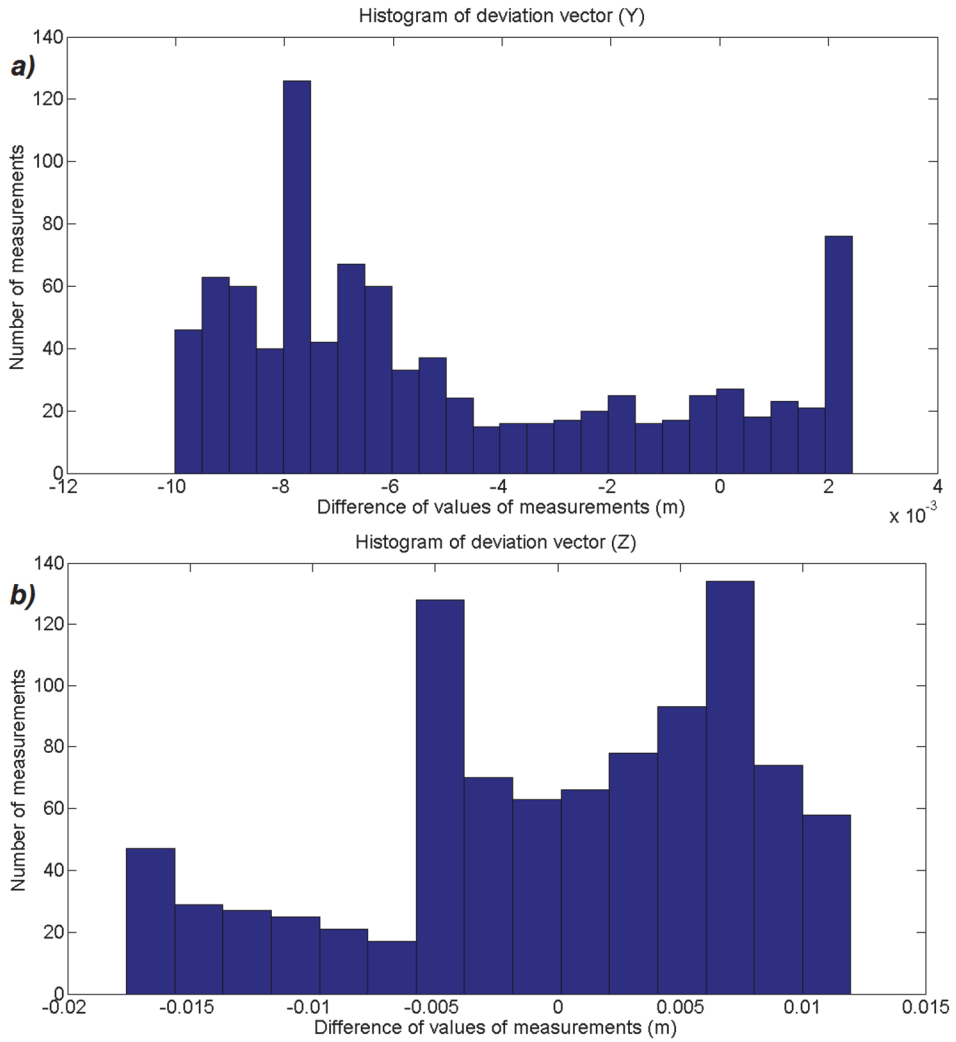


Figure 3.11. Histograms of distribution of deviation vector exements for: a) axis y ; b) axis z .

It should be noted that even data from similar experiments with walking can be very different because of distinctions in experimental planning, precision of marker or sensor installation, anthropometric properties of the measured person (subject), and so on.

4. IDENTIFICATION OF MECHANICAL HEEL-PELVIS SYSTEM

Since the main objective of this work is to create a mathematical model and to construct a mechanical heel-pelvis system motion simulation in the frontal plane for subsequent usage in human lower-limb recovery, 2 possible ways of its realisation were examined.

The first method, the consideration of the motion of the plate with the help of the laws of theoretical mechanics, followed the Lagrange equations of the second kind for each DOF of the experimental prototype and subsequent analytical solution of derived differential equations. However, the description of the motion of the experimental prototype units is very complicated (a large number of DOF of the mechanical system of the prototype, the presence of springs, the complexity of the mathematical apparatus of the analytical solutions of the Lagrange differential equations, etc.) and necessarily requires additional research. Thus, the second alternative method was chosen.

The alternative identification method is based on the finding of theoretical law of the plate movement in time by the creation of a dynamic linear stationary model, simulating the work of an experimental prototype using the command line of MATLAB and its functions. The state-space form is used to find parameters of all the matrices of dynamic systems for axes y and z . Thus, to simplify the systems, the maximal range of differential equations is chosen as 2. After that, from state-space matrix parameters, it is possible to find transfer functions for both axes as well as differential equations. Moreover, the use of identification method allows us to determine dynamical parameters of observing system.

4.1. Description of identification method

Various models are widely used in theoretical and experimental studies. They are applicable to study the phenomena of mechanisms occurring in systems and facilities or to predict their performance. On this point, we solve the problem of creating a model of the motion of the experimental prototype [69,70].

Under the model is generally understood some form or other information about the most significant characteristics of the object. By way of presenting this information, the following types of models exist:

- Verbal models;
- Physical models (decrease copies of real objects, and sometimes other physical nature, allowing simulation of processes in the object of study);
- Mathematical models (give information about the object or system is represented as mathematical terms).

In this work the identification of mathematical (analytical) models is used.

Analytical models are a reflection of the relationship between the variables of the object in the form of a mathematical formula or a group of such formulas.

The simulation is based on 2 fundamental features:

- The principle of the practical limitations of the number of fundamental laws of nature;
- The principle of similarity, meaning that the phenomenon of different physical natures can be described by the same mathematical relations.

The procedure for constructing the model is called identification, although the term usually refers to the construction of analytical mathematical models of dynamic objects. Identified objects can be represented as shown in Fig. 4.1, where t is time; $u(t)$ is controlled (with) the input signal; $\tilde{y}(t)$ is the theoretical yield of the object, and $er(t)$ is a random disturbance, reflecting the action of factors not considered (noise monitoring).

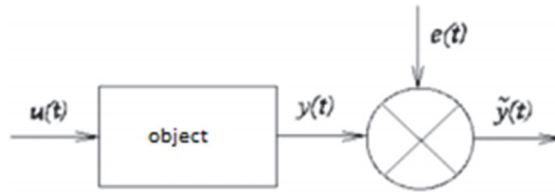


Figure 4.1. Common view of object identification.

Connection between the output and the ‘theoretical’ input signal is given by an operator Ψ :

$$\tilde{y}(t) = \Psi[u(t)] \quad (4.1)$$

Then, the observed output object can be described by the relation:

$$\tilde{y}(t) = \Psi[u(t)] + er(t) \quad (4.2)$$

The purpose of identification is the observations of the input $u(t)$ and output signal $y(t)$ at a certain interval of time for the operator to determine the binding theoretical output and input signals [71].

A short description of the identification method used in this work follows: first, the state-space representation in continuous time is identified. Then, the state-space representation in discrete- and continuous-time form must be found. Finally, using transfer functions, it is easy to express the differential system heel-pelvis motion.

Proposing the identification method offers the possibility to find the resulting differential equation for a multilink system situated between the input and output data, regardless of the number of mechanical system links [69,70].

Thus, identification method is based on experimental and analytical approach, closely interrelated with the results obtained in Chapter 3.

4.2. State-space representation. Vector-matrix form

Since we do not have the coefficients of the transfer function or the poles and zeros of the transfer function, we use the vector-matrix model of the dynamical system to describe the experimental plate motion. The dynamical system for vector-matrix models is represented as a ‘black box’ with one input signal (vertical displacements of summed left and right racks, simulating the human heel) and one output signal (displacements of plate, simulating pelvic motion by one of the 2 axes) for both axes and experimental modes. In summary, this vector-matrix model is shown in Fig. 4.2.

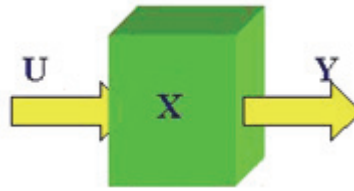


Figure 4.2. Simplified representation of the studied model [72].

All variables characterising the system can be divided into 3 groups [72,73]:

- 1) Input variables or input signals generated with systems, which are external to the studied system. They are characterised by the input vector:

$$u^T = [u_1, u_2, \dots, u_r], \quad (4.3)$$

where r is the number of inputs. In the case of our model (Fig. 4.2), $r = 1$.

- 2) The output variables that characterise the system response to input signals are represented as the output vector:

$$y^T = [y_1, y_2, \dots, y_m], \quad (4.4)$$

where m is the number of outputs. For observing model, $m = 1$.

- 3) Intermediate variables or state variables describing the internal state of the system and represented by the vector:

$$x^T = [x_1, x_2, \dots, x_{n_u}], \quad (4.5)$$

where n_u is the number of state variables of the system. For the studied model, $n_u = 2$.

In general, the dynamic system in the continuous state can be described by a pair of matrix equations:

$$\dot{x}(t) = N[x(t), u(t), t], \quad (4.6)$$

$$y(t) = O[x(t), u(t), t]. \quad (4.7)$$

Matrix Eq. 4.6 is called the equation of the system state. Its solution, corresponding to the initial condition $x_0 = x_0(t)$, defines the system state vector. Matrix Eq. 4.7, defining the output variables with dependence from $x(t)$ and $u(t)$, is the output equation.

In this particular case, dependences $N_i (i = 1, \dots, n_u)$ and $O_k (k = 1, \dots, m)$ can be linear combinations of state variables x_i and input variables u_q . The dynamic system is described in vector-matrix form [74]:

$$\dot{x} = A(t)x + B(t)u, \quad (4.8)$$

$$y = C(t)x + D(t)u, \quad (4.9)$$

The transition to stationary models allows operating with a coefficient matrix or with stationary equations [75]:

$$\dot{x} = Ax + Bu, \quad (4.10)$$

$$y = Cx + Du, \quad (4.11)$$

where the matrix A is a functional matrix of size $n_u \times n_u$, called the matrix of system state (object);

B denotes functional matrix sized $n_u \times r$, named control matrix (input);

C is a functional matrix with size $m \times n_u$, called the matrix of output state;

D denotes functional matrix with size $m \times r$, called the matrix of output control.

This system can be interpreted as:

$$\frac{d}{dt} \begin{pmatrix} x_1 \\ x_2 \end{pmatrix} = \begin{pmatrix} A_{11} & A_{12} \\ A_{21} & A_{22} \end{pmatrix} \begin{pmatrix} x_1 \\ x_2 \end{pmatrix} + \begin{pmatrix} B_1 \\ B_2 \end{pmatrix} (u_1 \ u_2) \quad (4.12)$$

$$y = (C_1 \ C_2) \begin{pmatrix} x_1 \\ x_2 \end{pmatrix} \quad (4.13)$$

Expressing matrices A , B , and C we obtain:

$$A = \begin{pmatrix} A_{11} & A_{12} \\ A_{21} & A_{22} \end{pmatrix}; B = \begin{pmatrix} B_1 \\ B_2 \end{pmatrix}; C = (C_1 \ C_2) \quad (4.14)$$

Figure 4.3 (a) shows plots of the input signals (displacement heel), wherein one input signal is shifted relatively to the other by the amount of π (half of a full step in time) and both of signals are summed; Fig. 4.3 (b) and 4.3 (c) show the experimental curves of the plate displacements by axes y and z .

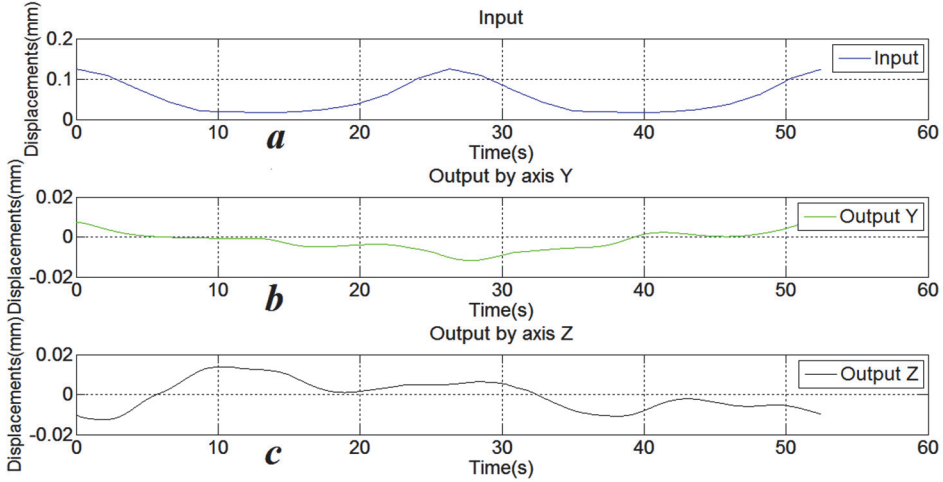


Figure 4.3. Graphical representation of studied system inputs and outputs; a) input signal; b) output signal by y -axis; c) output signal for z -axis.

Thus, we find the coefficients of the matrices of discrete spaces of states of the system for the axes y and z (equations 4.15–4.16) with the help of the application Control System Toolbox software environment MATLAB/Simulink [76].

Matrices in state-space representation in continuous-time form for axis y are:

$$A = \begin{pmatrix} 0 & 1 \\ -2,2619 & -2,5372 \end{pmatrix}; B = \begin{pmatrix} 0,1863 \\ -0,5688 \end{pmatrix}; C = (1 \ 0); D = (0), \quad (4.15)$$

For axis z the matrices are:

$$A = \begin{pmatrix} 0 & 1 \\ -0,0765 & 0,6317 \end{pmatrix}; B = \begin{pmatrix} -1,4 \cdot 10^{-3} \\ 2,4 \cdot 10^{-4} \end{pmatrix}; C = (1 \ 0); D = (0). \quad (4.16)$$

From these matrices, the state-space matrices coefficients (equations 4.15–4.16), we find the transfer function of a continuous-time dynamic system for y and z axes from Eq. (4.32):

$$W_y(s) = \frac{Y_y(s)}{U(s)} = \frac{0,1863s - 0,0961}{s^2 + 2,537s + 2,262} \quad (4.17)$$

$$W_z(s) = \frac{Y_z(s)}{U(s)} = \frac{1,7 \cdot 10^{-4}s - 8,5 \cdot 10^{-4}}{s^2 + 0,6317s + 0,0765} \quad (4.18)$$

where $U(s)$ is the input array of displacements; $Y_y(s)$ is the array of displacements by the y -axis, and $Y_z(s)$ is the array of displacements by the z -axis in continuous-time form.

4.3. Solution of discrete state-space equations using Laplace transform: calculation of the transfer function

To compare to the continuous-time state-space representation, we determine a discrete space.

Sometimes, it is convenient to explore linear systems with constant parameters using the Laplace transform. We define the Laplace transform of the vector function $Lap(t)$ as follows [77–79]:

$$Lap(s) = \mathcal{L}[Lap(t)] = \int_0^{\infty} e^{-st} Lap(t) dt, \quad (4.19)$$

where s is the complex variable. Symbol \mathcal{L} refers to the operation of the Laplace transform of the function in the square brackets.

Obviously, the Laplace transform of the vector-valued function $Lap(t)$ is a vector, whose components are the Laplace transform components of function $Lap(t)$.

Let us first observe the homogeneous differential equation of state:

$$\dot{x}(t) = Ax(t), \quad (4.20)$$

where A is the matrix of the system state. Performing the Laplace transform, we obtain:

$$sX(s) - x(0) = AX(s), \quad (4.21)$$

as all the usual Laplace transform theorems for scalar expressions are also valid in the vector case. The solution relative to $X(s)$ is:

$$X(s) = (sI - A)^{-1}x(0). \quad (4.22)$$

In the time domain, this corresponds to the expression:

$$x(t) = e^{At}x(0). \quad (4.23)$$

In the case of a non-homogeneous equation:

$$\dot{x}(t) = A(t)x + B(t)u, \quad (4.24)$$

where A and B are constant matrices, and by performing the Laplace transform, we obtain:

$$sX(s) - x(0) = AX(s) + BU(s), \quad (4.25)$$

where we find that

$$X(s) = (sI - A)^{-1}x(0) + (sI - A)^{-1}BU(s). \quad (4.26)$$

The equation for the output coordinate of the system has the form:

$$Y(t) = Cx(t), \quad (4.27)$$

where C is the matrix of output states. Using the Laplace transformation and substituting Eq. (4.27), we obtain:

$$Y(s) = CX(s) = C(sI - A)^{-1}x(0) + C(sI - A)^{-1}BU(s). \quad (4.28)$$

Then, we express $Y(t)$ as:

$$Y(t) = Ce^{At}x(0) + C \int_0^t e^{A(t-\tau)} Bu(\tau) d\tau. \quad (4.29)$$

Having, $x(0) = 0$, Eq. (4.21) becomes:

$$Y(s) = W(s)U(s), \quad (4.30)$$

where:

$$W(s) = C(sI - A)^{-1}B. \quad (4.31)$$

Matrix $W(s)$ is called a matrix-transfer function of the system. If $W(s)$ and $U(s)$ are known, the reaction of the system to the zero initial condition can be found using the Laplace inverse transform for Eq. (4.30).

From Eq. (4.31), it follows that the matrix form of the transfer function $W(s)$ is the Laplace transform for the matrix function:

$$K(t) = C \exp(A, t) B, t \geq 0 \quad (4.32)$$

It is obviously from Eq. (4.32) that

$$K(t - \tau), t \geq \tau \quad (4.32a)$$

is the matrix impulse transition function of the system. A matrix transform function can be introduced as:

$$W(s) = \frac{1}{\det(sI - A)} P(s), \quad (4.33)$$

where $P(s)$ is the matrix whose elements are polynomials of s . Consequently, the matrix elements of the transfer function $W(s)$ are rational functions of s . The common denominator of the $W(s)$ is the expression $\det(sI - A)$, if there is no cancellation of factors of type $s - \lambda_i$, where λ_i is characteristic number of matrix A for all elements of matrix $W(s)$.

Roots common denominator $W(s)$ called as the poles of the matrix transfer function W (Roots of common denominator $W(s)$ are called the poles of the matrix-transfer function $W(s)$). If there is no cancellation, the poles of the matrix-transfer function are the poles of the system or characteristic numbers of matrix A .

If both input $u(t)$ and output $y(t)$ variables are scalar, a matrix transfer function transforms to a scalar transfer function. In the case of multivariate systems, each element $W_{ij}(s)$ of the matrix transfer function $W(s)$ is a transfer function from the j^{th} component of input to the i^{th} component of output.

One way to transition from the continuous to the discrete function is the use of tables matching the Laplace transform and the z -image. This immediate transition from $W(s)$ to $W(z)$ can be matched with the next Eq. (4.34) [79–80]:

$$W(Z) = \text{Lap}\{W(s)\}. \quad (4.34)$$

A method for obtaining a discrete transfer function according to Eq. (4.30) is accurate, but its application to real systems of the second order and higher is difficult. Therefore, practical calculations of impulse systems use approximate methods of transition from the transfer function $W(s)$ to the discrete transfer function $W(z)$. These methods are based on the replacement of the derivative of time, appearing in the continuous part of the equation in the form of the first difference:

$$\frac{dy(t)}{dt} \approx \frac{\Delta y(t)}{\Delta t} = \frac{y(t_i) - y(t_{i-1})}{\Delta t} \quad (4.35)$$

We write the differential equation of a continuous integrator as:

$$\frac{dy(t)}{dt} = u(t). \quad (4.36)$$

Substituting Eq. (4.35) in Eq. (4.36), we obtain the residual equation of the integrator:

$$Y(iT) = y(iT - 1 \cdot T) + Tu(iT). \quad (4.37)$$

Writing Eq. (4.37) in form:

$$Y(z) = Y(z)z^{-1} + Tu(z), \quad (4.38)$$

we express the discrete transfer function of the integrator as:

$$W(z) = \frac{Y(z)}{U(z)} = \frac{T}{(1-z^{-1})} = \frac{Tz}{(z-1)}. \quad (4.39)$$

Considering that the usual transfer function of the integrator is:

$$W(s) = \frac{1}{s}, \quad (4.40)$$

we obtain one of the most commonly used equations for approximate transition from the transfer function of a continuous system to a discrete transfer function,

$$s = \frac{(z-1)}{Tz}. \quad (4.41)$$

A more precise transition from a continuous to a discrete system can be made using Tustin's substitution, according to which:

$$s = \frac{2(z-1)}{T(z+1)}. \quad (4.42)$$

Substitution Eq. (4.41) corresponds to the approximate (numerical) integration by the method of rectangles; the substitution Eq. (4.42) is the integration by the trapeze method.

Equations of observing discrete systems are usually not written in differential form but in residual form:

$$x(numT + T) = A(numT)x(numT) + B(numT)u(numT); \quad (4.43)$$

$$y(numT) = C(numT)x(numT) + D(numT)u(numT), \quad (4.44)$$

where num is the number of periods and T is the sample time.

In the case of the studied experimental prototype of a mechanical system for simulation of pelvic movements (displacements), we obtain the following values of the transfer functions for the y Eq. (4.45) and z Eq. (4.46) axes.

Thus, it is possible to find state-space matrices.

For the y -axis we have:

$$A = \begin{pmatrix} 0 & 1 \\ -0,8665 & 1,8597 \end{pmatrix}; B = \begin{pmatrix} 9,6 \cdot 10^{-3} \\ 8 \cdot 10^{-3} \end{pmatrix}; C = (1 \ 0); D = (0). \quad (4.45)$$

For the z -axis:

$$A = \begin{pmatrix} 0 & 1 \\ -0,9649 & 1,9647 \end{pmatrix}; B = \begin{pmatrix} 9,7 \cdot 10^{-5} \\ 9,6 \cdot 10^{-5} \end{pmatrix}; C = (1 \ 0); D = (0). \quad (4.46)$$

Finally, we obtain the transfer functions:

$$W_y(z) = \frac{Y_y(z)}{U(z)} = \frac{8,4 \cdot 10^{-3}z - 8,6 \cdot 10^{-3}}{z^2 - 1,8660z + 0,8718} \quad (4.47)$$

$$W_z(z) = \frac{Y_z(z)}{U(z)} = \frac{2 \cdot 10^{-5}z - 2,4 \cdot 10^{-5}}{z^2 - 1,9670z + 0,9669} \quad (4.48)$$

where $U(z)$ is the input array of displacements; $Y_y(z)$ is the array of displacements by y -axis, and $Y_z(z)$ is the array of displacements by z -axis in discrete-time form.

4.4. Dynamic parameters of automatic systems

The main characteristics of dynamic links of the transfer function can be divided into time, phase, and frequency characteristics [81]. Since we work with vibrations, created during the experimental prototype work, we will observe logarithmic and damping characteristics.

Using the second order of dynamic models for each axis, matrix coefficients in state-space representation describe the pattern between input and output signals. In this case, the main differential equation in generalized form can be written in Newton form [70]:

$$\frac{d^2u}{dt^2} + 2n_d \frac{du}{dt} + f^2u = f(t), \quad (4.49)$$

where u – input value, n_d – damping coefficient, f – natural frequency.

Then, after solving the characteristic equation and iterations of values of damping and natural frequency coefficients are obtained.

4.4.1. Bode diagram

To simplify the graphical representation of frequency characteristics as well as to facilitate the analysis of the processes in the frequency domain, the logarithmic frequency responses are used: logarithmic amplitude frequency response and logarithmic phase frequency response. During the building of logarithmic characteristics on the scale of frequencies, in spite of f lays off $\log(f)$ on horizontal axis and the measurement unit is the decade. The decade is the frequency range corresponding to 10 changes in frequency. The building logarithmic amplitude frequency response on the ordinate axis of the unit is the decibel (dB), which is the ratio of $L = 20 \log A(f)$. A decibel is an increase in output amplitude of $\sqrt[20]{10}$ times. The upper half of the plane of logarithmic amplitude response corresponds to values $Amp > 1$ (increasing amplitude), and the lower half of the plane corresponds to values $Amp < 1$ (decreasing amplitude). The point of intersection with the abscissa axis is equal to the cut-off frequency f_{cut} , at which the amplitudes of the input and output signals are equal [82].

We observe the logarithmic characteristics of the dynamic system of the studied prototype in the example of Bode diagrams (Fig. 4.4).

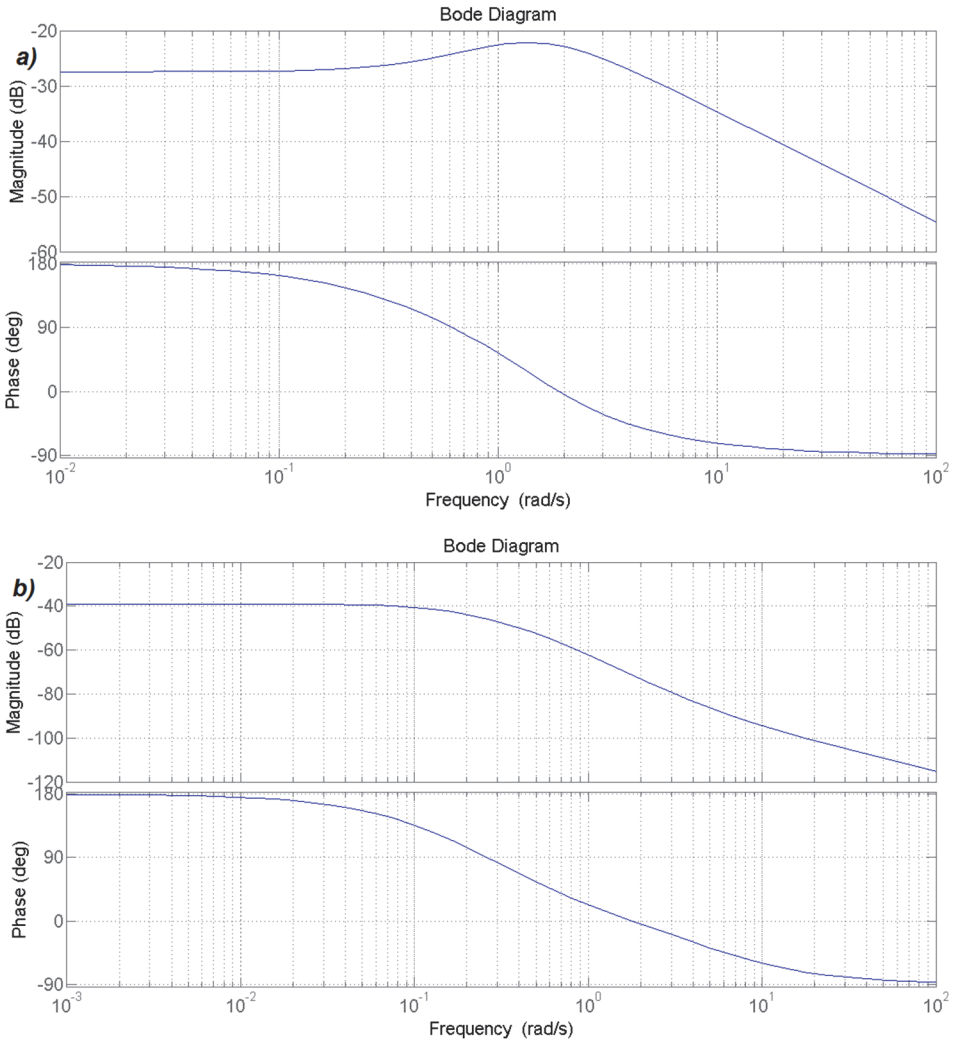


Figure 4.4. Bode diagram a) for axis y; b) for axis z.

For the Bode diagram on the frequency axis, we use a logarithmic scale and a natural scale for angles. In practice, the logarithmic frequency characteristics are based on the coincident coordinate system.

4.4.2. Damping

Damping of vibrations is the forced dampening of vibrations or the reduction of their amplitude to acceptable limits. Damping of mechanical vibrations is achieved by increasing the friction in the system. Thus, the damping coeffi-

cients show the influence of the frictional force on the vibrations of mechanical system elements [81].

Tables 4.1, 4.2 shows the main characteristics of vibrations damping along the axes y and z.

Figure 4.5 graphs the change of damping coefficients by axes y and z for the experimental prototype.

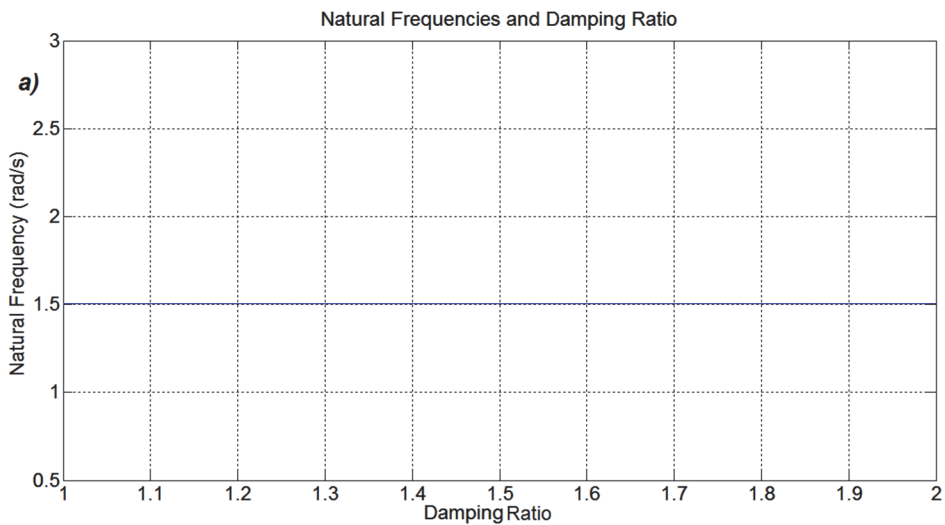
Tables 4.1 and 4.2 show the main characteristics of vibrations damping along the axes y and z. In addition, Fig. 4.5 graph the change of damping coefficients by axes y and z for the experimental prototype.

Table 4.1. Main features of vibrations damping by the axis y.

Eigenvalue	Magnitude	Damping	Frequency (rad/s)
$-9,30 \cdot 10^{-1} + 4,25 \cdot 10^{-2}i$	$-9,31 \cdot 10^{-1}$	$8,44 \cdot 10^{-1}$	1,50
$-9,30 \cdot 10^{-1} - 4,25 \cdot 10^{-2}i$	$-9,31 \cdot 10^{-1}$	$8,44 \cdot 10^{-1}$	1,50

Table 4.2. Main features of vibrations damping by the axis z.

Eigenvalue	Magnitude	Damping	Frequency (rad/s)
$-9,91 \cdot 10^{-1}$	$-9,91 \cdot 10^{-1}$	1,00	$1,63 \cdot 10^{-1}$
$-9,91 \cdot 10^{-1}$	$-9,74 \cdot 10^{-1}$	1,00	$4,68 \cdot 10^{-1}$



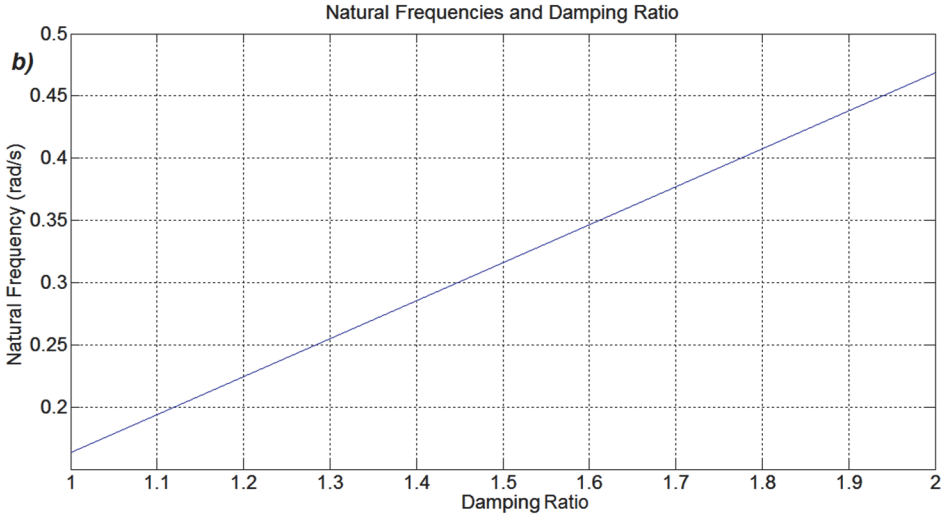


Figure 4.5. Plot of natural frequencies and damping ratio; a) for axis y ; b) for axis z .

4.5. Inverse Laplace transform: determination of the law of plate plane pelvic motion

The inversion formula allows finding the function $f(t)$ from its Laplace image of $F(s)$. On the basis of Jordan's lemma, integration in the range of $\delta - j\infty$ to $\delta + j\infty$ can be replaced by integration in a closed loop formed by the direct $R_e(s) = \delta$ and closing it ends the semicircle of radius R . In this case, for the right side signal, all the poles of $F(s)$ must lie to the left of the line $R_e(s) = \delta$ [83]:

$$f(t) = \frac{1}{2\pi j} \int_{\delta-jw}^{\delta+jw} F(s)e^{st} ds. \quad (4.50)$$

Then, according to the residue theorem, the integral Eq. (4.50) is equal to the sum of residues (Res) and the integrand $F(s)e^{st}$ with respect to all l singular points s_i of this function, lying inside the contour of integration, that is:

$$f(t) = \frac{1}{2\pi j} \int_{\delta-jw}^{\delta+jw} F(s)e^{st} ds = \sum_{i=1}^l Res[F(s_i)e^{s_i t}], \quad (4.51)$$

where $\delta_1 \geq \delta_{min}$.

Residues relative to a simple pole s_0 can be defined by the equation:

$$Res[\Phi(s_0)] = \lim_{s \rightarrow s_0} (s - s_0)\Phi(s) = e^{s_0 t} \lim_{s \rightarrow s_0} (s - s_0)F(s), \quad (4.52)$$

where:

$$\Phi(s) = F(s)e^{st}. \quad (4.53)$$

The residue with respect to the nl^{th} pole of multiplicity at s_0 is defined as:

$$\text{Res}[\Phi(s_0)] = \frac{1}{(1-n)!} \lim_{s \rightarrow s_0} \frac{d^{n-1}}{ds^{n-1}} [(s - s_0)^n \Phi(s)]. \quad (4.54)$$

To simplify the calculation of the inverse Laplace transform, there are special tables.

We find differential equations from transfer functions using the inverse Laplace transform. Because continuous-time and discrete-time transfer functions are identical, both of those forms will be shown as the differential equations.

From equations (4.18–4.19), it is possible to express the differential equations for axes y and z in continuous-time form.

For axis y :

$$Y_y(s)(s^2 + 2,5370s + 2,2620) = U(s)(0,1863s - 0,0961) \quad (4.55)$$

For axis z :

$$Y_z(s)(s^2 + 0,6317s + 0,0765) = U(s)(1,7 \cdot 10^{-4}s - 8,5 \cdot 10^{-4}) \quad (4.56)$$

Using inverse Laplace transforms, we obtain differential equations in time for both axes.

For axis y :

$$\frac{d^2y}{dt^2} + 2,5370 \frac{dy}{dt} + 2,2620y = 0,1863 \frac{du}{dt} - 0,0961u \quad (4.57)$$

For axis z :

$$\frac{d^2y}{dt^2} + 0,6317 \frac{dy}{dt} + 0,0765y = 1,7 \cdot 10^{-4} \frac{du}{dt} - 8,5 \cdot 10^{-4}u \quad (4.58)$$

From equations 4.48 and 4.49, it is possible to express the differential equations for axes y and z in discrete-time form.

For axis y :

$$Y_y(z)(z^2 - 1,8660z + 0,8718) = U(z)(8,4 \cdot 10^{-3}z - 8,6 \cdot 10^{-3}) \quad (4.59)$$

For axis z :

$$Y_z(z)(z^2 - 1,9670z + 0,9669) = U(z)(2 \cdot 10^{-5}z - 2,4 \cdot 10^{-5}) \quad (4.60)$$

The differential equations in discrete-time form are:

For axis y :

$$\frac{d^2y}{dt^2} - 1,8660 \frac{dy}{dt} + 0,8718y = 8,4 \cdot 10^{-3} \frac{du}{dt} - 8,6 \cdot 10^{-3}u \quad (4.61)$$

For axis z:

$$\frac{d^2y}{dt^2} - 1,9670 \frac{dy}{dt} + 0,9669y = 2 \cdot 10^{-5} \frac{du}{dt} - 2,4 \cdot 10^{-5}u \quad (4.62)$$

Chapter 4. Results and discussion

In Chapter 4, the identification method for the heel-pelvis mechanical system is introduced. First, the matrix coefficients in state-space representation were found for the continuous-time form with one input and one output signal for both axes, simulating the frontal plane motion. Then, the transfer functions for axes y and z were calculated. On the basis of defined transfer functions, the differential equations for a mechanical heel-pelvis system motion have been found. Moreover, damping and Bode plots have been represented. To check the correctness of the state-space representation results in continuous-time form, the same calculations have been made for system identification in discrete-time form, which has practically identical results for studied dynamic system.

One of the questions that can occur after reading Chapter 4 is how the calculated coefficients of the matrices in state-space form represent the real human heel-pelvis system motion? To answer this question, it is necessary to understand that the main elements of experimental prototype construction (leg-links, plate-pelvis lengths, and angles of the plate-pelvis tilt) are chosen to coincide with statistically average adult person pelvis geometry. The input data (vertical heel displacements) is obtained with IMUs during experiments with walking. The output signal for identification was captured with IMUs described in this work. So, calculated coefficients can be considered as conditionally responding to real human motion.

Conversely, there are some differences between the work of the construction of the experimental prototype and human lower-limb motions during walking, described in the discussion sections to the Chapters 2 and 3.

CONCLUSION

Scientific Results

This thesis describes the experimental and analytical approach for obtaining a mathematical model of the mechanical heel-pelvis system in the frontal plane, on the basis of input and output signals captured from 27 different experiments simulating human pelvic motion, with corrections for possible subsequent usage of scientific results in mechanotherapy.

The main scientific results of this work are the following:

- 1) The development of an algorithm for IMU data processing, considering the possibilities of measuring systems, construction of an experimental prototype, and the action of damping elements on the motion of the pelvic plate. The macroparameters and technical facilities for experimental research of the kinematic hip system are identified.
- 2) Identification of damping and frequency coefficients of the studied linear model of the heel-pelvis mechanical system.
- 3) Determination of a mathematical model of the mechanical heel-pelvis system motion, based on identification methods. Obtainment of transfer functions and differential equations of motion, describing the mathematical dependence between input and output signals.

Novelties

- 1) An algorithm for the analysis of experimental data, with the possibility of measuring system, is developed.
- 2) A mathematical model of the motion of the human mechanical heel-pelvis system is represented in the form of a differential equation, and its parameters are found for both axes. Moreover, the laws of human pelvic motion in time in the form of a Fourier series have been obtained for both axes for the first time for human motion in the frontal plane, taking into account the future use of the experimental prototype construction for medical purposes. The adequacy of the model for experimental data is shown by working with real experimental input (displacements of the heel) and output (plate-pelvis displacements by axes) data.

Future work

During this study, several ideas and problems emerged that require further investigation, including the following:

- Installation of an additional motor for automatic control of rotation was needed for the experimental plate, in order to imitate the pelvic supporting link.
- The addition of extra elements to make the experimental prototype work in space.
- Artificial simulation of knee motion for subsequent research of recovering trainer modelling.
- Creation of the mathematical basis for the determination of patient foot motion from the motion of the pelvis.
- Thorough selection and analysis of components for real therapeutic trainer, diagnostics of mechanical heel-pelvis system equipment, and details during scientific research.

REFERENCES

1. Report v.5 on musculoskeletal health in Europe, European Union project EUMUSK, 2013.
2. Bottcher, S., Principles of robot locomotion, Southern Illinois University, 2006.
3. Pamies I Vila, R., Application of multibody dynamics techniques to the analysis of human gait. *PhD thesis*, Polytechnic University of Catalonia, 2012.
4. Kljuno, E., Williams II, R. L., Humanoid walking robot: modeling, inverse dynamics, and gain scheduling control. *Journal of Robotics*, 2010, 2010, 1–19.
5. Saranli, U., Arslan, O., Ankarali, M. M., Morgul, O., Approximate analytic solutions to nonsymmetric stance trajectories of the passive springloaded inverted pendulum with damping. *Nonlinear Dynamics*, 2010, 62(4), 729–742.
6. Kuo A. D., The six determinants of gait and the inverted pendulum analogy: a dynamic walking perspective. *Human Movement Science*, 2007, 26, 617–656.
7. Kajita, S., Kanehiro, F., Kaneko, K., Yok, K., Hirukawa, H., The 3D linear inverted pendulum model: a simple modeling for a biped walking pattern generation. *Proceedings of the 2001 IEEE/RSJ, International Conference on Intelligent Robots and Systems*, Maui, 2001, 239–246.
8. R. M. Ghigliazza, R. M., Altendorfer, R., Holmes, P., D. Koditschek, D., A simply stabilized running model. *SIAM Journal on Applied Dynamical Systems*, 2013, 2(2), 187–218.
9. Otani, T., Hashimoto, K., Yahara, M., Miyamae, S., Isomichi, T., Hanawa, S., Sakaguchi, M., Kawakami, Y., Lim, H., Takanishi, A., Utilization of human-like pelvic rotation for running robot, *Frontiers in Robotics and AI*, 2015, 2 (article 17), 1–9.
10. Lim, H., Ogura, Y., Takanishi, A., Locomotion pattern generation and mechanisms of a new biped walking machine. *Proceedings of Royal Society, Proceeding A*, 2008, 464(2089), 273–288.
11. Chigarev, A., Borisov, A., Simulation of controlled motion of the bipedal anthropomorphic mechanism. *Russian Journal of Biomechanics*, 2010, 1(51), 74–88 (in Russian).

12. Zhang, L., Brunnett, G., Rusdorf, S., Real-time human motion capture with simple marker sets and monocular video. *Journal of Virtual Reality and Broadcasting*, 2011, 8(1) (Article 1), 1–14.
13. Dodd, K. E., Morris, M. E., Matyas, T. A., Wrigley, T. V., Goldie, P. A., Lateral pelvic displacement during walking: retest reliability of a new method of measurement. *Gait & Posture*, 1988, 7(3), 243–250.
14. Galdeano, D., Bonnet, V., Bennehar, M., Fraise, P., Chemori, A., Partial human data in design of human-like walking control in humanoid robotics. *10th IFAC Symposium on Robot Control*, Dubrovnik, 2012, 485–490.
15. Ito, T., Walking motion analysis using small acceleration sensors. *International Journal of Simulation: Systems, Science and Technology*, 2009, 10(3), 65–71.
16. Tanaka, S., Motoi, K., Nogawa, M., Yamakoshi, K., A new portable device for ambulatory monitoring of human posture and walking velocity using miniature accelerometers and gyroscope. *Engineering in Medicine and Biology Society, IEMBS '04. 26th Annual International Conference of the IEEE*, 2004, 1, 2283–2286.
17. Cross, R., Standing, walking, running, and jumping on a force plate. *American Journal of Physics*, 1999, 67(4), 304–309.
18. Marasovic, T., Cecic, M., Zanchi, V., Analysis and interpretation of ground reaction forces in normal gait. *WSEAS TRANSACTIONS on SYSTEMS*, 2009, 8(6), 1105–1114.
19. Yorozu, A., Moriguchi, T., Takahashi, M., Improved leg tracking considering gait phase and spline-based interpolation during turning motion in walk tests. *Sensors*, 2015, 15(9), 22451–22472.
20. de Araújo, V.M., Alsina, P.J., Soares, L.S., de Medeiros, A.A.D., Generation of anthropomorphic movements for an active orthosis for lower limbs. *ABCMSymposium Series in Mechatronics*, 2012, 5 (Section VII - Robotics), 1052–1057.
21. Yuan, K., Parri, A., Yan, T., Wang, L., Minih, M., Wang, Q., Vitiello, N., A realtime locomotion mode recognition method for an active pelvis orthosis. *2015 IEEE/RSJ International Conference on Intelligent Robots and Systems (IROS) proceedings*, 2015, 6196–6201.

22. Goodworth, A. D., Peterka R. J., Sensorimotor integration for multi-segmental frontal plane balance control in humans. *Journal of Neurophysiology*, 2012, 107(1), 12–28.
23. Suleiman, W., Monin, A., Laumond, J.-P., Synthesizing and modeling human locomotion using system identification. *IEEE International Conference on Intelligent Robots and Systems (IROS)*, Beijing, 2006, 1972–1977.
24. Xie, H.-L., He, N., Li, F., Yang, J.-Y., The bionic design and system identification of intelligent bionic leg with magneto-rheological. *Technical Gazette*, 2015, 22(5), 1093–1098.
25. Marholt, J., Gazdos, F., Modelling, identification and simulation of the inverted pendulum PS600. *Acta Montanistica Slovaca*, 2010, 15(1), 14–18.
26. Uyanik, I., Ankarali, M. M., Cowan N. J., Morgul, O., Saranli, U., Identification of a vertical hopping robot model via harmonic transfer functions. *Trans. Inst. Measurement Control*, 2015, 1–11 [Online].
27. Ankarali, M. M., Cowan, N. J., System identification of rhythmic hybrid dynamical systems via discrete time harmonic transfer functions. *53rd IEEE conference on decision and control (CDC'14)*, Los Angeles, 2014, 1017–1022.
28. Ankarali, M. M., Saranli, U., Control of underactuated planar pronking through an embedded spring-mass hopper template. *Autonomous Robots*, 2011, 30(2), 217–231.
29. Boonstra, T. A., Schouten, A. C., van der Kooji, H., Identification of the contribution of the ankle and hip joints to multi-segmental balance control. *Journal of NeuroEngineering and Rehabilitation*, 2013, 1–18.
30. Torres, S., Becerra, V. M., Nonlinear identification of a two link robotic system using dynamic neural networks. *SYSTEM IDENTIFICATION, A Proceedings volume from the 13th IFAC Symposium on System Identification*, Rotterdam, 2003, 363-368.
31. Harischandra, N., Computer simulation of the neural control of locomotion in the cat, *PhD thesis*, Royal Institute of Technology, Stockholm, 2011.
32. Ghan, J., Kazerooni, H., System identification for the Berkeley lower extremity exoskeleton (BLEEX). *Proceedings of the 2006 IEEE International Conference on Robotics and Automation*, Orlando, 2006, 3477–3484.

33. Park, H.-W., Sreenath, K., Hurst, J., Grizzle, J. W., Identification of a bipedal robot with a compliant drivetrain: Parameter estimation for control design. *IEEE Control Systems Magazine (CSM)*, 2011, 31(2), 63–88.
34. Ebnezar, J., Essentials of orthopedics and physiotherapists, *Jaypee Brothers*, New Delhi, 2003.
35. Valovska, A. T., Pelvic pain management, *Oxford University Press*, New York, 2016.
36. Tyler, T. F., Silvers, H. J., Gerhardt, M. B., Nicholas, S. J., Groin injuries in sports medicine. *Sports Health*, 2010, 2(3), 231–236.
37. Saxena, P., Sakale, H., Agrawal, Introduction to pelvic injury and its acute management. *Symposium on pelvic trauma*, 2014, 7(1), 1–7.
38. Chien, L.-C., Cheng, H.-M., Chen, W.-C., Tsai, M.-C., Pelvic fracture and risk factors for mortality: a population-based study in Taiwan. *European Journal of Trauma and Emergency Surgery*, 2009, 36(2), 131-137.
39. Matityahu, A., Elson, J., Morshed, S., Marmor, M., Survivorship and severe complications are worse for octogenarians and elderly patients with pelvic fractures as compared to adults: data from the national trauma data bank. *Journal of Osteoporosis*, 2012, 2012, 1–10.
40. Report on: age and sex composition in the United States, United States Census Bureau, 2012.
41. Hidler, J., Nichols, D., Pelliccio, M., Brady, K., Campbell, D. D., Kahn, J. H., Hornby, T. G., Multicenter randomized clinical trial evaluating the effectiveness of the Lokomat in subacute stroke. *Neurorehabilitation and Neural Repair*, 2009, 23(1), 5–13.
42. Vaney, C., Gattlen, B., Lugon-Moulin, V., Meichtry, A., Hausammann, R., Foinant, D., Anchisi-Bellwald, A. M., Palaci, C., Hilfiker, R., Robotic-assisted step training (lokomat) not superior to equal intensity of over-ground rehabilitation in patients with multiple sclerosis. *Neurorehabilitation and Neural Repair*, 2012, 26(3), 212–221.
43. Hilfiker, R., Vaney, C., Gattlen, B., Meichtry, A., Deriaz, O., Lugon-Moulin, V., Anchisi-Bellwald, A. M., Palaci, C., Foinant, D., Terrier, P., Local dynamic stability as a responsive index for the evaluation of rehabilitation effect on fall risk in patients with multiple sclerosis: a longitudinal study. *BMC Research Notes*, 2013, 6:230, [Online].

44. Verchenko, A., Design of a control system of experimental plant for pelvis movement imitation, *MSc. thesis*, Tallinn University of Technology, 2015.
45. Obusek, J. P., Holt, K. P., Rosestein, R. M., The hybrid mass-spring pendulum model of human leg swinging: stiffness in the control of cycle period. *Biological Cybernetics*, Springer-Verlag, 1995, 73, 139–147.
46. Bishop, M., Fiolkowski, P., Conrad, B., Brunt, D., Horodyski, M., Athletic footwear, leg stiffness, and running kinematics. *Journal of Athletic Training*, 2006, 41(4), 387–392.
47. Dudenhausen, J. W., Practical obstetrics, *Walter de Gruyter GmbH*, Berlin/Boston, 2014.
48. Neumann, D., Kinesiology of the musculoskeletal system, *2nd ed. Elsevier Health Sciences*, 2013.
49. Michaud, S. B., Gard, S. A., Childress, D. S., A preliminary investigation of pelvic obliquity patterns during gait in persons with transtibial and transfemoral amputation. *Journal of Rehabilitation Research and Development*, 2000, 37(1), 1–10.
50. Zhigailov, S., Musalimov, V., Aryassov, G., Design of experimental stand for human gait imitation, *Proceedings of the 9th International Conference of DAAAM Baltic*, Tallinn, 2014, 300–304.
51. Finni, T., Hodgson, J. A., Lai, A. M., Edgerton, V. R., Sinha, S., Nonuniform strain of human soleus aponeurosis-tendon complex during submaximal voluntary contractions in vivo. *Journal of Applied Physiology*, 2003, 95(2), 829–837.
52. Tao, W., Liu, T., Zheng, R., Feng, H., Gait analysis using wearable sensors. *Sensors*, 2012, 2(2), 2255–2283.
53. Korotkin, D., Kuznetcov, A., Inertial measurement system for human gait analysis, *Proceedings of 8th International Conference on Body Area Networks*, Brussels, 2013, 414–419.
54. Zhigailov, S., Kuznetcov, A., Musalimov, V., Aryassov, G., Measurement and analysis of human lower limbs movement parameters during walking. *Solid State Phenomena*, 2015, 220–221, 538–543.
55. Aryassov, G., Kuznetcov, A., Musalimov, V., Lower limb mathematical modeling with inertial motion capture during normal walking. *Proceedings of*

the International Conference on Integrity, Reliability and Failure, 2013, 505–506.

56. Zhigailov, S., Verchenko, A., Musalimov, V., Aryassov, G., Calculation of plate plane motion parameters using inertial measurement system. *Proceedings of the 10th International Conference of DAAAM Baltic*, Tallinn, 2015, 192–198.

57. Zhigailov, S., Musalimov, V., Aryassov, G., Penkov, I., Modelling and simulation of human lower-limb motion. *International Review on Modelling and Simulations (I.RE.MO.S.)*, 2016, 9(2), 114–123.

58. Kapandzhi, A., Lower limb. Functional anatomy, *Eksmo-press*, Moscow, 2010 (in Russian).

59. Mohamed, E. E., Useh, U., Mtshali, B. F., Q-angle, pelvic width, and intercondylar notch width as predictors of knee injuries in women soccer players in South Africa. *African Health Sciences*, 2012, 12(2), 174–180.

60. Milic, L., Multirate filtering for digital signal processing: matlab applications, University of Belgrad, Serbia, 2009.

61. Lutovac, M. D., Tosic, D. V., Evans, B. L., Filter design for signal processing using MATLAB and mathematica, *Prentice Hall*, 2001.

62. Engelberg, S., Digital signal processing, signals and communication technologies, *Springer*, 2008.

63. Kyu, M. T., Aung, Z. M., Naing, Z. M., Design and implementation of active filter for data acquisition system. *International conference on: Information Management and Engineering*, Kuala Lumpur, 2009, 406–410.

64. Euston, M., Coote, P., Mahony, R., Kim J., Hamel, T., A Complementary Filter for Attitude Estimation of a Fixed-Wing UAV. *Proceeding of 2008 IEEE/RSJ International Conference on Intelligent Robots and Systems*, 2008, 340–345.

65. Zhi, R., A drift eliminated attitude & position estimation algorithm in 3D, *MSc. thesis*, University of Vermont, 2016.

66. Smyth, G. K., Numerical integration, Encyclopedia of Biostatistics, *John Wiley & Sons*, 1998.

67. Young, T., Mohlenkamp M. J., Introduction to numerical methods and matlab programming for engineers, Department of Mathematics, Ohio University, 2015.

68. Rubinshtein, I., Modeling movement of the lower human limbs by using IT technology. *MSc. thesis*, Tallinn University of Technology, 2016.
69. Musalimov, V. M., Sizova, A. A., Ivanov, E. K., Krolov, N. A., Tkatchev, A. L., The basics of tribonics, Saint Petersburg National Research University of Information Technologies, Mechanics and Optics, Saint-Petersburg, 2009. (in Russian)
70. Musalimov, V., Valetov, V., Dynamics of frictional interaction, Saint Petersburg National Research University of Information Technologies, Mechanics and Optics, Saint-Petersburg, 2006 (in Russian).
71. Ljung, L., System identification toolbox. Getting started guide, *The MathWorks, Inc.*, 2015.
72. Kolganov, A., Main branches of modern control theory, Ivanovo State Energy University, 2013 (in Russian).
73. Miroshnik, I., Automatic control theory. Linear systems. *Piter*, Saint Petersburg, 2005.
74. Antsaklis, P. J., Michel, A. N., Response of linear systems, Linear systems, *Springer*, 2006.
75. Winston, A. B., Observer incorporated neoclassical controller design: a discrete perspective. *MSc thesis*, Marquette University, 2009.
76. Aldemir, A., Alpbaz, M., Discrete-time state-space modeling of a wireless control system with matlab. *International Journal of Modern Trends in Engineering and Research*, 2015, 2(8), 124–135.
77. Kwakernaak, H., Sivan, R., Linear optimal control systems, *John Wiley & Sons*, New York, 1972.
78. Doetsch, G., Guide to the practical application of the Laplace transform and Z-transform, *Nauka*, Moskow, 1971 (in Russian).
79. Bahar, E., The indefinite Z-transform technique and application to analysis of difference equations. *Journal of Engineering Mathematics*, 1972, 6(2), 125–132.
80. Krivosheev, V., Fundamentals of control theory, Vladivostok State University of Economics and Service, Russia, 2000 (in Russian).

81. Besekersky, V., Popov, E., Automatic control systems theory, Saint-Petersburg, 2003 (in Russian).
82. Bakaev, V., Automatic control theory, Vologda State Technical University, 2004 (in Russian).
83. Novikov, V., Fundamentals of signals wavelet-analysis, Saint-Petersburg, 1999 (in Russian).
84. Golodnaya, N., Shuman, G., Statistic control of statistic hypothesis. Vladivostok State University of Economics and Service, Russia, 2011 (in Russian).
85. Vogler, L. E., Norton, K. A., Graphs and tables of the significance levels $F(v_1, v_2, p)$ for the Fisher-Snedecor variance ratio, U.S. Department of Standarts, National Bureau of Statistics, Boulder, 1957.
86. Steiger, J. H., Introductory distribution theory, Department of psychology and human development, Vanderbilt University, 2012.
87. Dixon W. J., Dean, R. B., Simplified statistics for small numbers of observations. *Analytical Chemistry*, 1951, 23(4), 936–938.
88. Dixon, W. J., Ratios involving extreme values. *The Annals of Mathematical Statistics*, 1951, 22(1), 68–78.

OTHER PUBLICATIONS

1. Aryassov, G. Zhigailov, S. Zinovjev, E., Development of movement algorithms for a robot manipulator. *Proceedings of the 8th International Conference od DAAAM Baltic*, Tallinn, 2012, 262–267.
2. Aryassov, G., Zhigailov, S., Optimal Design of system of cross-beams. *Mechatronic Systems and Materials IV*, 2013, 675–680.
3. Gornostajev, D., Aryassov, G., Zhigailov, S., Development of the calculation method of plates for optimization of barge hull thickness. *Solid State Phenomena*, 2015, 220–221, 256–261.

ACKNOWLEDGEMENTS

I would like to express my deep gratitude to my supervisors, Gennady Aryassov and Victor Musalimov for their unmeasurable help during process of writing this PhD work. Playing different roles, they made everything they could this work be finished.

I would like to thank Mart Tamre, head of the Mechatronics Department, for his patience and giving me new chances.

I would also like to thank Igor Penkov personally and everyone who helped me to conduct the experiments and who gave good advice.

I greatly honour my family: my mom, dad, and sister for their love, moral support, and remarkable encouragement.

ABSTRACT

Experimental and Analytical Modelling of Pelvic Motion

According to statistics from the World Health Organization, today, the illnesses of the musculoskeletal system (MSS) rank second after heart diseases. In this case, the risk of diseases of the spine, bones, and joints are not attributable to any one group, regardless of age or gender. Difficulty walking often causes problems in other organs, making diseases of the MSS a serious problem. One of the methods of rehabilitation of the human MSS is the use of special methods of training in special rehabilitation trainers. However, such systems are often associated with high costs. Therefore, it was decided to develop a relatively inexpensive model of a rehabilitation trainer, which can be used even in small medical centres. The simulators invented by the engineer G. Zander have been chosen as the most similar to describing the experimental prototype in this work because of having saddle in some of his constructions. However, having only one degree of freedom (DOF), such trainers are not effective and have become out of date over the lack of recovering abilities.

The main objectives of this work are to create a mathematical model and construct a mechanical heel-pelvis system motion simulation in the frontal plane for its subsequent use in human lower-limb recovery in the near future.

This thesis consists of 4 parts: 1) an overview of the existing mathematical models for simulating human lower-limb motion and overview of the use of identification methods for human lower-limb motion simulation and the description of a new approach to mechanical heel-pelvis system mathematical modelling; 2) a short analysis of input data (heel displacements while walking/running) and description of the experimental prototype creation of a mechanical heel-pelvis motion system with some particularities of its usage; 3) the algorithm for the initial data captured by IMUs placed on a plate simulating pelvic processing; and 4) the use of the identification method for finding mechanical heel-pelvis motion system parameters and mathematical models shown in differential equations of the second kind.

Chapter 1 describes the classification of the mathematical models of lower limbs according to the simplicity of constructions and the possible precision of mathematical models. The foundation of a new experimental and analytical approach to biomechanical system modelling is represented on the example of dynamical system consisting of one input, the blackbox and one output. Moreover, the base steps of the work, used methodology and tools during this work are listed and explained.

Chapter 2 gives a short description of heel displacement curve selection and describes the technical tasks appearing in the process of design, assembly and work of the experimental prototype. The logical foundations of the design and

choice of mechanical, measurement and control system components specifying the motion of experimental prototype links are shown. In addition, the principles of choice of 3 experimental parameters are explained.

Chapter 3 explains the entire process of experimental data processing to obtain the output signal of plate-pelvis motion by axes, which is later used for identification of the mechanical heel-pelvis system motion parameters and the mathematical models. The main part of this chapter is dedicated to the work of the algorithm for IMU signal processing for plate-pelvis plane motion, shown in the example of one of the experimental modes. First, the IMU unprocessed data was statistically prepared for subsequent steps. After that, a low-pass Butterworth filter for accelerometer signal filtering was designed. The evaluation of the results of the unprocessed and filtered signal comparison (F -test, Appendix 2) was made to approve the need for filter use. Then, the average signals of IMU accelerometers to simplify data processing and evaluate the accelerometer similarity results (Appendix 3) were found for axes y and z . The next step is the design and usage of a complimentary filter to avoid the effect of angle floating. Afterwards, the gravity forces acting on IMUs during the experiments were assigned for both axes and subtracted from the filtered accelerations. A choice of integration method was made to obtain the arrays of velocities and displacements from filtered accelerations without gravity force saving the shape of filtered accelerations profiles. The combination of chosen low-pass and complimentary filters and the method of integration made it possible to avoid difficult calculations from theoretical mechanics and to replace them with a simpler algorithm. After that, the shape of the displacements was corrected with the use of cubic splines. Then, the absence of the presence of outliers was determined from the obtained maximal values of displacements (Q -test, Appendix 4) for axes y and z . Finally, the laws of motion of a plate pelvis by axes were finally determined.

Chapter 4 provides an identification method in this work based on the mechanical heel-pelvis system. First, the state-space representation was found in continuous-time form with one input and one output along both axes and the black box between input and output. Then, the transfer functions for axes y and z were calculated. On the basis of defined transfer functions, the differential equations of mechanical system motions have been found. To control the determination of state-space representation in continuous-time form, state-space matrix coefficients and transfer functions were found in discrete-time form too, which has practically no difference from continuous-time representation.

Finally, it can be concluded that all aims proposed in this work were completely achieved.

KOKKUVÕTE

Vaagna liikumise eksperimentaalne ja analüütiline modelleerimine

Vastavalt Maailma Tervishoiuorganisatsiooni statistikale on lihasluukonna haigused ühed levinumad ning on oma leviku poolest teisel kohal peale südameveresoonekonna haigusi. Seetõttu ei ole selja, luude ja liigeste haiguste riski eest kindlustatud ükski isik sõltumata vanusest ja soost. Tihti põhjustavad inimese kõndimisraskused probleeme ka teiste organite töös, mistõttu lihas-luukonna haigused on tõsine probleem.

Üks meetod inimeste lihasluukonna taastusravis on kasutada spetsiaalseid liikumist taastavaid trenadžõure, kuid sellised süsteemid on sageli kallid ja seotud suurte kulutustega. Seetõttu otsustati projekteerida odav taastusravi trenadžõör, mille saaksid soetada ka väikesed meditsiinikeskused. Antud töös loodud eksperimentaalse prototüübi iseloomustamiseks on kasutatud Zanderi simulaatoreid nende lähima sarnasuse tõttu. Kuna aga Zanderi simulaatoritel on ainult üks vabadusaste, siis on need väikese efektiivsusega ja tänaseks vananenud.

Käesoleva töö eesmärgiks on identifitseerimise meetodi alusel mehaanilise süsteemi jalakand-vaagen matemaatilise mudeli ja võimaliku konstruktsiooni väljatöötamine, mida saaks kasutada inimeste liikumiskõnnakute taastamiseks lähitulevikus.

Doktoritöö koosneb neljast osast: 1) lihas-luukonna alumise osa liikumise simuleerimiseks kasutatavate eksisteerivate matemaatiliste mudelite ülevaade, lihas-luukonna alumise osa liikumise simuleerimiseks kasutatavate identifitseerimismeetodite ülevaade ning uue eksperimentaalse ja analüütilise meetodi kirjeldamine; 2) sisendandmete lühianalüüs (jalakanna siirded) ning mehaanilise süsteemi jalakand-vaagen liikumise simuleerimiseks loodava eksperimentaalse prototüübi kirjeldus; 3) sisendandmete töötlemise algoritm, mis saadud vaagna liikumise jäljendamiseks kasutatud katseplaadile paigaldatud kiirendusanduritest; 4) identifitseerimise meetodi kasutamine mehaanilise süsteemi jalakand-vaagen parameetrite leidmiseks ning süsteemi liikumise kirjeldus diferentsiaalvõrranditega.

Peatükk 1 kirjeldab lihas-luukonna alumise osa matemaatiliste mudelite klassifikatsiooni nende lihtsuse ja täpsuse järgi. Peatüki teine osa annab ülevaate identifitseerimise meetoditest, mida on kasutatud lihas-luukonna alumise osa liikumise kirjeldamisel. Peatüki viimases osas on kirjeldatud uut eksperimentaalset ja analüütilist lähenemist biomehaaniliste süsteemide modelleerimiseks.

Peatükis 2 on antud jalakanna siirete kõverjoonte valiku analüüs ning samuti on kirjeldatud eksperimentaalse prototüübi väljatöötamisel tekkivaid tehnilisi ülesandeid ja nende lahendusi. Samuti on esitatud eksperimentaalse prototüübi mehaanilise konstruktsiooni ja mõõtesüsteemi komponentide valikute põhimõtt-

ted. Kirjeldatud konstruktsioon võimaldab saada väljundsignaali, mida kasutatakse edasi identifitseerimise meetodis.

Kolmas peatükk selgitab eksperimentaalse andmetöötluse kogu protsessi, selleks et saada kätte plaadi-vaagna telgedesuunalise liikumise väljundsignaal. Antud signaali kasutatakse hiljem mehhaanilise süsteemi jalakand-vaagen liikumise parameetrite ja matemaatiliste mudelite identifitseerimiseks. Antud peatüki põhiosa on pühendatud inertsiaal mõõteandurite (IMA) signaalide töötlemise algoritmidele plaadi-vaagna tasapinnalises liikumises ning selle kohta on esitatud ka näide ühe eksperimentaalse režiimi kohta. Esmalt valmistati statistiliselt ette IMA töötlemata andmed järgnevateks etappideks. Peale andmete statistilist töötlust töötati välja Butterworth'i madalpääsfilter kiirendusandurite signaalide filtreerimiseks. Seejärel võrreldi töötlemata ja filtreeritud signaalide tulemusi (F -test, Lisa 2), mis kinnitas filtri kasutamise vajalikkust. Andmete töötlemise lihtsustamiseks ning kiirendusandurite signaalide sarnasuse hindamiseks leiti IMA signaalide keskmised väärtused ka telgede y ja z jaoks. Järgmise sammuna töötati välja ja võeti kasutusele lisafiltrid, et vältida signaalide nihutamist. Seejärel määrati gravitatsioonijõudude väärtused, mis mõjusid IMA-le katsete käigus telgede suhtes ning lahutati need filtreeritud kiirendustest. Integreerimismeetodi valik põhines asjaolul, et see võimaldas saada kiiruste ja siirete massiivid filtreeritud kiirenduste väärtustest ilma gravitatsioonijõudude mõjuta säilitades samal ajal signaalide kuju. Madalpääs- ja lisafiltrite kasutamine kombineerituna integreerimismeetodiga võimaldas vältida teoreetilise mehaanika keerukaid arvutusi ning asendada need lihtsama algoritmiga. Seejärel korregeeriti siirete kõverate kujud kolmandat järku joontega. Võõrväärtuste puudumine määrati telgede y ja z suunaliste maksimaalsete siirete kaudu (Q -test, Lisa 4). Lõpuks määrati süsteemi plaat-vaagen telgedesuunalised liikumisseadused.

Peatükis 4 on esitatud mehhaanilise süsteemi jalakand-vaagen identifitseerimise meetod. Esiteks leiti süsteemi pidevaja olekuvõrrandid ühe sisendi ja väljundi korral iga telje jaoks ning must kast sisendi ja väljundi vahel. Seejärel leiti y ja z telje ülekandefunktsioonid. Defineeritud ülekandefunktsiooni põhjal koostati mehhaanilise süsteemi liikumise võrrandid. Süsteemi pidevaja olekuvõrrandite kontrollimiseks koostati süsteemi ka diskreetaja olekuvõrrandid ning ülekandefunktsioon, mis praktiliselt ei erinev pidevaja olekuvõrranditest ning ülekandefunktsioonist.

Kokkuvõtlikult võib öelda, et kõik selle töö eesmärgid olid saavutatud.

the supporting part (6,7,18), the restrictive elements (24,25,26,27,28,29,30,31), additional loads (13) and IMUs (12).

The mechanical construction of the prototype works in the following way. After launching the motors (1 and 8), the left rack (2) starts to go up and the right rack (9) goes down (Fig. 2.2(a)). At the same time, the compensating plate of right leg (10) and bearing (23) gets up from outer shelf of the bent plate (25), and the compensating plate of the left leg gradually falls on the shelf (24). With further movement of the left foot the up springs (17) and the pull (16) become weakened, and the angle between the plates (3 and 4) on the bearing (15) decreases. Together with this, the bearing (22) of the right leg moves down, rests on the plate (27), and bends it inwardly due to the bolt without locking nuts (31) until the moment when the bearing (22) will not enter into the space limited by the plates (25 and 27) and lift the plate (10) up the shelf. Accordingly, the angle between the plates (10 and 11) on the bearing (23) increase until the rack (9) reaches the lowest point. At the same time, the hinge (21) rises and gives force to the spring (20). This simulates the right side elevation of the pelvic plate (5) (lifting of the thigh). Rotation takes place around the middle point of the plate (5), the hinge (18) and the force are transmitted to the spring (19). The resistance to this by the left leg does not occur because the left leg elements at this point are weakened. When a certain angle of inclination of the horizontal plate occurs, the support plate (7) and the rotation support bearing (6) begin to move left until the moment when the plate (7) abuts on the restrictive removable plates (29) (Fig. 2.2(b)). When the right rack reaches its lower position point, the left rack reaches its highest point (Fig. 2.2(c)). This point is the end of the first half step.

The second half step occurs in a similar manner, but the left foot goes down, and the right leg goes up. At the same time, the thigh of the left leg is lifted, and the connecting plate is rotated to the right until it stops at the right restrictive plate (29). The bearings (28) are needed to fix the plate (5) in the frontal plane. The restrictive plates (29) can be removed and delivered to form a new angle of rotation of supporting bearing plates (6). Three combinations of angles are needed for different models of the experiment. In addition, load (13) is also used in various models of experiments (Chapters 3 and 4 of the thesis).

Appendix 2. Statistical evaluation of signals (*F*-test)

Statistical evaluation of the measured unprocessed and processed signals in order to confirm the need to use filters and estimate the level of noise in the unprocessed signals is shown in Appendix 2.

To avoid the presence of failed cycles of experimental steps, we select the least noisy periods of full steps for all modes. Choosing such periods, the measurements are 911 (0,021 s), 930 (0,025 s), and 978 (0,035 s) for each of the experimental modes.

Common statistical parameters of the unprocessed and processed signals are found using standard functions of the software package MATLAB. Tables A2.1 and A2.2 show the main parameters of the measured unprocessed and processed low-pass filter signals for axes *y* and *z*, where the letters *un* in brackets next to the name of the experimental mode indicates an unprocessed signal, and the letters *pr* indicate processed signals, respectively.

Table A2.1. Statistical parameters of unprocessed and processed signals for the *y*-axis,

	Dy_{min}	Dy_{max}	μ_y	M_y	σ_y
$\alpha 1 w 1 t_{m1}(un)$	5,8192	4,8339	-0,4328	-0,6411	0,6030
$\alpha 1 w 1 t_{m1}(pr)$	-1,4796	1,1860	-0,2574	-0,4101	0,4831
$\alpha 1 w 1 t_{m2}(un)$	-4,0035	4,3408	-0,4985	-0,7055	0,5727
$\alpha 1 w 1 t_{m2}(pr)$	-1,6458	1,1694	-0,3554	-0,5377	0,4890
$\alpha 1 w 1 t_{m3}(un)$	-3,4173	3,9019	-0,8290	-0,9576	0,5464
$\alpha 1 w 1 t_{m3}(pr)$	-2,0521	0,6732	-0,7019	-0,8501	0,4905
$\alpha 1 w 2 t_{m1}(un)$	-4,4425	3,8275	-0,5755	-0,7518	0,6292
$\alpha 1 w 2 t_{m1}(pr)$	-2,0260	1,0946	-0,4837	-0,6910	0,5619
$\alpha 1 w 2 t_{m2}(un)$	-3,1499	4,2603	-0,2242	-0,2064	0,5423
$\alpha 1 w 2 t_{m2}(pr)$	-1,5232	1,1933	-0,1469	-0,0875	0,4799
$\alpha 1 w 2 t_{m3}(un)$	-2,9100	3,2715	-0,4532	-0,4312	0,5709
$\alpha 1 w 2 t_{m3}(pr)$	-1,8413	1,0614	-0,3642	-0,3567	0,5320
$\alpha 1 w 3 t_{m1}(un)$	-4,7122	3,6152	-0,8421	-0,9401	0,6476
$\alpha 1 w 3 t_{m1}(pr)$	-2,0491	0,9280	-0,6817	-0,8025	0,5148
$\alpha 1 w 3 t_{m2}(un)$	-4,0735	5,2551	-0,6718	-0,8163	0,6118
$\alpha 1 w 3 t_{m2}(pr)$	-1,8883	1,1427	-0,4997	-0,6585	0,5171
$\alpha 1 w 3 t_{m3}(un)$	-3,4984	2,3598	-0,7406	-0,9213	0,5558
$\alpha 1 w 3 t_{m3}(pr)$	-1,9300	0,9627	-0,5672	-0,7177	0,5001
$\alpha 2 w 1 t_{m1}(un)$	-4,0127	2,7508	-0,6552	-0,5639	0,6222
$\alpha 2 w 1 t_{m1}(pr)$	-2,2140	1,0708	-0,5509	-0,4564	0,5801
$\alpha 2 w 1 t_{m2}(un)$	-3,1640	2,0811	-0,3737	-0,3810	0,5364
$\alpha 2 w 1 t_{m2}(pr)$	-1,7342	1,1273	-0,2748	-0,1975	0,5124
$\alpha 2 w 1 t_{m3}(un)$	-2,6610	1,7818	-0,5184	-0,4887	0,5514
$\alpha 2 w 1 t_{m3}(pr)$	-1,9291	1,0398	-0,4273	-0,3884	0,5437
$\alpha 2 w 2 t_{m1}(un)$	-5,4022	3,6414	-0,4810	-0,3175	0,5828
$\alpha 2 w 2 t_{m1}(pr)$	-1,8946	0,9104	-0,3561	-0,2128	0,4914
$\alpha 2 w 2 t_{m2}(un)$	-3,8974	3,4913	-0,4849	-0,3312	0,5487
$\alpha 2 w 2 t_{m2}(pr)$	-1,9482	0,9195	-0,3779	-0,2889	0,5214

$\alpha 2w2t_m3(\text{un})$	-3,3691	2,8483	-0,4217	-0,2532	0,5739
$\alpha 2w2t_m3(\text{pr})$	-1,9363	1,0680	-0,3003	-0,1752	0,5306
$\alpha 2w3t_m1(\text{un})$	-5,2624	4,5859	-1,0691	-1,0113	0,7236
$\alpha 2w3t_m1(\text{pr})$	-3,2069	0,8465	-0,8584	-0,7667	0,6165
$\alpha 2w3t_m2(\text{un})$	-4,4959	2,9933	-0,8461	-0,7980	0,5989
$\alpha 2w3t_m2(\text{pr})$	-2,2591	0,7331	-0,6262	-0,5562	0,5344
$\alpha 2w3t_m3(\text{un})$	-3,8398	4,5284	-0,7646	-0,6520	0,5949
$\alpha 2w3t_m3(\text{pr})$	-2,1643	0,8175	-0,5859	-0,5124	0,5379
$\alpha 3w1t_m1(\text{un})$	-3,5715	3,3381	-0,7038	-0,6376	0,6315
$\alpha 3w1t_m1(\text{pr})$	-2,2270	0,9779	-0,5390	-0,4301	0,5901
$\alpha 3w1t_m2(\text{un})$	-2,9650	3,9135	-0,7251	-0,6610	0,6049
$\alpha 3w1t_m2(\text{pr})$	-2,1596	0,9110	-0,5656	-0,4346	0,5661
$\alpha 3w1t_m3(\text{un})$	-3,0111	2,0567	-0,7389	-0,6017	0,5949
$\alpha 3w1t_m3(\text{pr})$	-2,1916	0,9414	-0,5916	-0,5228	0,5757
$\alpha 3w2t_m1(\text{un})$	-6,0494	2,8768	-0,7350	-0,5792	0,6899
$\alpha 3w2t_m1(\text{pr})$	-2,5526	0,9492	-0,5932	-0,4197	0,6218
$\alpha 3w2t_m2(\text{un})$	-4,7920	3,5211	-0,6222	-0,5529	0,6612
$\alpha 3w2t_m2(\text{pr})$	-2,2811	1,0326	-0,4937	-0,3326	0,5974
$\alpha 3w2t_m3(\text{un})$	-4,0463	3,4214	-0,6212	-0,5376	0,6687
$\alpha 3w2t_m3(\text{pr})$	-2,3341	1,2431	-0,5147	-0,4422	0,6443
$\alpha 3w3t_m1(\text{un})$	-8,9892	5,6731	-0,7524	-0,7192	0,7749
$\alpha 3w3t_m1(\text{pr})$	-2,5732	0,9590	-0,6754	-0,5637	0,6246
$\alpha 3w3t_m2(\text{un})$	-6,3609	3,6119	-0,6556	-0,5602	0,7188
$\alpha 3w3t_m2(\text{pr})$	-2,4801	1,0503	-0,5772	-0,4337	0,6301
$\alpha 3w3t_m3(\text{un})$	-5,3456	3,3254	-0,6356	-0,5432	0,6721
$\alpha 3w3t_m3(\text{pr})$	-2,5213	1,0053	-0,5423	-0,4323	0,6219

where Dy_{min} is the minimal value of sample, Dy_{max} is the maximal value of sample, μ_y is the expected value, M_y is the median, and σ_y is the standard deviation.

Table A2.2. Statistical parameters of unprocessed and processed signals for the z-axis,

	Dz_{min}	Dz_{max}	μ_z	M_z	σ_z
$\alpha 1w1t_m1(\text{un})$	2,3522	17,2731	9,8434	9,8510	0,74195
$\alpha 1w1t_m1(\text{pr})$	9,5418	10,3834	9,8239	9,7772	0,0834
$\alpha 1w1t_m2(\text{un})$	1,3767	19,1525	9,8588	9,8191	0,80425
$\alpha 1w1t_m2(\text{pr})$	9,4308	10,5045	9,8533	9,8310	0,10165
$\alpha 1w1t_m3(\text{un})$	3,4589	16,4926	9,7434	9,7290	0,63175
$\alpha 1w1t_m3(\text{pr})$	9,2751	10,0474	9,7714	9,7615	0,0747
$\alpha 1w2t_m1(\text{un})$	-2,5230	16,5389	9,7816	9,8089	0,89305
$\alpha 1w2t_m1(\text{pr})$	9,4399	10,1615	9,7897	9,7810	0,0879
$\alpha 1w2t_m2(\text{un})$	2,7159	18,8703	9,8596	9,8076	0,6771
$\alpha 1w2t_m2(\text{pr})$	9,4131	10,4387	9,8210	9,7496	0,1311
$\alpha 1w2t_m3(\text{un})$	5,4078	13,2060	9,7579	9,8338	0,42215
$\alpha 1w2t_m3(\text{pr})$	9,5123	10,0869	9,7659	9,7259	0,06805
$\alpha 1w3t_m1(\text{un})$	-0,1784	19,5800	9,7530	9,8089	1,13535
$\alpha 1w3t_m1(\text{pr})$	9,3373	10,2514	9,8194	9,8285	0,0959
$\alpha 1w3t_m2(\text{un})$	1,2856	19,5709	9,9108	9,8573	0,9094

$\alpha 1w3t_m2(\text{pr})$	9,1887	10,6977	9,8876	9,8608	0,1214
$\alpha 1w3t_m3(\text{un})$	0,0364	19,5791	9,8068	9,8032	0,75235
$\alpha 1w3t_m3(\text{pr})$	9,4352	10,1513	9,7972	9,7973	0,082
$\alpha 2w1t_m1(\text{un})$	0,0657	19,1516	9,7648	9,8134	0,82545
$\alpha 2w1t_m1(\text{pr})$	9,2338	10,2778	9,7788	9,7447	0,11055
$\alpha 2w1t_m2(\text{un})$	0,5355	19,5083	9,7737	9,7803	0,7474
$\alpha 2w1t_m2(\text{pr})$	9,3152	10,3561	9,7870	9,7776	0,0899
$\alpha 2w1t_m3(\text{un})$	4,8891	14,6608	9,7184	9,7486	0,49275
$\alpha 2w1t_m3(\text{pr})$	9,5012	10,0391	9,7360	9,6923	0,07175
$\alpha 2w2t_m1(\text{un})$	1,6522	18,5371	9,8439	9,8575	0,8702
$\alpha 2w2t_m1(\text{pr})$	9,5210	10,2635	9,8193	9,7555	0,09705
$\alpha 2w2t_m2(\text{un})$	0,1989	19,2632	9,8127	9,8173	0,95095
$\alpha 2w2t_m2(\text{pr})$	9,3713	10,4302	9,7935	9,7664	0,09315
$\alpha 2w2t_m3(\text{un})$	3,6335	17,5437	9,8349	9,8461	0,55275
$\alpha 2w2t_m3(\text{pr})$	9,5738	10,1625	9,8345	9,7939	0,07265
$\alpha 2w3t_m1(\text{un})$	-0,3106	19,5196	9,8102	9,8275	0,97925
$\alpha 2w3t_m1(\text{pr})$	9,3275	10,3965	9,8002	9,8002	0,1084
$\alpha 2w3t_m2(\text{un})$	-0,0853	16,0692	9,8194	9,8301	0,7845
$\alpha 2w3t_m2(\text{pr})$	9,3335	10,3879	9,8160	9,8016	0,09435
$\alpha 2w3t_m3(\text{un})$	-1,0833	16,9991	9,7531	9,7901	0,6916
$\alpha 2w3t_m3(\text{pr})$	9,4124	10,0901	9,7940	9,7892	0,08025
$\alpha 3w1t_m1(\text{un})$	1,3436	17,1866	9,8193	9,8195	0,7341
$\alpha 3w1t_m1(\text{pr})$	9,4487	10,4547	9,8301	9,8054	0,08945
$\alpha 3w1t_m2(\text{un})$	1,4930	19,5508	9,7765	9,7654	0,7196
$\alpha 3w1t_m2(\text{pr})$	9,4672	10,0653	9,7643	9,7585	0,0633
$\alpha 3w1t_m3(\text{un})$	2,9666	15,2579	9,8070	9,8547	0,57855
$\alpha 3w1t_m3(\text{pr})$	9,5315	10,1573	9,7850	9,7624	0,0662
$\alpha 3w2t_m1(\text{un})$	2,5383	19,4992	9,6985	9,7497	1,0072
$\alpha 3w2t_m1(\text{pr})$	9,3080	10,3402	9,7232	9,6931	0,0965
$\alpha 3w2t_m2(\text{un})$	1,4385	19,4892	9,8763	9,8163	0,8349
$\alpha 3w2t_m2(\text{pr})$	9,5345	10,2577	9,8275	9,7853	0,08185
$\alpha 3w2t_m3(\text{un})$	4,5535	17,1345	9,7727	9,7483	0,58945
$\alpha 3w2t_m3(\text{pr})$	9,4177	10,2209	9,7978	9,7818	0,0827
$\alpha 3w3t_m1(\text{un})$	0,9470	19,5342	9,8037	9,8661	1,10225
$\alpha 3w3t_m1(\text{pr})$	9,3365	10,8426	9,7915	9,7580	0,14035
$\alpha 3w3t_m2(\text{un})$	2,8944	19,5081	9,8764	9,8160	0,9158
$\alpha 3w3t_m2(\text{pr})$	8,7473	10,2666	9,7579	9,7846	0,1283
$\alpha 3w3t_m3(\text{un})$	3,9834	18,7442	9,6789	9,6722	0,8867
$\alpha 3w3t_m3(\text{pr})$	8,8845	10,7835	9,7923	9,7867	0,1339

where Dz_{min} is the minimal value of sample, Dz_{max} is the maximal value of sample, μ_z is the expected value, M_z is the median, and σ_z is the standard deviation.

In one example of the same mode of experiments ($\alpha 2w2t_m2$), as we observed in previous chapters, we try to determine the general need of usage filters. For this kind of problem, it is logical to use statistical methods to compare each experimental sample of the unprocessed and processed signals on the respective axes for the same experimental mode. Among these comparative methods are

widely used techniques associated with the definition of the t -test (Student's test) and the F -test (Fisher's test) results. Since the t -test in our case is not rational (noisy signal, a large number of experimental data in the sample, average shift of processed and unprocessed signals according to the horizontal axis), the choice is the F -test.

The main reason we use the F -test is to determine whether the null hypothesis H_0 works or, in other words, whether the requirement of lack uniformity is satisfied in the distributions of 2 samples of unprocessed and processed signals for each model experiment on each axis. From hypothesis H_0 , it follows that the obtained values correspond to the statistical chi-square distribution. However, if the hypothesis H_0 is not satisfied, hypothesis H_1 is true. This indicates the inequality of sample variances of samples of experimental data and a significant excess of the sample variance of the experimental data of the unprocessed signal with respect to the sample variance of experimental data of processed (filtered) signals [84].

Assuming that the experimental values of both samples are considered to have a normal distribution, we find the value of the sample variance for a sample of unprocessed and processed data for the y -axis of the experiment $a2w2t_m2$.

Thus, $\sigma_{y(un)}^2 = 0,3011$; $\sigma_{y(pr)}^2 = 0,2719$.

We define the ratio between the highest and lowest sample variances for the same experimental mode:

$$F_{emp.} = \frac{\sigma_{y(u)}^2}{\sigma_{y(p)}^2} = \frac{0,3011}{0,2719} = 1,1074 \quad (A2.1)$$

Then, we compare the value obtained in Eq. (A2.1) with the empirical values from the Fisher-Snedecor used for the chosen DOF of samples ($th_1 = th_2 = 929$) as the nearest to the quantity of measurement points. Thus, $F_{table} = 1.11$ for 1000 measurements (the next number of table values after the number of measurements) [85].

Because $F_{emp} < F_{table}$, the hypothesis H_0 is approved.

In Fig. A2.1, the chi-square distribution for DOF $th_{1,1} = th_{2,1} = 10$ is shown graphically [86]. The number of degrees of freedom was reduced to improve the shape of plotted curve of probability density function of the chi-squared distribution.

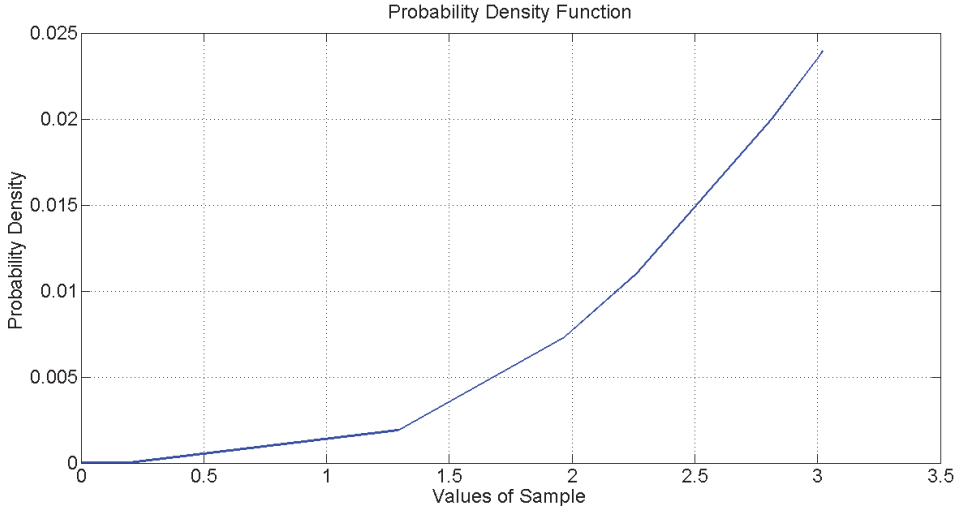


Figure A2.1. Chi-square distribution for experimental data with $th_{1,1,2,1} = 10$.

We find the F -test results for data of the experimental model $\alpha 2w 2t_m 2$ for the z -axis.

We obtain $\sigma_{z(u)}^2 = 0,9043$, $\sigma_{z(p)}^2 = 0,0087$.

Substituting values from Table A2.2, we obtain the empirical value for the F -test for the axis z :

$$F_{emp} = \frac{\sigma_{z(u)}^2}{\sigma_{z(p)}^2} = \frac{0,9043}{0,0087} = 103,9425 \quad (A2.2)$$

This means hypothesis H_1 is accepted, by which $F_{emp} > F_{table}$. It can be concluded that samples of unprocessed and processed signals are not uniform.

Using analogical calculations for all experimental modes, we can make 2 main conclusions:

- 1) Filtering is necessary because the noises (especially for the z -axis) are strong.
- 2) Results of the F -test for all experimental models for the y -axis are on the border between hypotheses H_0 and H_1 .

Appendix 3. Filtered accelerations averaging

The plot for averaging the filtered accelerations for the experimental mode $\alpha 2w2t_m 2$ is shown in Fig. 3.3. In Table A3.1, the parameters of the difference of the filtered acceleration curves, measured with both IMU, are introduced.

Table A3.1. Table of deviations of data from averaged acceleration and accelerations from both IMUs accelerometers for all experimental modes,

Mode	IMU №	T_{total}	T_{exp}	$Dif_y(m^2)$	$Dif_z(m^2)$	$Dif_{ymid}(\frac{m}{s^2})$	$Dif_{zmid}(\frac{m}{s^2})$
$\alpha 1w1t_m 1$	1	340	282	0,108	0,11	$3,840 \cdot 10^{-4}$	$3,794 \cdot 10^{-4}$
	2	340	282	0,122	0,01	$4,348 \cdot 10^{-4}$	$1,773 \cdot 10^{-5}$
$\alpha 1w1t_m 2$	1	272	245	0,109	0,11	$4,441 \cdot 10^{-4}$	$4,489 \cdot 10^{-4}$
	2	272	245	0,131	0,01	$5,343 \cdot 10^{-4}$	$4,081 \cdot 10^{-6}$
$\alpha 1w1t_m 3$	1	304	255	0,126	0,15	$4,937 \cdot 10^{-4}$	$5,803 \cdot 10^{-4}$
	2	304	255	0,150	0,03	$5,898 \cdot 10^{-4}$	$1,254 \cdot 10^{-4}$
$\alpha 1w2t_m 1$	1	307	235	0,138	0,09	$5,889 \cdot 10^{-4}$	$3,872 \cdot 10^{-4}$
	2	307	235	0,155	0,07	$6,583 \cdot 10^{-4}$	$2,808 \cdot 10^{-4}$
$\alpha 1w2t_m 2$	1	280	245	0,136	0,18	$5,563 \cdot 10^{-4}$	$7,265 \cdot 10^{-4}$
	2	280	245	0,155	0,02	$6,310 \cdot 10^{-4}$	$6,530 \cdot 10^{-5}$
$\alpha 1w2t_m 3$	1	303	255	0,144	0,16	$5,659 \cdot 10^{-4}$	$6,431 \cdot 10^{-4}$
	2	303	255	0,165	0,07	$6,482 \cdot 10^{-4}$	$2,549 \cdot 10^{-4}$
$\alpha 1w3t_m 1$	1	232	188	0,116	0,40	$6,149 \cdot 10^{-4}$	$2,127 \cdot 10^{-4}$
	2	232	188	0,139	0,01	$7,378 \cdot 10^{-4}$	$5,851 \cdot 10^{-5}$
$\alpha 1w3t_m 2$	1	270	245	0,103	0,05	$4,225 \cdot 10^{-4}$	$2 \cdot 10^{-4}$
	2	270	245	0,128	0,01	$5,208 \cdot 10^{-4}$	$4,897 \cdot 10^{-5}$
$\alpha 1w3t_m 3$	1	228	204	0,100	0,04	$4,902 \cdot 10^{-4}$	$2,009 \cdot 10^{-4}$
	2	228	204	0,124	0,01	$6,093 \cdot 10^{-4}$	$3,431 \cdot 10^{-5}$
$\alpha 2w1t_m 1$	1	352	282	0,141	0,12	$5,025 \cdot 10^{-4}$	$4,432 \cdot 10^{-4}$
	2	352	282	0,181	0,10	$6,429 \cdot 10^{-4}$	$3,652 \cdot 10^{-4}$
$\alpha 2w1t_m 2$	1	282	245	0,124	0,11	$5,094 \cdot 10^{-4}$	$4,612 \cdot 10^{-4}$
	2	282	245	0,164	0,07	$6,731 \cdot 10^{-4}$	$3,142 \cdot 10^{-4}$
$\alpha 2w1t_m 3$	1	446	306	0,140	0,16	$4,582 \cdot 10^{-4}$	$5,228 \cdot 10^{-4}$
	2	446	306	0,178	0,08	$5,837 \cdot 10^{-4}$	$2,679 \cdot 10^{-4}$
$\alpha 2w2t_m 1$	1	290	235	0,141	0,11	$6,013 \cdot 10^{-4}$	$4,893 \cdot 10^{-4}$
	2	290	235	0,172	0,10	$7,323 \cdot 10^{-4}$	$4,340 \cdot 10^{-4}$
$\alpha 2w2t_m 2$	1	230	196	0,141	0,12	$7,230 \cdot 10^{-4}$	$6,326 \cdot 10^{-4}$
	2	230	196	0,170	0,07	$8,699 \cdot 10^{-4}$	$3,775 \cdot 10^{-4}$
$\alpha 2w2t_m 3$	1	286	255	0,131	0,13	$5,149 \cdot 10^{-4}$	$5,450 \cdot 10^{-4}$
	2	286	255	0,158	0,03	$6,204 \cdot 10^{-4}$	$1,450 \cdot 10^{-4}$
$\alpha 2w3t_m 1$	1	274	235	0,125	0,10	$5,340 \cdot 10^{-4}$	$4,340 \cdot 10^{-4}$
	2	274	235	0,139	0,01	$5,945 \cdot 10^{-4}$	$6,382 \cdot 10^{-5}$
$\alpha 2w3t_m 2$	1	275	245	0,114	0,08	$4,686 \cdot 10^{-4}$	$3,551 \cdot 10^{-4}$
	2	275	245	0,134	0,02	$5,502 \cdot 10^{-4}$	$1,020 \cdot 10^{-4}$
$\alpha 2w3t_m 3$	1	266	255	0,109	0,07	$4,282 \cdot 10^{-4}$	$2,823 \cdot 10^{-4}$
	2	266	255	0,129	0,02	$5,078 \cdot 10^{-4}$	$7,843 \cdot 10^{-5}$
$\alpha 3w1t_m 1$	1	272	235	0,120	0,11	$5,144 \cdot 10^{-4}$	$4,680 \cdot 10^{-4}$

	2	272	235	0,142	0,03	$6,081 \cdot 10^{-4}$	$1,574 \cdot 10^{-4}$
$\alpha 3w1t_m2$	1	282	245	0,123	0,07	$5,033 \cdot 10^{-4}$	$2,857 \cdot 10^{-4}$
	2	282	245	0,148	0,03	$6,053 \cdot 10^{-4}$	$1,265 \cdot 10^{-4}$
$\alpha 3w1t_m3$	1	287	255	0,122	0,11	$4,800 \cdot 10^{-4}$	$4,352 \cdot 10^{-4}$
	2	287	255	0,148	0,01	$5,808 \cdot 10^{-4}$	$7,058 \cdot 10^{-5}$
$\alpha 3w2t_m1$	1	284	235	0,141	0,12	$6,004 \cdot 10^{-4}$	$5,191 \cdot 10^{-4}$
	2	284	235	0,163	0,05	$6,940 \cdot 10^{-4}$	$2,425 \cdot 10^{-4}$
$\alpha 3w2t_m2$	1	327	294	0,135	0,13	$4,616 \cdot 10^{-4}$	$4,523 \cdot 10^{-4}$
	2	327	294	0,157	0,05	$5,354 \cdot 10^{-4}$	$1,836 \cdot 10^{-4}$
$\alpha 3w2t_m3$	1	281	255	0,136	0,12	$5,365 \cdot 10^{-4}$	$4,862 \cdot 10^{-4}$
	2	281	255	0,154	0,03	$6,055 \cdot 10^{-4}$	$1,294 \cdot 10^{-4}$
$\alpha 3w3t_m1$	1	285	235	0,152	0,08	$6,486 \cdot 10^{-4}$	$3,702 \cdot 10^{-4}$
	2	285	235	0,167	0,05	$7,110 \cdot 10^{-4}$	$2,468 \cdot 10^{-4}$
$\alpha 3w3t_m2$	1	338	294	0,144	0,11	$4,915 \cdot 10^{-4}$	$3,843 \cdot 10^{-4}$
	2	338	294	0,160	0,04	$5,452 \cdot 10^{-4}$	$1,632 \cdot 10^{-4}$
$\alpha 3w3t_m3$	1	285	255	0,152	0,12	$5,969 \cdot 10^{-4}$	$4,745 \cdot 10^{-4}$
	2	285	255	0,160	0,07	$6,302 \cdot 10^{-4}$	$2,941 \cdot 10^{-4}$

where: T_{total} is the total time of measurements for corresponding experiments in seconds; T_{exp} is the pure time of experiments with the moving prototype in seconds;

$Dif_y(m^2)$ is the deviation of accelerometer filtered data from average acceleration by the y-axis; $Dif_z(m^2)$ is the deviation of accelerometer filtered data from average acceleration by the z-axis; $Dif_{ymid}(\frac{m}{s^2})$ is the average difference between each measurement of filtered accelerometer data and averaged acceleration data by the y-axis (Eq. (A3.1)); $Dif_{zmid}(\frac{m}{s^2})$ is the average difference between each measurement of filtered accelerometer data and average acceleration data by the z-axis (Eq. (A3.2)).

$$Dif_{ymid} = \frac{Dy}{T_{exp}} \quad (A3.1)$$

$$Dif_{zmid} = \frac{Dz}{T_{exp}} \quad (A3.2)$$

Appendix 4. Determination of outliers presence (Q-test)

On the basis of the data of experimental plate movements (Table A4.1), we conduct a brief assessment to determine the strength of the influence of 1) changes in the angle of rotation of the plate on the support joint, 2) the additional load on the test plate, and 3) the increase/decrease of the step time of the stepper motor on the values of motions of an experimental plate. To assess this, we create a separate table (Table A4.2), which traces the relationship between the variable experimental setting parameters and the arithmetic mean of the plate movements, holding for these regime experiments.

Table A4.1. Dependence between arithmetic means of experimental displacements and setting parameters,

	α ($^{\circ}$)	\bar{y} (m)	\bar{z} (m)
$\alpha 1$	4,8	0,0165	0,0253
$\alpha 2$	6,4	0,0190	0,0256
$\alpha 3$	8,0	0,0208	0,0251
$\alpha(max) - \alpha(min)$	–	0,0043	0,0005
	w (N)	\bar{y} (m)	\bar{z} (m)
w1	16,54	0,0180	0,0252
w2	13,44	0,0190	0,0258
w3	9,08	0,0193	0,0278
$w(max) - w(min)$	–	0,0013	0,0026
	s (s)	\bar{y} (m)	\bar{z} (m)
s1	0,021	0,0189	0,0273
s2	0,025	0,0187	0,0257
s3	0,035	0,0187	0,0259
$s(max) - s(min)$	–	0,0002	0,0016

where \bar{y}, \bar{z} are the arithmetic means by axes y and z .

Three major conclusions can be made from Table A4.1:

- 1) The maximum values of the y -axis movements of the experimental plate are in straight dependence on the change of the angle of the observed plate rotation around the support hinge. At the same time, the z -axis movement is practically independent on changes in the angle of rotation around the support hinge.
- 2) The displacements of the experimental plate are more dependent by the y -axis than by z -axis from the values of additional load.
- 3) Changing the duration of steps of stepper motors has almost no movement effect on the experimental plate.

Assuming that all of the experimental movements have a normal distribution, we use Dixon's Q -test to identify potential outliers in the results [87].

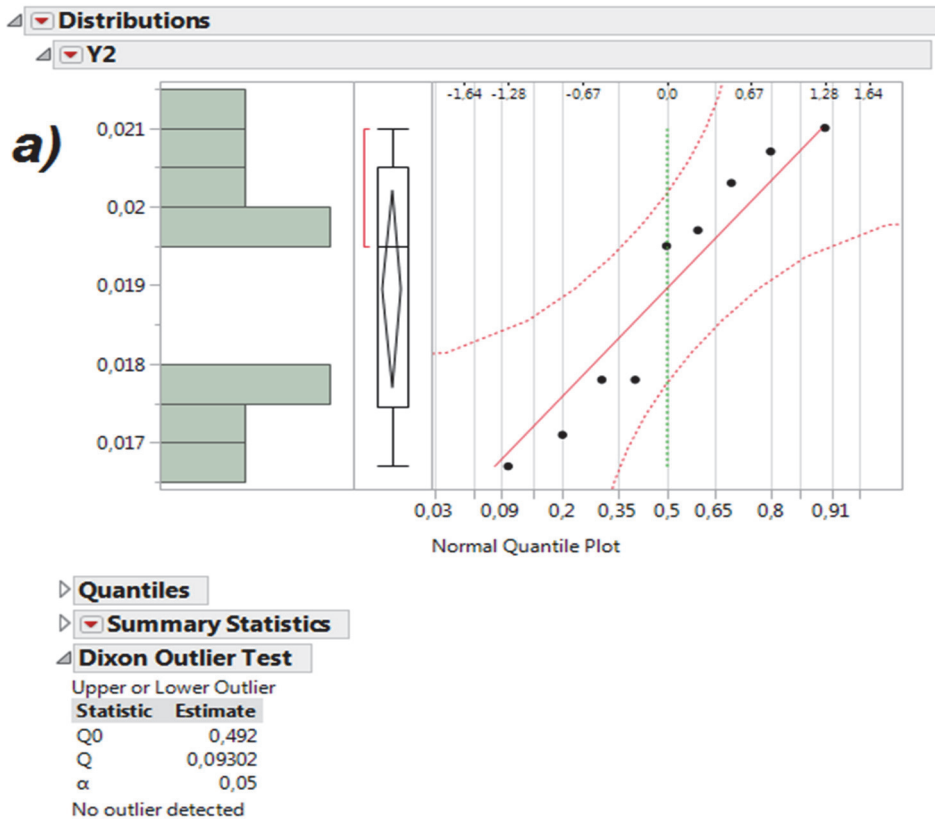
The main expression of Dixon's test is Eq. (A4.1), where the numerator denotes the difference between evaluating an adjacent number of a sample row, and the denominator denotes the difference between the maximum and estimated value of the sample row. All elements of the sample row are placed in ascending order (Eq. (A4.2)) [87,88]:

$$Q = \frac{\gamma_2 - \gamma_1}{\gamma_n - \gamma_1} \quad (\text{A4.1})$$

$$\gamma_1 \leq \gamma_2 \dots \leq \gamma_{n-1} \leq \gamma_n \quad (\text{A4.2})$$

For this purpose, we divide all values of displacements along the y-axis into 3 parts, as they are strongly dependent on the angle of experimental plate rotation around the support hinge. Movements by the z-axis do not have a strict dependence on one of the parameters, so they can be evaluated as a single sample row [56].

Figure A4.1 shows graphical results of the Q -test for movements along the y and z axes at a confidence level of 95%, obtained with the help of an application written for statistical software package, JMP (SAS), to calculate the Q -test.



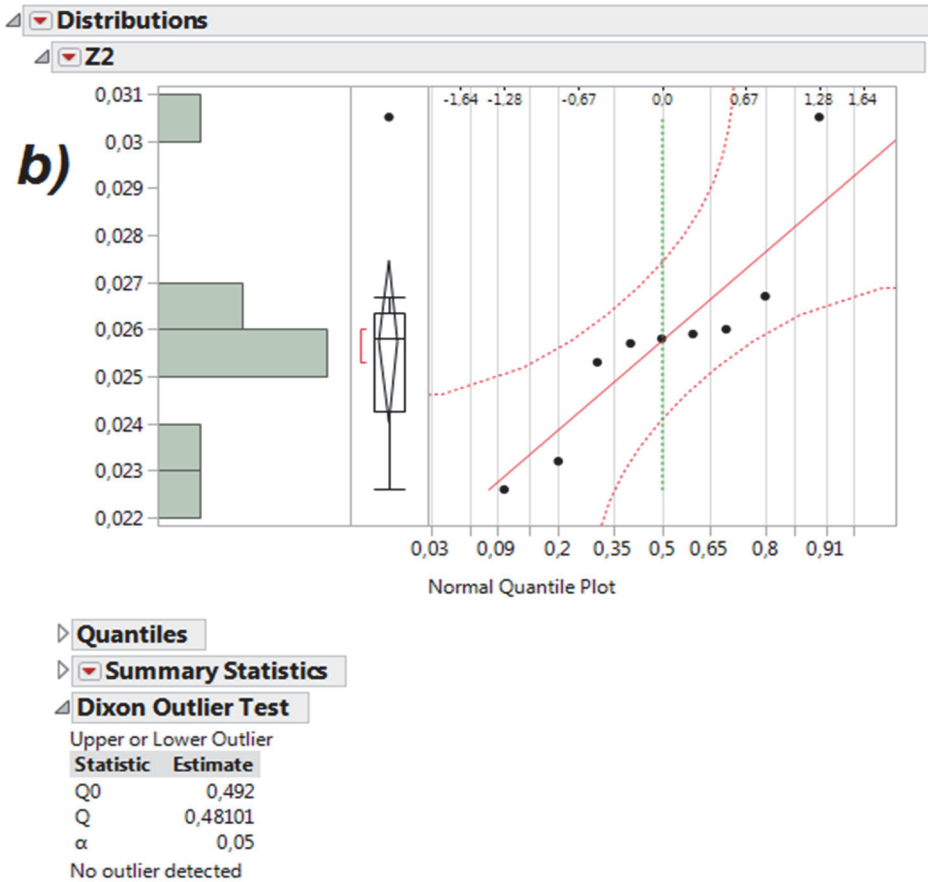


Figure A4.1 Dixon's Q-test results for displacements of the experimental plate by: a) y-axis; b) z-axis.

In Table A4.2 the main statistical parameters for each of the designated samples (arrays) of movements based on the results of Dixon's Q-test for determination of outliers can be seen.

Table A4.2. The main statistical parameters for each of the designated samples (arrays) of movements based on the results of Dixon's Q-test for determination of outliers.

Statistical parameter	y_1	y_2	y_3	z_1	z_2	z_3
Mean	0,0165	0,0190	0,0208	0,0253	0,0257	0,0279
Standard deviation	0,0008	0,0016	0,0012	0,0020	0,0022	0,0010
Standard error mean	0,0003	0,0005	0,0004	0,0007	0,0007	0,0003
Confidence coefficient 95%	No outliers					
Confidence coefficient 99%	No outliers					

The main conclusion of this brief statistical research is that the experiment for simulation of the experimental plate movement was carried out correctly. The experimental plate motion parameters, captured with the measurement system and the proposed data processing algorithm, can be used in further studies. In addition, the importance of each of the 3 variable setting parameters for final experimental results is established.

ELULOOKIRJELDUS

1. Isikuandmed

Ees- ja perekonnanimi
Sünniaeg ja -koht
Kodakondsus
E-posti aadress

Sergei Žigailov
16.04.1986, Sillamäe, Eesti
Eesti
sergsil@gmail.com

2. Hariduskäik

Õppeasutus (nimetus lõpetamise ajal)	Lõpetamise aeg	Haridus (eriala/kraad)
Tallinna Tehnikaülikool	2008	Mehhatroonika, bakalaureusekraad
Tallinna Tehnikaülikool	2010	Mehhatroonika, magistrikraad

3. Keelteoskus (alg-, kesk- või kõrgtase)

Keel	Tase
Vene	Emakeel
Ukraina	Väga hea
Eesti	Hea
Inglise	Hea

4. Teenistuskäik

Töötamise aeg	Tööandja nimetus	Ametikoht
2008–2011	Stoneridge Electronics Eesti	Lihttööline
2011	Esfitech OU	Insener
2011–2014	E.R.S. AS	Insener
2015–2016	Metallurg Engineering OU	Insener

CURRICULUM VITAE

1. Personal data

Name	Sergei Zhigailov
Date and place of birth	16.04.1986, Sillamae, Estonia
Citizenship	Estonia
E-mail address	sergsil@gmail.com

2. Education

Institution	Graduation year	Education (field of study/degree)
Tallinn University of Technology	2008	B. Sc. In Mechatronics
Tallinn University of Technology	2010	M. Sc. In Mechatronics

3. Language competence/skills

Language	Level
Russian	Native
Ukrainian	Very good
Estonian	Good
English	Good

4. Professional Employments

Working period	Organization	Position
2008–2011	Stoneridge Electronics Estonia	Worker
2011	Esfitech OU	Engineer
2011–2014	E.R.S. AS	Engineer
2015–2016	Metallurg Engineering OU	Engineer

**DISSERTATIONS DEFENDED AT
TALLINN UNIVERSITY OF TECHNOLOGY ON
*MECHANICAL ENGINEERING***

1. **Jakob Kübarsepp**. Steel-Bonded Hardmetals. 1992.
2. **Jakub Kõo**. Determination of Residual Stresses in Coatings & Coated Parts. 1994.
3. **Mart Tamre**. Tribocharacteristics of Journal Bearings Unlocated Axis. 1995.
4. **Paul Kallas**. Abrasive Erosion of Powder Materials. 1996.
5. **Jüri Pirso**. Titanium and Chromium Carbide Based Cermets. 1996.
6. **Heinrich Reshetnyak**. Hard Metals Serviceability in Sheet Metal Forming Operations. 1996.
7. **Arvi Kruusing**. Magnetic Microdevices and Their Fabrication methods. 1997.
8. **Roberto Carmona Davila**. Some Contributions to the Quality Control in Motor Car Industry. 1999.
9. **Harri Annuka**. Characterization and Application of TiC-Based Iron Alloys Bonded Cermets. 1999.
10. **Irina Hussainova**. Investigation of Particle-Wall Collision and Erosion Prediction. 1999.
11. **Edi Kulderknup**. Reliability and Uncertainty of Quality Measurement. 2000.
12. **Vitali Podgurski**. Laser Ablation and Thermal Evaporation of Thin Films and Structures. 2001.
13. **Igor Penkov**. Strength Investigation of Threaded Joints Under Static and Dynamic Loading. 2001.
14. **Martin Eerme**. Structural Modelling of Engineering Products and Realisation of Computer-Based Environment for Product Development. 2001.
15. **Toivo Tähemaa**. Assurance of Synergy and Competitive Dependability at Non-Safety-Critical Mechatronics Systems design. 2002.
16. **Jüri Resev**. Virtual Differential as Torque Distribution Control Unit in Automotive Propulsion Systems. 2002.
17. **Toomas Pihl**. Powder Coatings for Abrasive Wear. 2002.
18. **Sergei Letunovič**. Tribology of Fine-Grained Cermets. 2003.
19. **Tatyana Karaulova**. Development of the Modelling Tool for the Analysis of the Production Process and its Entities for the SME. 2004.
20. **Grigori Nekrassov**. Development of an Intelligent Integrated Environment for Computer. 2004.

21. **Sergei Zimakov**. Novel Wear Resistant WC-Based Thermal Sprayed Coatings. 2004.
22. **Irina Preis**. Fatigue Performance and Mechanical Reliability of Cemented Carbides. 2004.
23. **Medhat Hussainov**. Effect of Solid Particles on Turbulence of Gas in Two-Phase Flows. 2005.
24. **Frid Kaljas**. Synergy-Based Approach to Design of the Interdisciplinary Systems. 2005.
25. **Dmitri Neshumayev**. Experimental and Numerical Investigation of Combined Heat Transfer Enhancement Technique in Gas-Heated Channels. 2005.
26. **Renno Veinthal**. Characterization and Modelling of Erosion Wear of Powder Composite Materials and Coatings. 2005.
27. **Sergei Tisler**. Deposition of Solid Particles from Aerosol Flow in Laminar Flat-Plate Boundary Layer. 2006.
28. **Tauno Otto**. Models for Monitoring of Technological Processes and Production Systems. 2006.
29. **Maksim Antonov**. Assessment of Cermets Performance in Aggressive Media. 2006.
30. **Tatjana Barashkova**. Research of the Effect of Correlation at the Measurement of Alternating Voltage. 2006.
31. **Jaan Kers**. Recycling of Composite Plastics. 2006.
32. **Raivo Sell**. Model Based Mechatronic Systems Modeling Methodology in Conceptual Design Stage. 2007.
33. **Hans Rämmal**. Experimental Methods for Sound Propagation Studies in Automotive Duct Systems. 2007.
34. **Meelis Pohlak**. Rapid Prototyping of Sheet Metal Components with Incremental Sheet Forming Technology. 2007.
35. **Priidu Peetsalu**. Microstructural Aspects of Thermal Sprayed WC-Co Coatings and Ni-Cr Coated Steels. 2007.
36. **Lauri Kollo**. Sinter/HIP Technology of TiC-Based Cermets. 2007.
37. **Andrei Dedov**. Assessment of Metal Condition and Remaining Life of In-service Power Plant Components Operating at High Temperature. 2007.
38. **Fjodor Sergejev**. Investigation of the Fatigue Mechanics Aspects of PM Hardmetals and Cermets. 2007.
39. **Eduard Ševtšenko**. Intelligent Decision Support System for the Network of Collaborative SME-s. 2007.
40. **Rünno Lumiste**. Networks and Innovation in Machinery and Electronics Industry and Enterprises (Estonian Case Studies). 2008.

41. **Kristo Karjust.** Integrated Product Development and Production Technology of Large Composite Plastic Products. 2008.
42. **Mart Saarna.** Fatigue Characteristics of PM Steels. 2008.
43. **Eduard Kimmari.** Exothermically Synthesized B₄C-Al Composites for Dry Sliding. 2008.
44. **Indrek Abiline.** Calibration Methods of Coating Thickness Gauges. 2008.
45. **Tiit Hindreus.** Synergy-Based Approach to Quality Assurance. 2009.
46. **Karl Raba.** Uncertainty Focused Product Improvement Models. 2009.
47. **Riho Tarbe.** Abrasive Impact Wear: Tester, Wear and Grindability Studies. 2009.
48. **Kristjan Juhani.** Reactive Sintered Chromium and Titanium Carbide-Based Cermets. 2009.
49. **Nadežda Dementjeva.** Energy Planning Model Analysis and Their Adaptability for Estonian Energy Sector. 2009.
50. **Igor Krupenski.** Numerical Simulation of Two-Phase Turbulent Flows in Ash Circulating Fluidized Bed. 2010.
51. **Aleksandr Hlebnikov.** The Analysis of Efficiency and Optimization of District Heating Networks in Estonia. 2010.
52. **Andres Petritšenko.** Vibration of Ladder Frames. 2010.
53. **Renee Joost.** Novel Methods for Hardmetal Production and Recycling. 2010.
54. **Andre Gregor.** Hard PVD Coatings for Tooling. 2010.
55. **Tõnu Roosaar.** Wear Performance of WC- and TiC-Based Ceramic-Metallic Composites. 2010.
56. **Alina Sivitski.** Sliding Wear of PVD Hard Coatings: Fatigue and Measurement Aspects. 2010.
57. **Sergei Kramanenko.** Fractal Approach for Multiple Project Management in Manufacturing Enterprises. 2010.
58. **Eduard Latõsov.** Model for the Analysis of Combined Heat and Power Production. 2011.
59. **Jürgen Riim.** Calibration Methods of Coating Thickness Standards. 2011.
60. **Andrei Surzhenkov.** Duplex Treatment of Steel Surface. 2011.
61. **Steffen Dahms.** Diffusion Welding of Different Materials. 2011.
62. **Birthe Matsi.** Research of Innovation Capacity Monitoring Methodology for Engineering Industry. 2011.
63. **Peeter Ross.** Data Sharing and Shared Workflow in Medical Imaging. 2011.
64. **Siim Link.** Reactivity of Woody and Herbaceous Biomass Chars. 2011.

65. **Kristjan Plamus**. The Impact of Oil Shale Calorific Value on CFB Boiler Thermal Efficiency and Environment. 2012.
66. **Aleksei Tšinjan**. Performance of Tool Materials in Blanking. 2012.
67. **Martinš Sarkans**. Synergy Deployment at Early Evaluation of Modularity of the Multi-Agent Production Systems. 2012.
68. **Sven Seiler**. Laboratory as a Service – A Holistic Framework for Remote and Virtual Labs. 2012.
69. **Tarmo Velsker**. Design Optimization of Steel and Glass Structures. 2012.
70. **Madis Tiik**. Access Rights and Organizational Management in Implementation of Estonian Electronic Health Record System. 2012.
71. **Marina Kostina**. Reliability Management of Manufacturing Processes in Machinery Enterprises. 2012.
72. **Robert Hudjakov**. Long-Range Navigation for Unmanned Off-Road Ground Vehicle. 2012.
73. **Arkadi Zikin**. Advanced Multiphase Tribo-Functional PTA Hardfacings. 2013.
74. **Alar Konist**. Environmental Aspects of Oil Shale Power Production. 2013.
75. **Inge Roos**. Methodology for Calculating CO₂ Emissions from Estonian Shale Oil Industry. 2013.
76. **Dmitri Shvarts**. Global 3D Map Merging Methods for Robot Navigation. 2013.
77. **Kaia Lõun**. Company's Strategy Based Formation of e-Workplace Performance in the Engineering Industry. 2013.
78. **Maido Hiimaa**. Motion Planner for Skid-Steer Unmanned Ground Vehicle. 2013.
79. **Dmitri Goljandin**. Disintegrator Milling System Development and Milling Technologies of Different Materials. 2013.
80. **Dmitri Aleksandrov**. Light-Weight Multicopter Structural Design for Energy Saving. 2013.
81. **Henrik Herranen**. Design Optimization of Smart Composite Structures with Embedded Devices. 2014.
82. **Heiki Tiikoja**. Experimental Acoustic Characterization of Automotive Inlet and Exhaust System. 2014.
83. **Jelena Priss**. High Temperature Corrosion and Abrasive Wear of Boiler Steels. 2014.
84. **Aare Aruniit**. Thermoreactive Polymer Composite with High Particulate Filler Content. 2014.
85. **Dmitri Gornostajev**. Development of the Calculation Method for Barge Hull. 2014.

86. **Liina Lind.** Wear of PVD Coatings on Fineblanking Punches. 2014.
87. **Nikolai Voltšihhin.** Design and Technology of Oxides-Containing Ceramic-Based Composites. 2014.
88. **Aleksander Šablinski.** RANS Numerical Modelling of Turbulent Polydispersed Flows in CFB Freeboard. 2015.
89. **Tanel Aruväli.** Wireless Real-time Monitoring of Machining Processes. 2015.
90. **Andrei Bogatov.** Morphological Changes on Diamond and DLC Films During Sliding Wear. 2015.
91. **Raimo Kabral.** Aero-Acoustic Studies and Innovative Noise Control with Application to Modern Automotive Gas Exchange System. 2015.
92. **Jevgeni Sahnö.** Dynamic Management Framework for Continuous Improvement of Production Processes. 2015.
93. **Ott Pabut.** Optimal Design of Slotless Permanent Magnet Generators. 2015.
94. **Merili Kukuškin.** Value Centric Business Development for Estonian Manufacturing Small and Medium Sized Enterprises. 2015.
95. **Kaimo Sonk.** Development of Additive Manufacturing Based on Functional Requirements. 2015.
96. **Marina Aghayan.** Functionalization of Alumina Nanofibers with Metal Oxides. 2016.
97. **Marek Jõelett.** Titanium Carbide Cermet as Ballistic Protection Material. 2016.
98. **Heikki Sarjas.** Novel Synthesized and Milled Carbide-based Composite Powders for HVOF Spray. 2016.
99. **Klodian Dhoska.** Measurement Methods with 3D Coordinate Measuring Machine and Improved Characterization Setup for Detector Performance. 2016.
100. **Aleksei Snatkin.** Development and Optimisation of Production Monitoring System. 2016.
101. **Igor Poljantšikov.** Partners Selection Tool for Virtual Enterprise in SMEs Network. 2016.